AD-A235 522

AFOSR-TR- 91 [illegible]6

Final Report • February 1991

CALCULATIONS OF ELECTRON ATTACHMENT AND RECOMBINATION IN A HYDROGEN PLASMA

A. Peet Hickman, Senior Physicist
Molecular Physics Laboratory

AIR FORCE OFFICE OF SCIENTIFIC RESEARCH (AFSC)
NOTICE OF TRANSMITTAL TO DTIC
This technical report has been reviewed and is approved for public release IAW AFR 190-12.
Distribution is unlimited.
MATTHEW J. KERPER
Chief, Technical Information Division

Prepared for:

Air Force Office of Scientific Research
Building 410
Bolling Air Force Base
Washington, DC 20332-6448

Attn: Lt. Col. James A. Lupo

Contract No. F49620-88-K-0005
SRI Project PYU-5549
MP 91-045

COPY

91 4 26 005

Final Report • February 1991

CALCULATIONS OF ELECTRON ATTACHMENT AND RECOMBINATION IN A HYDROGEN PLASMA

A. Peet Hickman, Senior Physicist
Molecular Physics Laboratory

Prepared for:

Air Force Office of Scientific Research
Building 410
Bolling Air Force Base
Washington, DC 20332-6448

Attn: Lt. Col. James A. Lupo

Contract No. F49620-88-K-0005
SRI Project PYU-5549
MP 91-045

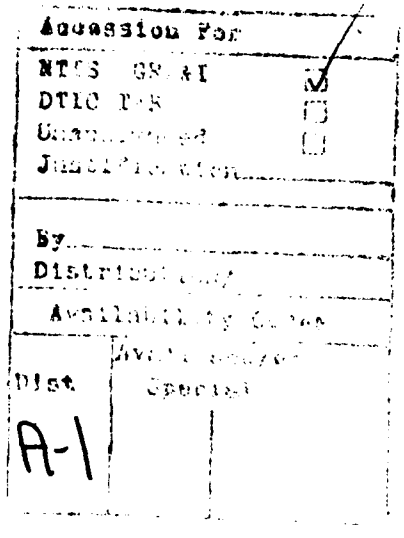

Approved by:

D. J. Eckstrom, Director
Molecular Physics Laboratory

David M. Golden
Vice President
Physical Sciences Division

SRI International 333 Ravenswood Avenue • Menlo Park, CA 94025-3493 • (415) 326-6200 • FAX: (415) 326-5512 • Telex: 334486

REPORT DOCUMENTATION PAGE

Form Approved OMB No. 0704-0188

Public reporting burden for this collection of information is estimated to average 1 hour per response, including the time for reviewing instructions, searching existing data sources, gathering and maintaining the data needed, and completing and reviewing the collection of information. Send comments regarding this burden estimate or any other aspect of this collection of information, including suggestions for reducing this burden, to Washington Headquarters Services, Directorate for Information Operations and Reports, 1215 Jefferson Davis Highway, Suite 1204, Arlington, VA 22202-4302, and to the Office of Management and Budget, Paperwork Reduction Project (0704-0188), Washington, DC 20503

1. AGENCY USE ONLY *(Leave blank)*	2. REPORT DATE	3. REPORT TYPE AND DATES COVERED
	910414	Final Report 880215 to 910214

4. TITLE AND SUBTITLE
CALCULATIONS OF ELECTRON ATTACHMENT AND RECOMBINATION IN A HYDROGEN PLASMA

5. FUNDING NUMBERS

6. AUTHOR(S)
Hickman, A. Peet

7. PERFORMING ORGANIZATION NAME(S) AND ADDRESS(ES)
SRI International
333 Ravenswood Avenue
Menlo Park, California 94025-3493

8. PERFORMING ORGANIZATION REPORT NUMBER
F49620-88-K-0005

9. SPONSORING/MONITORING AGENCY NAME(S) AND ADDRESS(ES)
Air Force Office of Scientific Research/NP
Building 410
Bolling AFB, DC 20332
Lt Col James A. Lupo
202-767-4908

10. SPONSORING/MONITORING AGENCY REPORT NUMBER

11. SUPPLEMENTARY NOTES

12a. DISTRIBUTION/AVAILABILITY STATEMENT
Approved for public release;
Distribution unlimited

12b. DISTRIBUTION CODE

13. ABSTRACT *(Maximum 200 words)*

This project involved theoretical calculations of microscopic atomic and molecular processes in the generation of H^- in a hydrogen plasma. Efficient production of H^- is essential for practical applications such as particle beams and fusion plasmas. The specific objectives of the project were: (1) to calculate cross sections for dissociative recombination of electrons with H_2^+, (2) to provide theoretical analysis for ongoing experiments that use multiphoton ionization to investigate the spectroscopy of excited states of molecular hydrogen, and (3) to calculate cross sections for dissociative attachment of electrons with vibrationally excited hydrogen molecules.

14. SUBJECT TERMS	15. NUMBER OF PAGES
Hydrogen Negative Ion Formation, Electron Recombination, Electron Attachment	91
	16. PRICE CODE

17. SECURITY CLASSIFICATION OF REPORT	18. SECURITY CLASSIFICATION OF THIS PAGE	19. SECURITY CLASSIFICATION OF ABSTRACT	20. LIMITATION OF ABSTRACT
UNCLASSIFIED	UNCLASSIFIED	UNCLASSIFIED	Unlimited

CONTENTS

OBJECTIVES 1

RESEARCH ACCOMPLISHMENTS 2
Electron Recombination with H_2^+ 2
Multiphoton Ionization of H_2 2
Electron Attachment to H_2 4

LIST OF PUBLICATIONS 6

PROFESSIONAL PERSONNEL 6

PAPERS PRESENTED AT MEETINGS 6

REFERENCES 7

APPENDICES

A Resonances in Dissociative Recombination of Electrons with H_2^+ A-1

B Dissociative Recombination of H_2^+: Comparison of Theory and Experiment B-1

C Two-Photon Excitation and Excited-State Absorption Cross Sections for H_2 E,F $^1\Sigma_g$ (v = 6): Measurement and Calculation C-1

D Photoelectron Spectroscopy of Vibrationally Excited H_2 (E,F $^1\Sigma_g^+$) D-1

E Dissociative Attachment of Electrons to Vibrationally Excited H_2 ..... E-1

OBJECTIVES

This project involved theoretical calculations of microscopic atomic and molecular processes important in the generation of H^- in a hydrogen plasma. Efficient production of H^- is essential for many practical applications such as particle beams and heating fusion plasmas. The calculations performed provided detailed information about the effect of the internal energy of the reactants. Such data are necessary to determine the optimal conditions for operating the plasma. In more general terms, the theoretical analysis and close interaction with experiments led to a better understanding of the basic physics of the plasma.

The specific objectives of the project were (1) to calculate cross sections for dissociative recombination of electrons with H_2^+ for various values of the vibrational quantum number v, (2) to provide theoretical analysis for ongoing experiments using multiphoton ionization to investigate the spectroscopy of excited states of molecular hydrogen, and (3) to calculate cross sections for dissociative attachment of electrons with vibrationally excited H_2 molecules. The following sections report the accomplishments of all these investigations.

RESEARCH ACCOMPLISHMENTS

ELECTRON RECOMBINATION WITH H_2^+

Dissociative recombination involves the capture of an electron by a molecular ion, formation of a compound state, and subsequent dissociation into fragments. The process may be written schematically as

$$e + H_2^+ \rightarrow H_2^* \rightarrow H^* + H$$

Initial calculations performed for $e + H_2^+$ illuminated the mechanisms that come into play as the process unfolds. Our calculations treated in detail the so-called indirect mechanism. The calculations[1] were published in 1988, and a copy of the work is included as Appendix A.

We have an ongoing collaboration with Professor Brian Mitchell at the University of Western Ontario, and in 1990 we compared our calculations with the most recent experiments of his group. The new data show dramatic oscillations in the cross sections as a function of the electron energy. These results are of sufficient accuracy to associate particular features of the cross sections with specific compound states of the neutral, excited hydrogen molecule. Additional theoretical analysis was performed to allow comparison of our calculations with experiments at this level of accuracy.

Our new work clearly shows that both $s\sigma$ and $d\sigma$ Rydberg series of H_2^{**} contribute to the oscillations in the cross section, and we were able to make tentative assignments of the quantum numbers of these states that contribute to the observed resonances. A joint manuscript with Professor Mitchell's group has been submitted to *Physical Review Letters*, and a copy is included as Appendix B. The excellent agreement achieved between theory and experiment is shown in Figure 1.

MULTIPHOTON IONIZATION OF H_2

Two experiments performed in the Molecular Physics Laboratory at SRI are related to the detection of vibrationally excited hydrogen by multiphoton ionization. This detection is an important diagnostic for hydrogen plasma sources of H^-. Theoretical calculations have made key contributions to the analysis of these experiments.

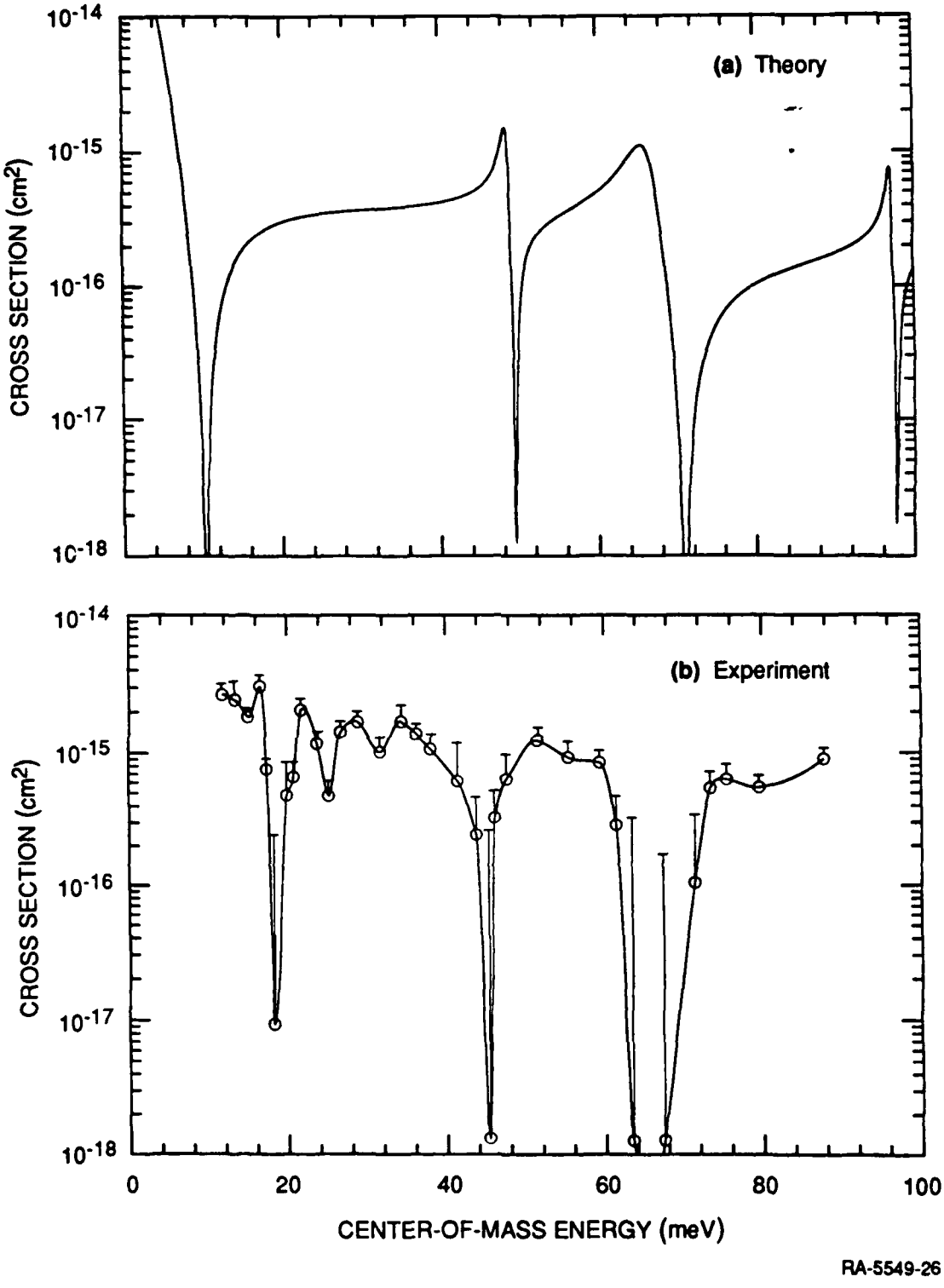

Figure 1. Comparison of theory and experiment for dissociative recombination of electrons with H_2^+.

The first set of experiments was performed in Dr. William K. Bischel's research group. Absolute cross sections were measured for two-photon excitation of molecular hydrogen to the EF state and for subsequent ionization of this state. Theoretical calculations were performed to clarify the mechanism of the ionization of the EF state. These calculations were recently published,[2] and a copy is attached as Appendix C. The main conclusion was that an autoionizing state provides an important indirect pathway for photoionization. The additional photoionization signal caused by the indirect ionization is frequency-dependent. Understanding these effects is necessary for plasma diagnostics, because the strength of the photoionization signal as a function of frequency must be correlated with the population of various vibrationally excited states of H_2.

The second set of experiments was performed by Dr. Ravinder Kachru, Dr. Hanspeter Helm, and their associates. The same multiphoton ionization process of molecular hydrogen was studied. The energy distribution of the photoelectrons was measured, and calculations of this energy distribution were compared with the experimental data. Good agreement was achieved, leading to confidence in our understanding of the physics of the process. A joint experimental and theoretical paper was published[3] describing the work, and a copy of this paper is attached as Appendix D.

ELECTRON ATTACHMENT TO H_2

The process of electron attachment to H_2 may be written

$$e + H_2 \rightarrow H^- + H$$

We are performing calculations of dissociative attachment of low energy (< 5eV) electrons to molecular hydrogen in vibrational states v = 0 to v = 9, using a nonlocal complex potential. Knowledge of these cross sections is important for optimizing the operating conditions of hydrogen plasmas from which H^- will be extracted. The present work is particularly concerned with the difference between the rigorous formulation using nonlocal potentials (that is, integro-differential equations) and the simpler approximation assuming local potentials (differential equations).

A manuscript describing the calculations has been accepted for publication and is attached as Appendix E. The calculations include the nonlocal and energy-dependent width and shift operators that are defined by resonant scattering theory.

We compared the use of local and nonlocal potentials by performing calculations with several approximate forms of the full nonlocal potential. We found that in certain cases we could define an appropriate local potential, but only by first calculating and then modifying the full nonlocal coupling terms. This result explains the relative accuracy of earlier work based on fitting experimental data using local potentials, because it shows that one does expect an approximate local potential to exist. Unfortunately, the appropriate local potential is not the one that can easily be identified with fixed-nuclei properties of the resonant electronic state. In fact, using the fixed-nuclei curve led to serious errors. Our conclusion is that detailed calculations of the electronic coupling matrix elements, and inclusion of the nonlocal width and shift, are necessary for definitive calculations of electron attachment.

LIST OF PUBLICATIONS

The following publications resulted from work under this contract.

A. P. Hickman, "Resonances in Dissociative Recombination of Electrons with H_2^+," in *Dissociative Recombination: Theory, Experiment, and Applications*, J.B.A. Mitchell and S. Guberman, Eds. (World Scientific Publishing Co., 1988).

J. D. Buck, D. C. Robie, A. P. Hickman, D. J. Bamford, and W. K. Bischel, "Two-Photon Excitation and Excited-State Absorption Cross Sections for H_2 E,F $^1\Sigma_g^+$: Measurement and Calculations," Phys. Rev. A **39**, 3932 (1989).

E. Xu, A. P. Hickman, R. Kachru, T. Tsuboi, and H. Helm, "Photoelectron Spectroscopy of Vibrationally Excited H_2 (E,F $^1\Sigma_g^+$)," Phys. Rev. A **40**, 7031 (1989).

A. P. Hickman, "Dissociative Attachment of Electrons to Vibrationally Excited H_2," Phys. Rev. A, **43**, in press (1991).

P. Van der Donk, F. B. Yousif, J.B.A. Mitchell, and A. P. Hickman, "Dissociative Recombination of H_2^+: Comparison of Theory and Experiment," Phys. Rev. Lett., submitted for publication.

PROFESSIONAL PERSONNEL

Dr. A. Peet Hickman, project leader.

PAPERS PRESENTED AT MEETINGS

The following papers were presented at meetings during this project.

A. P. Hickman, "Theory of Dissociative Electron Recombination," presented at the Division of Atomic, Molecular, and Optical Physics sessions of the American Physical Society Meeting, Baltimore, April 18-20, 1988.

A. P. Hickman, "Resonances in Dissociative Recombination of Electrons with H_2^+," presented at the Workshop on Dissociative Recombination at Lake Louise, Canada, May 28-31, 1988.

E. Xu, A. P. Hickman, R. Kachru, and H. Helm, "Photoelectron Spectroscopy of Vibrationally Excited H_2 E,F States," presented at the XVI International Conference on the Physics of Electronic and Atomic Collisions, New York, July 25-August 1, 1989.

REFERENCES

1. A. P. Hickman, "Resonances in Dissociative Recombination of Electrons with H_2^+," in *Dissociative Recombination: Theory, Experiment, and Applications,* J.B.A. Mitchell and S. Guberman, Eds. (World Scientific Publishing Co., 1988).

2. J. D. Buck, D. C. Robie, A. P. Hickman, D. J. Bamford, and W. K. Bischel, "Two-Photon Excitation and Excited-State Absorption Cross Sections for H_2 E,F $^1\Sigma_g^+$: Measurement and Calculations," Phys. Rev. A **39**, 3932 (1989).

3. E. Xu, A. P. Hickman, R. Kachru, T. Tsuboi, and H. Helm, "Photoelectron Spectroscopy of Vibrationally Excited H_2 (E,F $^1\Sigma_g^+$)," Phys. Rev. A **40**, 7031 (1989).

APPENDIX A

Resonances in Dissociative Recombination of Electrons with H_2^+

From *Dissociative Recombination: Theory, Experiment, and Applications*
Edited by J.B.A. Mitchell and S. Guberman (World Scientific Publishing Co., 1988).

Resonances in Dissociative Recombination of Electrons with H_2^+

A. P. Hickman
Molecular Physics Department
SRI International
Menlo Park, CA 94025

ABSTRACT

Dissociative recombination of electrons with diatomic molecular ions is reviewed, with emphasis on the qualitative description of the "direct" and "indirect" mechanisms involved. Calculations for H_2^+ are presented and compared with the recent experimental results of Hus et al. The calculations confirm the importance of the "indirect" mechanism, which accounts for the resonant structure observed in the cross section.

1. INTRODUCTION

Dissociative recombination (DR) involves the capture of an electron by a molecular ion, the formation of a compound state, and the subsequent dissociation into fragments. This paper discusses the mechanisms that come into play as the process unfolds and presents specific calculations for $e + H_2^+$. This system is an important prototype because it involves the simplest molecular ion, because experimental data[1,2] is available, and because the relevant excited state potential curves of H_2 have been calculated.[3,4]

Section 2 discusses the so-called "direct" and "indirect" mechanisms. Section 3 summarizes the theory. A single resonance in the DR cross section may be described by a Beutler-Fano profile,[5] but the general approach treats overlapping resonances. Section 4 pre sents calculations for H_2^+. Section 5 contains concluding remarks.

2. MECHANISMS FOR DISSOCIATIVE RECOMBINATION

2.1 Direct Recombination

The physical picture of direct DR, treated by Bardsley[6] in 1968, may be understood using the potential curves sketched in Fig. 1a and the following symbolic representation:

$$e + AB^+ \rightleftarrows AB^{**} \rightarrow A + B^* \qquad (1)$$

After capture into the dissociating state AB^{**}, the nuclei follow the dissociating potential curve V^*. The excess electronic energy of the resonant state is converted to kinetic energy of the dissociating products. These products must separate to the point where V^* crosses V^+ for the recombination to be complete. Competing with the stabilization of the resonant state by dissociation is electronic autoionization [indicated by the leftward pointing arrow in Eq. (1)]. For H_2, classical mechanics predicts that a time on the order of 10^{-15} sec is required for dissociation. Typical calculated values[4] of the autoionization lifetime are also on the order of 10^{-15} sec. The conclusion is that dissociation provides a stabilization mechanism fast enough to compete effectively with autoionization.

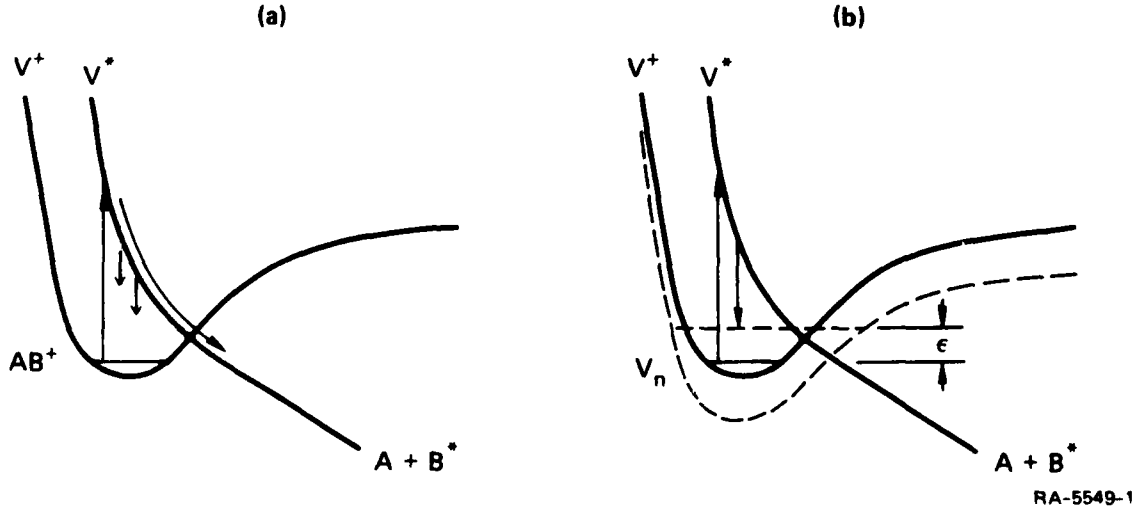

Figure 1. Illustration of direct (a) and indirect (b) recombination.

The details of the theoretical analysis of direct DR are available in the literature.[6-10] The result is that the cross section is approximately proportional to the square of the following integral:

$$\xi_{v_0} = \left(\frac{2M\pi}{k}\right)^{1/2} \int \chi_{v_0}(R)\, V_{el}(R)\, F(R)\, dR \qquad (2)$$

χ_{v_0} is the wave function of the initial vibrational level of the molecular ion, V_{el} is the matrix element for electron capture (or autoionization), and F(R) is the regular solution to the Schroedinger equation for the final state potential $V^*(R)$ at energy $E = \hbar^2k^2/2M$. This integral is essentially a Franck-Condon factor between the initial and final states, mediated by the electronic coupling V_{el}.

Direct DR for thermal energy electrons is expected to have a large cross section when the Franck-Condon factor is large. This situation usually occurs when the dissociating potential V^* crosses the ionic potential V^+ near the minimum of the latter. Conversely, when the dissociating curve does not cross V^+ near the minimum, one expects the thermal energy cross section for direct DR to be small. However, even when direct DR is small, other mechanisms may be significant and may lead to a large total cross section. A qualitative discussion of this possibility is presented in the next subsection.

2.2 Indirect Recombination

At certain well-defined energies, the incident electron may be captured into compound resonant states, here denoted $AB^{\#}(n,v)$. These states provide an alternative pathway to the final state $A + B^*$. The situation represented by Eq.(1) must therefore be generalized:

$$\begin{array}{ccccc} e + AB^+ & \longrightarrow & AB^{**} & \longrightarrow & A + B^* \\ & \searrow & \uparrow & & \\ & & AB^{\#}(n,v) & & \end{array} \qquad (3)$$

The additional states are labelled by the indices n and v. Their physical form is an ion core AB^+ in vibrational level v, and a Rydberg electron in an orbital whose principle quantum number is n. (We omit discussion of the electron's angular momentum).

One way to consider these resonant states is the following. Beginning with the ionic potential $V^+(R)$, define the series of Rydberg potential energy curves $V^n(R) = V^+(R) - 0.5\,[n-\mu(R)]^{-2}$. The quantum defect $\mu(R)$ defines the binding energy of the Rydberg electron. Each potential $V^n(R)$ of the molecule AB has a set of vibrational energy levels. One of the $V^n(R)$ is shown in Fig. 1b, and one of its vibrational energy levels is drawn. For an incident electron of the proper energy, the total energy of the system will be close to that of this particular $AB^{\#}(n,v)$. One expects the cross section for recombination to have additional structure near this energy.

3. THEORY

The theory of DR may be formulated[6-8] using the matrix elements

$$g_{v'v} = \frac{2M}{k} \int \chi_{v'}(R')\, V_{el}(R')\, G(R',R)\, V_{el}(R)\, \chi_v(R)\, dR'\, dR$$

where $G(R',R)$, defined explicitly in ref. 8, is a Green function for the Schroedinger equation with potential V^*. The matrix element $g_{v'v}$ is related to the amplitude for capture into the resonant state $AB^{\#}(n,v')$ from the initial vibrational state v of AB^+. The mechanism for this capture is a second order (in V_{el}) electronic coupling via the resonant state AB^{**}. The momentum transfer from the light electron to the heavy nuclei via potential scattering is neglected. This approximation is well-fulfilled in practice for H_2^+.

For the present discussion, it is sufficient to note that G corresponds to outgoing-wave boundary conditions (i.e., dissociation) and is therefore a complex-valued function. We may write

$$g_{v'v} = \mathrm{Re}\; g_{v'v} + (i/\pi)\xi_{v'}\xi_v \qquad (4)$$

where the ξ_v are defined in Eq. (2).

Giusti[9] first treated DR including both direct and indirect mechanisms, using "first order" Multichannel Quantum Defect Theory (MQDT). The terms Re $g_{v'v}$ were neglected. Later calculations for

$e + H_2^+$ by Giusti et al.[7] and Nakashima et al.[10] also neglected Re $g_{v'v}$. Hickman[8] included Re $g_{v'v}$ in an approach based on the Independent Resonance Approximation (IRA) and discovered that the previously neglected terms were quite important for $e + H_2^+$. However, the relation between the two theories (MQDT and IRA) was obscure. Our recent work, summarized here, clarifies this relation and ...fies the two theories.

MQDT is formulated in terms of a reactance matrix coupling several different arrangement channels. These channels have the asymptotic forms $A + B^*$ (labelled d), and $AB^+(v) + e$, for v=0,1,... The specific form of the matrix that we use is

	d	v=0	v=1	v=2	v=3	
d	0	ξ_0	ξ_1	ξ_2	ξ_3	. . .
v=0	ξ_0					
v=1	ξ_1		π Re $g_{v'v}$			
v=2	ξ_2					
⋮						

(5)

This matrix may be "contracted" into an S matrix using the general MQDT prescription.[11] S may have a smaller dimension than the reactance matrix, because some of the arrangement channels are closed.

We have found a limiting case in which the MQDT contraction can be explicitly compared with the IRA. Consider the channels d, v=0 (the initial channel), and v=1 (a closed channel). The effect of a single resonance on the recombination may then be described in terms of a background process (direct DR) that is modified in a restricted energy range by the resonance. Identical result are obtained with the IRA and MQDT:

$$\sigma(\epsilon) = \sigma^{direct}(\epsilon)\ (x + q)^2/(x^2 + 1) \qquad (6)$$

where $x = (E-E_{res})/(\Gamma/2)$, and $\Gamma = 2\xi_v^2/\pi n^3$ is the width of the resonance. We find that q is given by $-(\text{Re } g_{01})/(\text{Im } g_{01})$. This result demonstrates the equivalence of MQDT and the IRA for single resonances, provided that one includes the effect of the full Green function as shown in Eq. (5). The "first-order" limit of MQDT discussed by Giusti[9] corresponds to neglecting the block of terms in

Eq. (5) whose values are π Re $g_{v',v}$. For the calculations reported here, we use the full MQDT approach based on the reactance matrix, Eq. (5).

4. RESULTS FOR e + H_2^+

Fig. 2 shows the intermediate states $AB^{\#}(n,v)$ introduced in 2.2. The vibrational levels of the ion AB^+ are drawn, as well as an electronic Rydberg series converging to each ionization limit. Clearly, for many incident electron energies, contributions from more than one intermediate state must be included.

Two limiting cases may be identified: small Δv and large n (the left hand side of Fig. 2), and large Δv and small n (the right hand side of Fig. 2). The discussion in 2.2 and Fig. 1b correspond to resonances of the first type. One may wonder whether resonances of the second type, involving up to seven quanta of vibrational energy transfer, are important. Following the arguments of O'Malley,[12] one

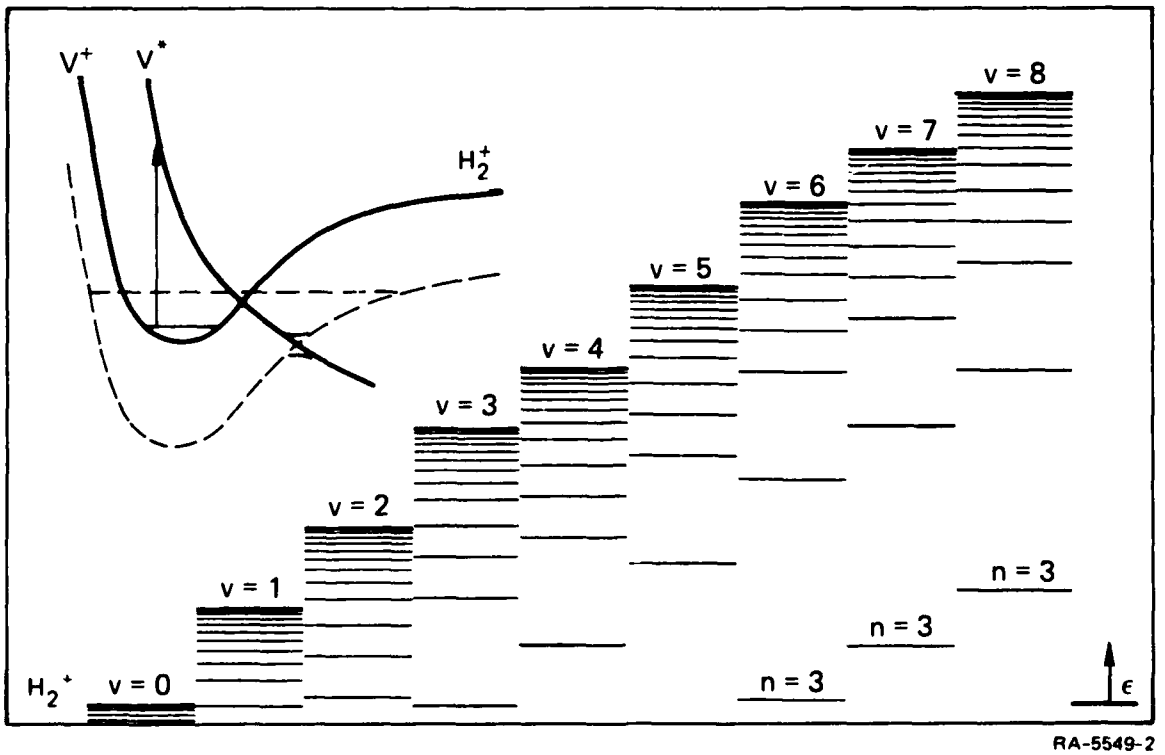

Figure 2. Rydberg energy levels of H_2. Inset: Curve crossing mechanism for high v, low n resonances.

sees that such resonances may be interpreted in terms of a curve crossing as shown in the upper left of Fig. 2. The electron is captured into the dissociating state, but during dissociation the system undergoes a curve crossing to the potential curve $V^n(R)$, where n=3 (the smallest value of n possible for the $d\sigma$ waves considered here).

The effect of the overlapping resonances may be probed by model calculations that include only selected resonances. Two series of such calculations are presented in Fig. 3. First, we consider the case v_0=0. (v_0 denotes the initial vibrational level of H_2^+). In this case the Franck-Condon factor is low and one expects the direct mechanism to be small. Panel (a) shows a dotted line corresponding to the direct process; the transition probability is indeed small, about 10%. This panel also shows the regular structure arising from the Rydberg series converging to v=1 (cf. Fig. 2). The structure defined by Eq. (7), which could be obtained by the IRA, is essentially repeated, properly scaled, by each member of the Rydberg series. Panel (b) shows the result if one considers a single resonance corresponding to v=7 and n=3. Panel (c) shows the combined results. The overall pattern is more complicated, but still reminiscent of the simpler results obtained in (a) and (b). Note that the deep minimum seen in (b) near 0.20 eV persists.

Panels (d)-(f) show a parallel calculation for the case v_0=1. In this case the Franck-Condon factor is large, and the direct mechanism (dotted line) is much larger, about 70%. The series of resonances for v=1 to v=2 excitation [panel (d)] are "window" resonances, that is, purely destructive interference. The single resonance for v=1 to v=8 excitation is also of this type. Again, the composite case [panel (f)] exhibits features that are similar to those of each contributing resonance.

Our results suggest that the indirect mechanism tends to inhibit recombination when the direct mechanism is large. When the direct mechanism is small, however, the indirect mechanism may enhance or inhibit the cross section. Having a smaller cross section when the indirect mechanism is included is consistent with the physical picture

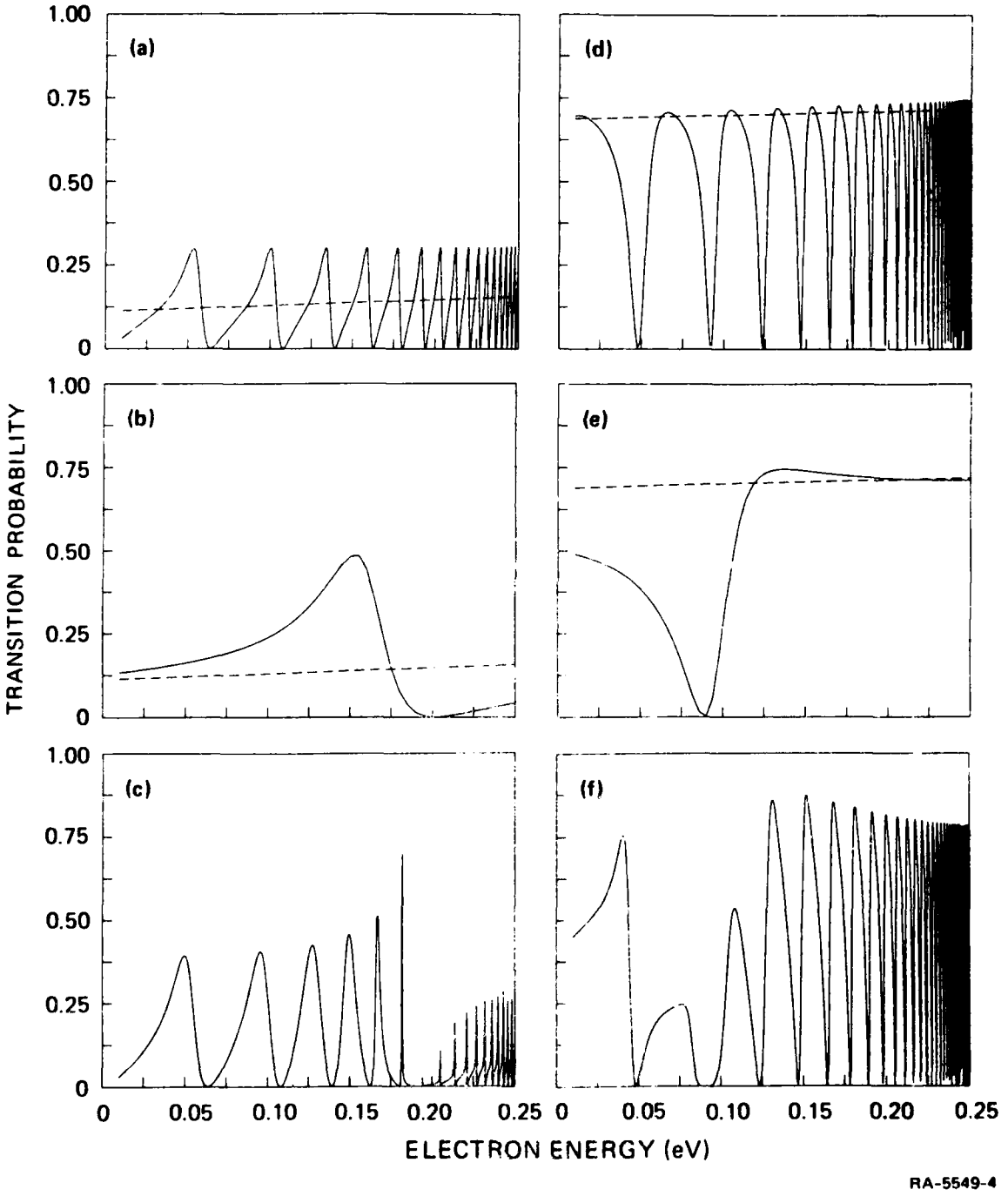

Figure 3. Effect of selected resonant states for e + H_2^+.

developed by O'Malley based on classical trajectories. The curve crossings in the outgoing channel make dissociation more difficult.

The exact energies of the resonances corresponding to large Δv are sensitive to the molecular potential curves. We find that different values of $\mu(R)$ from the literature lead to different values of the resonance energies. For $\Delta v \sim 7\text{-}8$, the discrepancies are large, on the order of tenths of eV. (Another contribution to the resonance energy comes from Re $g_{vv'}$). Since the effect of these large v resonances is often to reduce substantially the cross section over a particular energy range, it is essential to calculate accurately the location of each resonance.

These uncertainties preclude a definitive calculation even though the MQDT formalism provides the computational framework. Nevertheless, Fig. 4 presents calculations including the vibrational levels v=0-9 for H_2^+. Separate calculations for v_0=0 and v_0=1 were performed; the experimental values of Hus et al., shown for comparison in both panels, correspond to a mixture of these two initial states. Some testing of the effects of using different functions $\mu(R)$ from the literature was carried out. Our results tend to favor the $\mu(R)$ of Nakashima et al.,[10] which is numerically much smaller than the other functions. Those results are shown.

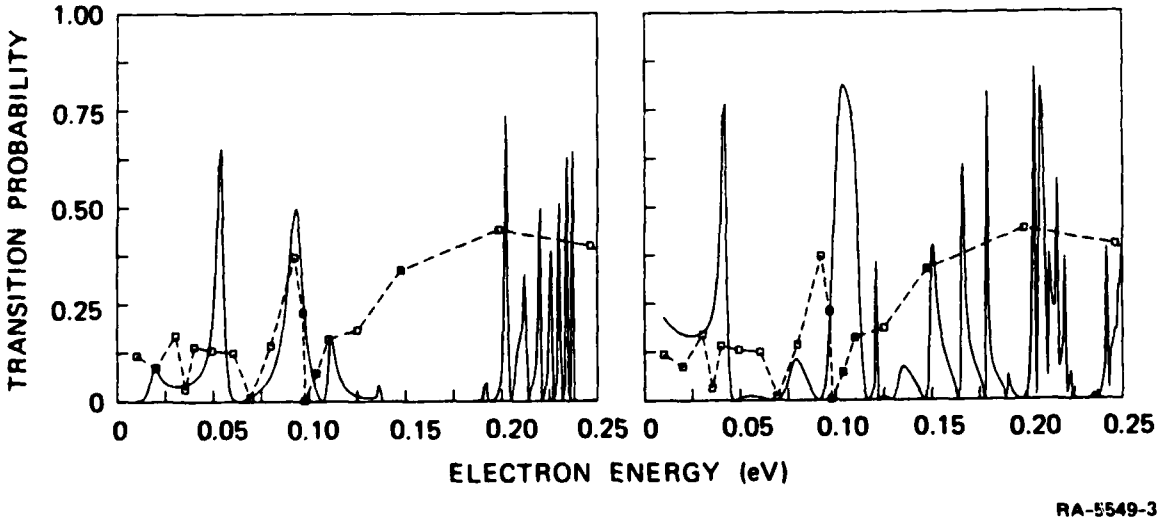

Figure 4. Comparison with experiment (Hus et al.[2]) for e + H_2^+.

5. CONCLUDING REMARKS

There has been considerable progress in the understanding of DR of molecular ions in the past few years. The recent experimental studies of Hus et al. have an electron energy resolution of about 0.02 eV, and reveal a complex structure of the cross section. Theoretical calculations confirm that the structure arises from the pattern of overlapping Rydberg series converging to the various vibrational levels of the target molecular ion. These Rydberg states collectively contribute to the "indirect" mechanism of recombination, which is of prime importance for $e + H_2^+$. This indirect mechanism should be assessed in future calculations on other systems, particularly in cases where Franck-Condon arguments suggest that the direct mechanism will be small.

ACKNOWLEDGMENT

This work was supported by AFOSR contract No. F49620-88-K-0005.

REFERENCES

1. Auerbach, D., Cacak, R., Caudano, R., Gaily, T. D., Keyser, C. J., McGowan, J. W., Mitchell, J.B.A. and Wilk, S.F.J., J. Phys. B 10, 3797 (1977).
2. Hus, H., Yousif, F., Noren, C., Sen, A. and Mitchell, J.B.A., Phys. Rev. Lett. 60, 1006 (1988).
3. Guberman, S., J. Chem. Phys. 78, 1404 (1983).
4. Hazi, A. U., Derkits, C. and Bardsley, J. N., Phys. Rev. A 27, 1751 (1983).
5. Fano, U., Phys. Rev. 124, 1866 (1961).
6. Bardsley, J. N., J. Phys. B 1, 349 (1968).
7. Giusti-Suzor, A., Bardsley, J. N. and Derkits, C., Phys. Rev. A 28, 682 (1983).
8. Hickman, A. P., J. Phys. B 20, 2091 (1987).
9. Giusti, A., J. Phys. B 13, 3867 (1980).
10. Nakashima, K., Takagi, H. and Nakamura, H., J. Chem. Phys. 86, 726 (1987).
11. Seaton, M. J., Rep. Prog. Phys. 46, 167 (1983).
12. O'Malley, T. F., J. Phys. B 14, 1229 (1981).
13. Ross, S. and Jungen, Ch., Phys. Rev. Lett. 59, 1297 (1987).

APPENDIX B

Dissociative Recombination of H_2^+: Comparison of Theory and Experiment

Submitted to *Physical Review Letters*

Dissociative Recombination of H_2^+. Comparison of Theory and Experiment.

P. Van der Donk, F.B. Yousif, J.B.A. Mitchell
Dept. of Physics, University of Western Ontario
London, Ontario, Canada, N6A 3K7
and
A.P. Hickman
Molecular Physics Laboratory
SRI International
Menlo Park, CA 94025

ABSTRACT.

High resolution measurements for the dissociative recombination of H_2^+ (v=0) are presented and compared with theoretical calculations. The observed structure is explained with a model that invokes the coupling to intermediate electronic states belonging to two separate Rydberg series.

INTRODUCTION.

The complex collision process of dissociative recombination (DR) can be better understood by comparing high quality experimental results with theoretical models. The most likely candidate for such a comparison is H_2^+, the simplest molecular ion.

For this system, DR can be schematically written

$$e + H_2^+ \rightarrow H + H^* \quad ...(4)$$

A number of theoretical calculations have been performed for this ion[1-4]. These calculations have predicted that the cross section for electrons recombining with H_2^+ in a specific vibrational state should display a series of narrow resonances due to the influence of the neutral Rydberg states lying below the ion state. In order to observe these resonances it is necessary to prepare the ions in a single vibrational state and to have a collision at a well defined energy. The most suitable method for doing this is to use the merged beam technique which has been developed at the University of Western Ontario. A preliminary measurement that demonstrated the existence of the resonances has already been published[5]. This paper describes some recent measurements that were performed using very high energy resolution and a fine energy mesh. The results are now of sufficient accuracy to associate particular features of the cross section with specific Rydberg states. Additional theoretical work is necessary to compare experiment and theory at this level of accuracy. Extensions to previous theory[4], and the very good comparison with experiment thereby obtained, are also presented in this paper.

EXPERIMENTAL METHOD.

The Merged Beam Electron Ion Beam Experiment at the University of Western Ontario has been described in detail elsewhere[6] and only a brief overview of the apparatus will be presented here. A beam of H_2^+ ions are produced by electron impact in a radiofrequency ion

trap source located in the terminal of a Van de Graaff accelerator. This source, when operated with a low extraction potential is capable of producing ions with very low internal energies[5,7]. The ions are accelerated to 400 kev, mass analyzed and passed into the interaction region where they are merged with a beam of electrons derived from an indirectly-heated, barium oxide cathode, using a trochoidal analyzer. The two beams interact over a distance of 8.6 cm before being demerged. The electron beam is collected in a Faraday cup, the ion beam is deflected electrostatically into a second Faraday cup and the undeflected neutrals impinge upon a surface barrier detector and are detected. The electron beam is modulated and the signals are measured in and out of phase with the modulation in order to distinguish true recombination signals from neutrals produced in collisions between the ion beam and the background gas. The overlap of the two beams is measured at two places in the interaction region and the effective collision area, F, is determined.

The cross section for recombination is determined using the formula

$$\sigma = \frac{C_n e^2}{I_i I_e L} \frac{|\mathbf{v}_i \cdot \mathbf{v}_e|}{|\mathbf{v}_i - \mathbf{v}_e|} F \quad \ldots(1)$$

where C_n is the neutral count rate, e, the electronic charge, I_i, v_i, I_e, and v_e are the ion and electron beam currents and velocities respectively, L is the length of the interaction region and F is the effective collision area.

The energy in the center-of-mass is given by:

$$E_{CM} = (E_e^{1/2} - E_+^{1/2})^2 + E_e^{1/2} E_+^{1/2} \theta^2 \quad \ldots(2)$$

where θ is the intersection angle between the two beams, E_e is the electron beam energy and E_+ the reduced ion energy is given by $E_+ = E_i . m_e/m_i$, E_i being the ion beam energy. By differentiating this equation with respect to E_+, E_e and θ, it is possible to write down an expression for the uncertainty in the center-of-mass in this measurement.

$$\Delta E_{CM} = \left[\left(\left[\left(1 - \left(\frac{E_+}{E_e}\right)^{1/2}\right] \Delta E_e \right)^2 + \left(\left[1 - \left(\frac{E_e}{E_+}\right)^{1/2}\right] \Delta E_+ \right)^2 + \right.\right.$$

$$\left.\left. + \left[2 (E_e E_+)^{1/2} \theta \Delta\theta\right]^2 \right]^{1/2} \ldots (3)$$

It can be seen from equation (3) that when $E_e = E_+$, the first two terms go to zero and the uncertainty is determined mainly by the uncertainty in the intersection angle. Using well collimated beams and careful alignment this can be made quite small. The unique property of the merged beam technique is that the ultimate energy resolution at low energies is rather insensitive to spreads in the energies of the electron and ion beams.

The energy scale of the measurement was calibrated using a method described in ref.[8] in which the ion beam energy is first determined using a nuclear resonance technique and the electron energy is subsequently obtained from the position of the maximum in the DR signal as the electron energy is scanned through the $E_e \approx E_+$ energy region. E_{cm} can then be calculated using Eq.2. The largest uncertainty associated with this calibration is in the determination of E_e and this amounts to ± 0.5 eV. From Eq.2 it can be seen that this inaccuracy leads to an uncertainty in the center-of-mass energy of ± 7meV at 20 meV and ±15 meV at 100 meV.

RESULTS AND DISCUSSION.

The cross sections for the dissociative recombination of H_2^+ ions with low internal energy, measured in the present study are shown in figure 1a. The ion and electron beam currents used were 20μA and $1x10^{-14}$A respectively and more than 24 hours per point were needed in order to achieve the level of statistical accuracy shown here. The error bars shown represent one standard deviation and systematic errors, mainly associated with measurement of F,provide an uncertainty in the absolute cross sections of ± 20%. The effect of systematic errors on the relative uncertainty in the data points is about 4% however since F is a quantity which changes slowly with energy.

The merged beam technique is very stable regarding the collision energy and measured points are very repeatable. Three well defined window resonances are clearly apparent in the data. From the figure it can be seen that at the low end of the energy scale, the resolution must be of the order of 5 mev. Using equation (3) this translates to a value of about 10 meV at the upper end. At a higher extraction potential the central resonance was found to disappear and this is due the population of v=1 states in the beam increasing causing this resonance to be washed out. By comparison with theoretical results it is believed that the results presented in figure 1a refer only to v=0 ions. This is discussed further below. No effort was made to restrict the rotational population of the beam and the source gas was undoubtedly a mixture of ortho and para hydrogen. The rotational population must therefore be reflect a thermal distribution of odd and even J

levels.

The direct and indirect mechanisms of dissociative recombination have been identified and discussed in the literature [1-4]. One can augment Eq.(1) as follows

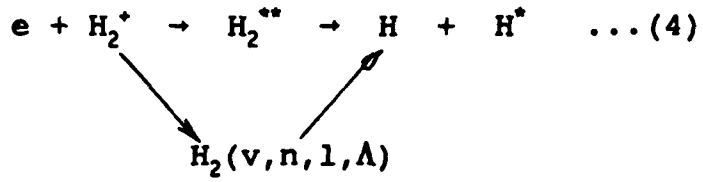

The top line of Eq.(4) corresponds to direct recombination: an incident electron is captured directly into the dissociating $^1\Sigma_g^+$ state and the nuclear motion on this potential leads to the final products. At certain well-defined energies, the electron may also be captured into compound resonance states, here denoted on the second line by $H_2(v,n,l,\Lambda)$. The physical form of such a state is an *ion core* H_2^+ *in* vibrational level v and a Rydberg electron whose quantum numbers are n, l and Λ (projection on the internuclear axis). This state is formed when an electron, incident on H_2^+ (v=0) vibrationally excites the ion to v=1, thereby losing energy and dropping down into a Rydberg orbital. The state $H_2(v,n,l,\Lambda)$ may decay to H + H^* by predissociation. This sequence of events provides an alternative mechanism for recombination, and leads to classic interference phenomena. The direct mechanism provides a slowly varying background cross section; at those energies for which the intermediate compound state is allowed, the cross section exhibits rapidly varying resonance structure. By analyzing this structure, we can infer information about the compound states.

The specific resonant states $H_2(v,n,l,\Lambda$ involved have l=0 or 2 and Λ= 0, since the coupling is through the $^1\Sigma_g^+$ (predominantly

$2p\sigma^2$) state. These resonances correspond to $s\sigma$ and $d\sigma$ Rydberg series. Our analysis indicates that both series must be included. We do this by generalizing the theoretical approach used in ref. 4. The matrix element leading to direct recombination was written

$$\xi_v = \left(\frac{2M\pi}{k}\right)^{1/2} \int \chi_v(R) \cdot V_{el}(R) \cdot F(R) \cdot dR \quad \ldots (5)$$

where M is the reduced mass of H_2, $\chi_v(R)$ is the wave function of the v^{th} vibrational level of $H2^+$, $V_{el}(R)$ is the matrix element for electron capture (or autoionization), F(R) is the regular solution to the Schrödinger equation for the final state potential $V^+(R)$ at energy $E=\hbar^2k^2/2M$. This integral is essentially a Franck-Condon factor between initial and final states, mediated by the electronic coupling V_{el}.

The indirect mechanism is introduced using the matrix element

$$g_{v'v} = \int \chi_{v'}(R') \cdot V_{el}(R') \cdot G(R',R) \cdot V_{el}(R) \cdot \chi_v(R) \cdot dR'dR \quad \ldots (6)$$

where G(R',R), defined explicitly in ref.3, is a Green function for the Schrödinger equation with potential $V^+(R)$. The matrix element $g_{v'v}$ is related to the amplitude for vibrational excitation of H_2^+ from state v to v' by an incident electron. The two vibrational states are not directly coupled to each other, but each is coupled electronically to the resonant state H_2^{**}.

The coupling of the resonant state H_2^{**} to both $s\sigma$ and $d\sigma$ electrons is treated in an approximate way by assuming that the ratio of the couplings to the two partial waves is a constant,

independent of R. Then we can extract the necessary matrix elements from available literature values of the total widths by replacing the coupling matrix element $V_{el}(R)$ by $\alpha_l V_{el}(R)$ (l=0 for coupling to sσ and l=2 for dσ). Then $\alpha_0^2 + \alpha_2^2 = 1$, and we can write

$$\xi_{vl} = \alpha_l \xi_v \quad \ldots (7)$$

$$g_{vl,v'l'} = \alpha_l \alpha_{l'} g_{vv'} \quad \ldots (8)$$

We use a theoretical approach based on Multichannel Quantum Defect Theory (MQDT), which was formulated by Giusti[9] and modified by Hickman[4] to include higher order effects. MQDT is formulated in terms of a reactance matrix K coupling to different arrangement channels. These channels have the asymptotic form H + H* (labelled d) and $H_2^+(v)$ + e(lσ) (v=0,1,... and l=0,2). The rotational state of the H_2^+ ion has not been included. The specific states we include in the present calculation are therefore (d), (sσ, v=0), (dσ, v=0), (sσ, v=1), and (dσ, v=1), and the K matrix is

K =

0	$\alpha_0\xi_0$	$\alpha_2\xi_1$	$\alpha_0\xi_1$	$\alpha_2\xi_1$
$\alpha_0\xi_0$	$\tan\pi\mu_s$	0	$\Pi\alpha_0^2 R_e(g_{01})$	$\Pi\alpha_0\alpha_2 R_e(g_{01})$
$\alpha_2\sigma_0$	0	$\tan\pi\mu_s$	$\Pi\alpha_2\alpha_0 R_e(g_{01})$	$\Pi\alpha_2^2 R_e(g_{01})$
$\alpha_0\xi_1$	$\Pi\alpha_0^2 R_e(g_{10})$	$\Pi\alpha_0\alpha_2 R_e(g_{10})$	$\tan\pi\mu_s$	0
$\alpha_2\xi_1$	$\alpha_2\alpha_0 R_e(g_{10})$	$\Pi\alpha_2^2 R_e(g_{10})$	0	$\tan\pi\mu_d$

...(9)

The diagonal blocks contain the phase shifts μ_s and μ_d, which are related to the energies of the autoionizing states $H_2(v=1,n,l,\Lambda)$. This matrix is "contracted " into an S matrix for DR using the general MQDT prescription[10]. S has a smaller dimension that the K matrix for the energies of interest, for which the v=1 channels are closed.

The K matrix given in equation (6) provides flexibility to model the data. The quantum defects μ_s and μ_d determine the positions of the two series of resonances, given by

$$\varepsilon - \Delta E - \frac{1}{2(n-\mu_l)^2} \quad \ldots(8)$$

where ΔE is the vibrational excitation energy from v=0 to v=1, l=0 and 2 and n takes on integral values. By inverting equation (7), we can estimate the effective values $n^*=n-\mu_l$ of the resonances observed experimentally. The three resonances shown in figure 1 correspond to n^*=7.3, 7.7 and 8.1. Taking into account the uncertainty in the energy scale of the data, we can approximately model the data by assuming that the middle resonance (n^* =7.7) belongs to one series and the other two (n^* =7.3, 8.1) to the other series.

Calculations have been performed to investigate these alternatives. The values of the parameters in equation 6 were estimated from the literature and then systematically varied to achieve a good fit. Hazi et al.[11] determined α^0 = 0.86 and α_2 = 0.54. The quantum defects can be taken from ref.[11] or directly estimated

to be μ_s=-0.108 and μ_d =0.053 from the H_2 GK or HH[bar] potential curves. These values can only be considered guidelines; adjusting them is not unreasonable. The quantum defects are expected to vary weakly with energy, and their value the $^1\Sigma_g^+$ continuum state will certainly differ from their value in the region of the GK and HH[bar] states.

Determining which resonances are sσ and which are dσ is not possible on the basis of the quality of the fit to the data. Both alternatives lead to a plausible fit for the appropriate values of the quantum defects μ_s and μ_d and the branching ratios α_0 and α^2.)n physical grounds, one generally expects the d quantum defect to be smaller than the s. Also Hazi et al.[11] considered a fit to the EF and GK potential curves of H_2 and concluded that the width of the sσ partial wave is smaller than the dσ. Based on these considerations, we favour the assignment that the 45 meV resonance is an sσ state and the other two are dσ states. For this assignment, we used μ_s=0.4 and μ_d=-0.1.

Figure 1b shows the comparison calculated DR cross section. The model based on two rydberg series provides an excellent interpretation of the data. Furthermore, the data cannot be fit by assuming a single rydberg series.

ACKNOWLEDGEMENTS.

Financial support of the U.S. Air Force Office of Scientific Research, contracts F49620-88-K-0005 and AFOSR-90-0042 and the Canadian Natural Sciences and Engineering Research Council is gratefully acknowledged.

REFERENCES.

1. A. Giusti-Suzor, J.N. Bardsley and C. Derkits Phys. Rev. A 28, 682, 1983.
2. K. Nakashima, H. Takagi and H. Nakamura J. Chem. Phys. 86, 726, 1987.
3. A.P. Hickman J. Phys. B. 20, 2991, 1987.
4. A.P. Hickman in *Dissociative Recombination: Theory, Experiment and Applications* (eds. J.B.A. Mitchell and S.L. Guberman) World Scientific, Singapore, 1989, p.
5. H. Hus, F.B. Yousif, C. Noren, A. Sen and J.B.A. Mitchell Phys. Rev. Lett. 60, 1006, 1988.
6. D. Auerbach, R. Cacak, R. Caudano, T.D. Gaily, C.J. Keyser, J.Wm. McGowan, J.B.A. Mitchell and S.F.J. Wilk J. Phys. B. 10. 3797, 1977.
7. F.B. Yousif and J.B.A. Mitchell Phys. Rev. A 40, 4318, 1989.
8. F.B. Yousif, P. Van der Donk, M. Orakzai and J.B.A. Mitchell (Accepted for publication, Phys. Rev. 1991).
9. A. Giusti J. Phys. B. 13, 3867, 1980.
10. M.J. Seaton Rep. Prog. Phys. 46, 167, 1983.
11. A.U. Hazi, C. Derkits and J.N. Bardsley Phys. Rev. A 27, 1751, 1983.

FIGURE CAPTIONS.

1. Experimental (a) and theoretical (b) cross sections for the dissociative recombination of $H_2^+(v=0)$.

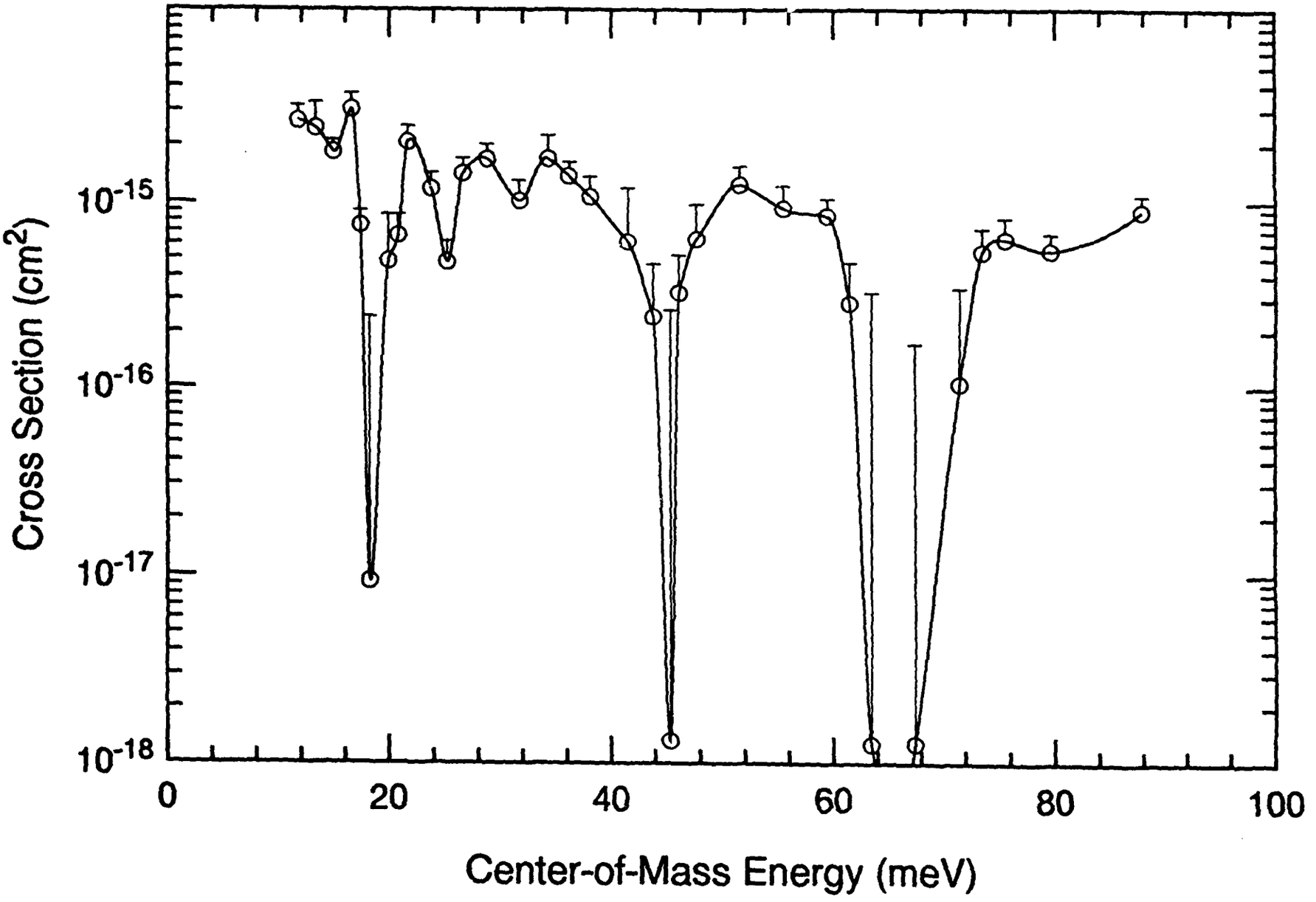
Cross Section (cm^2)
10^{-15}
10^{-16}
10^{-17}
10^{-18}
0
20
40
60
80
100
Center-of-Mass Energy (meV)

Fig 1a.

Cross Section (cm²)
10⁻¹⁵
10⁻¹⁶
10⁻¹⁷
10⁻¹⁸
0
20
40
60
80
100
Center-of-Mass Energy (meV)

APPENDIX C

Two-Photon Excitation and Excited-State Absorption Cross Sections for H_2 E,F $^1\Sigma_g$ (v = 6): Measurement and Calculations

Phys. Rev. A, **39**, 3932 (1989).

Two-photon excitation and excited-state absorption cross sections for H_2 $E,F\ ^1\Sigma_g$ ($v=6$): Measurement and calculations

Jesse D. Buck,* Daniel C. Robie, A. P. Hickman,
Douglas J. Bamford,† and William K. Bischel
Molecular Physics Laboratory, SRI International, Menlo Park, California 94025
(Received 21 November 1988)

The absolute two-photon excitation cross section for the H_2 $E,F\ ^1\Sigma_g$ ($v'=6$)←$X\ ^1\Sigma_g$ ($v''=0$) $Q(1)$ transition at 193 nm has been measured by observing the $E,F\ ^1\Sigma_g^+$ ($v'=6$)→$B\ ^1\Sigma_u^+$ ($v''=0$) fluorescence at ~750 nm. The measured integrated two-photon excitation cross section, $(2.0\pm0.9)\times10^{-36}$ cm^4, is in good agreement with the theoretical value of 2.8×10^{-36} cm^4, which is obtained from previously published calculations [Huo and Jaffe, Chem. Phys. Lett. **101**, 463 (1983)]. The absolute cross section for photoabsorption by the E,F state at 355 and 193 nm was also measured by monitoring the depletion of the 750-nm fluorescence caused by a second laser. The measured cross sections for photoabsorption by the E,F ($v=6$) state are $(9.7\pm2.4)\times10^{-18}$ cm^2 at 355 nm and $(6.4\pm1.3)\times10^{-18}$ cm^2 at 193 nm. Comparison with theoretical estimates [Cohn, J. Chem. Phys. **57**, 2456 (1972)] of the direct photoionization cross section of this state (8.5×10^{-18} cm^2 at 355 nm and 3.2×10^{-18} cm^2 at 193 nm) suggests that other processes may contribute to the photoabsorption. Photoexcitation of the dissociating $^1\Sigma_u$ autoionizing state is found to be important. Cross sections for this additional channel, which may lead to dissociation (H^*+H or H^++H^-) or autoionization ($H_2^++e^-$), are calculated to be 3.6×10^{-18} cm^2 at 355 nm and 7.6×10^{-18} cm^2 at 193 nm. The calculated branching ratio strongly favors dissociation at 355 nm and autoionization at 193 nm.

I. INTRODUCTION

Molecular hydrogen occupies a position of unique importance in chemical physics because it is the simplest neutral molecule. As such, it supports a rich interplay between experiment and theory, due largely to the relative tractability of large-scale calculations on this four-particle molecular system. Hydrogen is also of considerable practical importance in areas such as combustion,[1] extraterrestrial atmospheres,[2] vacuum-uv laser sources,[3] laser-based analytical probes,[4] and numerous others. In view of this, we have undertaken a series of experiments to compare absolute cross-section measurements to calculations for two-photon resonant multiphoton transitions in H_2. *Ab initio* calculations of the two-photon transition moment[5] for H_2 E,F ($v'=6$)←X ($v''=0$) have been available in the literature for several years and can be used to compare to quantitative measurements. In addition, this research was motivated by the need to develop detection methods for vibrationally excited ground electronic state hydrogen for application to the diagnostics of H^- plasma sources.[6,7] We expect the results reported here for the $v''=0$ ground vibrational state will serve as a benchmark for determining the sensitivity for H_2 ($v''>0$) detection using two-photon excitation.

In this paper we report absolute measurements of both the two-photon cross section for excitation in the transition from the X ($v''=0$) to the E,F ($v'=6$) state of H_2, and cross sections for absorption by the excited state. The wavelength dependence of the absorption cross section σ_{abs} is of particular interest since several mechanisms in addition to direct photoionization can contrib-

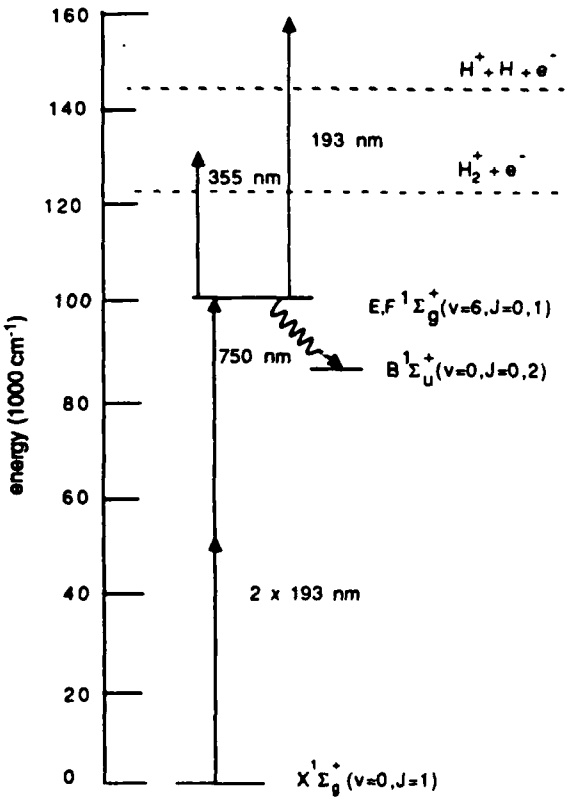

FIG. 1. Selected energy levels for H_2. The threshold for ionization is 124 417 cm^{-1}; for dissociative ionization the threshold is 145 796 cm^{-1} (Ref. 35).

 ©1989 The American Physical Society

ute.[8-10] As a first experiment in this direction, we have measured the total absorption cross section at two wavelengths (193 and 355 nm). These results are compared to theoretical calculations of the cross sections for direct photoionization and for other channels contributing to absorption.

The H_2 energy levels relevant to the work reported here are given in Fig. 1. The $J'=1$ rotational level of the E,F ($v'=6$) level was excited using two-photon absorption at 193 nm. The excited level either fluoresced in the near-ir region (750–840 nm) or absorbed a third photon (either at 193 or 355 nm). The experiment consisted of quantitatively measuring either the fluorescence produced in the two-photon process or the depletion of fluorescence caused by absorption of a third photon, and measuring the laser intensity in the observation volume. Using techniques previously developed in this laboratory,[11,12] two-photon excitation cross sections were derived from the data. Using the fluorescence depletion technique,[13] excited-state absorption cross sections were also obtained.

The paper is organized as follows. Section II describes the experiment, including a detailed description of two methods used to produce tunable radiation at 193 nm. Section III describes the theoretical calculations. Two-photon excitation cross sections for the $E,F \leftarrow X$ transition, and for the direct photoionization of the E,F state, are derived from work already in the literature. Photoexcitation to a dissociating, autoionizing $^1\Sigma_u$ state from the E,F state is treated. Section IV compares and discusses the experimental and theoretical results, and Sec. V presents concluding remarks.

II. EXPERIMENT

A. Apparatus and procedure

The apparatus, methods of data acquisition, and analysis used here for the two-photon absorption cross-section measurements have been previously described in detail for atomic oxygen.[12] The apparatus is diagramed in Fig. 2. Tunable laser radiation at 193 nm was generated using two different methods. This allowed the comparison of cross-section measurements using coherent sources that had significantly different photon statistics, bandwidths, and spatial temporal characteristics. In the first method a frequency-doubled Nd:yttrium-aluminum-garnet (YAG)-pumped dye laser (Quanta-Ray DCR2+PDL) was Raman shifted in H_2 to generate over 100 μJ in the fourth anti-Stokes (AS) order at 193 nm. Because the first Stokes order of the Raman-shifted dye laser fundamental has nearly the same wavelength as the fluorescence being observed ($\sim$750 nm), it was necessary to prevent any stray light from the Raman cell from reaching the photomultiplier. This was achieved by focusing the 193-nm beam (fourth AS order) with a 20-cm lens through a small pinhole in an opaque enclosure which surrounded the Raman cell output and the Pellin-Broca prism used to separate the various beams. A second 20-cm lens outside the enclosure then reconverged the 193-nm beam to a focus $\sim$100 cm away in the experimental cell. Pulse energies of up to 50 μJ were focused into the experimental cell. The pulse length was 4 ns, and the fourth AS bandwidth was $\sim 1\ cm^{-1}$.

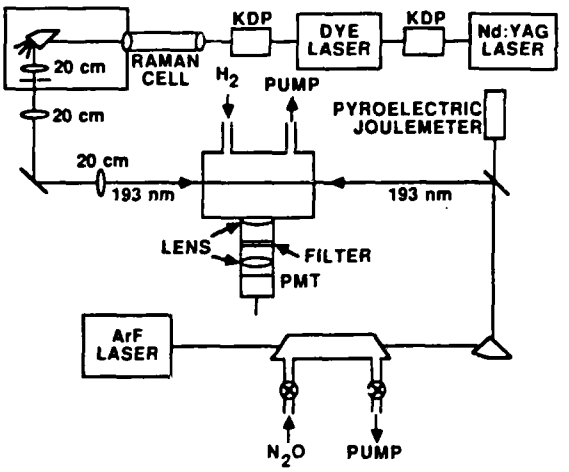

FIG. 2. Apparatus for measurement of the excited-state absorption cross section at 193 nm in H_2. The E,F ($v'=6$)$\leftarrow X$ ($v''=0$) $Q(1)$ two-photon absorption cross section was measured in a similar apparatus, with the ArF laser beam blocked, and the last 20-cm lens removed. To measure the excited-state single-photon absorption cross section at 355 nm, the potassium dihydrogen phosphate (KDP) crystal was used to generate both 532-nm radiation (to pump the dye laser) and 355-nm radiation. The latter follows a path like that of the ArF laser beam.

The second laser source of tunable 193-nm radiation was a commercial two-cavity excimer laser with a grating-tuned oscillator-amplifier system (Lambda Physik EMG150). The beam from the oscillator was amplified with a single pass through the amplifier cavity to an energy of 1–2 mJ/pulse, with a pulse width of 12 ns and a bandwidth of 0.3 cm^{-1}. Much higher pulse energies could be obtained by using unstable resonator optics on the amplifier and injection locking it with the oscillator output, and this configuration was used for the two-laser

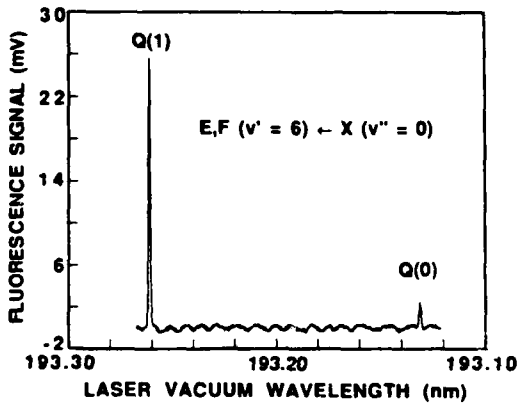

FIG. 3. Fluorescence signal as a function of ArF excimer wavelength. These scans were used to calibrate the wavelength scale.

depletion studies described below. The single-pass configuration eliminated effects from unlocked broadband output on the two-photon absorption measurements, which are sensitive to the laser bandwidth.

The laser energy at 193 nm was varied by admitting 5 mol% N_2O in Ar into a 50-cm-long cell equipped with Brewster windows which the laser beam passed through prior to entering the fluorescence cell. (5 mol% Cl_2 in Ar was used to attenuate the 355-nm beam.) A few hundred Torr of the N_2O mixture was sufficient to extinguish the laser beam, and the attenuation could be continuously varied by pumping out the mixture. The laser energy was measured at the cell exit, with a correction made for the window loss in the single laser experiments.

The wavelength of the excimer laser was calibrated by observing the fluorescence excitation spectrum with both the $E,F\ (v'=6)\leftarrow X\ (v''=0)\ Q(1)$ and $Q(0)$ lines shown in Fig. 1. Typical data for this calibration scan are given in Fig. 3. Additional wavelength calibration experiments were performed using 1+1 two-photon ionization in NO.[14]

Radiation at 355 nm was obtained from frequency tripling for the Nd:YAG laser. This produced 30 mJ in a pulse 5 ns long. The beam had a roughly top-hat spatial profile, but exhibited considerable spatial mode structure.

The experimental cell was equipped with parallel electrodes running the length of the cell for ion detection, and a fast aspheric lens to collect the near-ir fluorescence from the excited molecules due to the transition $E,F\ (v'=6,\ J'=1)\rightarrow B\ (v''=0,\ J''=0,2)$. H_2 flowed through the cell at pressures of 0.2–0.3 Torr. We detected a multiphoton ionization signal. However, small quantities of easily ionized impurities in the gas system (presumably vacuum pump oil) interfered with the resonant ionization signal giving a relatively large background signal.

Fluorescence collimated by the aspheric lens and transmitted by a 750-nm bandpass filter was refocused by a second lens (nominal f number ~ 0.7) onto an RCA C31034A photomultiplier tube. The fluorescence signal was integrated with an Ortec 113 preamplifier for all the two-photon absorption measurements. The fluorescence signal was recorded while scanning the laser through the $E,F\ (v'=6)\leftarrow X\ (v''=0)\ Q(1)$ transition at various pulse energies.

The excited-state decay rate was measured by fitting a single exponential to the time-resolved fluorescence signal (acquired on a Tektronix 2430 digital oscilloscope in averaging mode without the Ortec 113 preamplifier). This was used for the total decay rate $\sum_{v''} A_{6v''}+Q$ [see Eq. (1)]. The collisional quenching rate by H_2 was measured to be $1.95\times 10^{-9}\ cm^3 s^{-1}$, close to the value previously measured by Kligler and Rhodes.[15]

The spatial beam profile was measured with a pyroelectric detector array which has 100-μm resolution (Spiricon LP-256-11-SP). Scanning a pinhole across the beam gave the same result as the more convenient pyroelectric array. The temporal pulse profiles were measured by reflecting a fraction of the beam onto a fast photodiode (100-ps rise time, Instrument Technology Limited) and observing the output on a 1-GHz oscilloscope (Tektronix 7104). Several pulses were photographed for each run, then digitized by hand. They were subsequently integrated (or squared and integrated) and averaged.

Excited-state absorption cross sections were measured in a pump-probe arrangement in which the fourth AS beam pumped some molecules into the E,F state and either the excimer beam or the tripled Nd:YAG beam depleted a fraction of the excited population after a several nanosecond time delay.[13] The two-laser fluorescence depletion experiments had the advantage that the absolute number density of excited molecules did not need to be known, since the fractional depletion of the lower level in the absorption of the third photon was directly measured. A short focal length ($f=20$ cm) lens was used in the pump laser beam, generating a high density of excited molecules in a small volume which was viewed by the photomultiplier. A significant fraction of the excited molecules absorbed a third pump laser photon. Because the absorption cross-section measurement did not depend on the excited-state density, this did not affect the result. A second laser pulse spatially overlapped the pump laser focus, and was delayed in time by ~ 10 ns. [The excimer laser was tuned to a wavelength near the $E,F\ (v'=6)\leftarrow X\ (v''=0)\ Q(1)$ two-photon transition. No fluorescence could be detected with the pump beam blocked. The wavelength of the excimer laser beam was then within 0.05 nm of 193.26 nm.] In order to be certain that all the excited population was subjected to the same ionizing laser fluence, the time-delayed probe beam was not focused. High pulse energies were then required to produce measurable depletion. By placing a gate on the fluorescence signal ~ 20 ns after the delayed laser pulse had ended, the fluorescence was observed to be depleted by the delayed laser. A second gate was placed at the peak of the fluorescence signal prior to the delayed probe laser pulse; this provided a signal proportional to the density of two-photon excited molecules for shot-to-shot normalization. This signal was unaffected by the probe laser. The ratio (delayed fluorescence signal)/(peak fluorescence signal) at each delayed probe laser power was divided by the value of the ratio with the delayed probe laser absent.

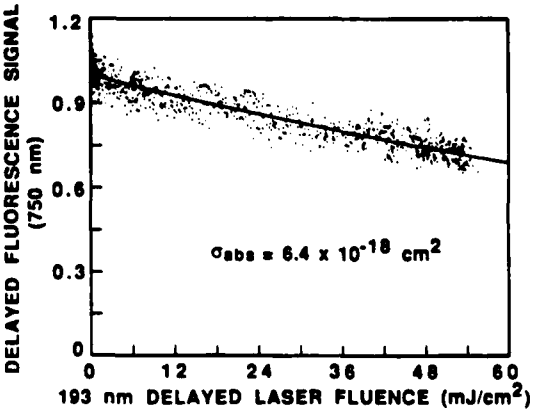

FIG. 4. Fluorescence depletion measurement at 193 nm. The solid curve shows a least-squares fit to an exponential decay.

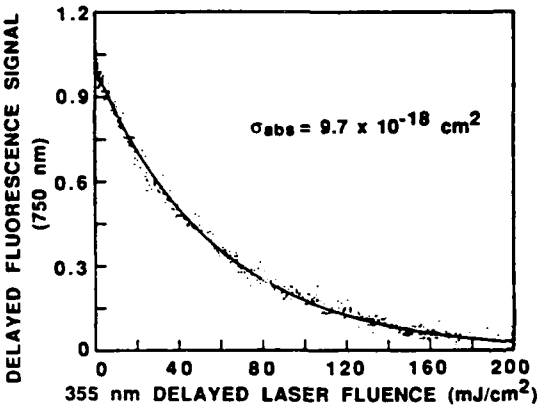

FIG. 5. Fluorescence depletion measurement at 355 nm. The solid curve shows a least-squares fit to an exponential decay.

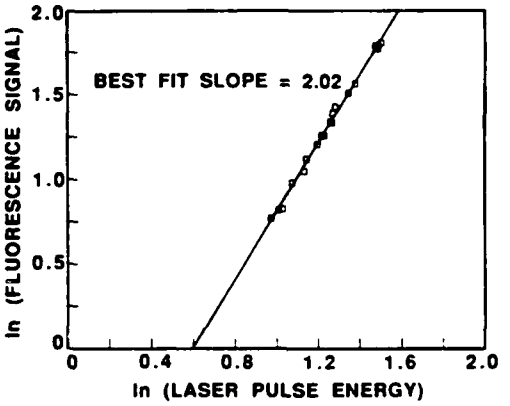

FIG. 6. Intensity dependence of the fluorescence signal for data given in run 2 of Table II.

Because the decay rate of the excited population by fluorescence or collisional quenching was unaffected by the probe laser, this normalization eliminated effects of those processes on the results.

The pulse energy of the delayed laser was varied from zero to full power, and a plot of delayed fluorescence versus delayed laser was recorded. Typical depletion plots are shown in Fig. 4 for 193-nm absorption, and in Fig. 5 for 355-nm absorption. The plots show an exponential decay. The decay constant of the delayed fluorescence as a function of the fluence of the delayed laser (in photons/cm^2) equals the cross section in cm^2 for absorption of a photon from the delayed laser beam. The fluence of the delayed laser was determined by removing the fluorescence cell and placing a 100-μm-diam pinhole at the waist of the focused pump beam, and then measuring the energy of the delayed laser beam which went through the pinhole. Since the delayed laser beam was not focused, the 100-μm pinhole had adequate resolution to measure the laser fluence.

B. Measurements

Plots of ln(peak signal) versus ln(laser energy) for one-laser data were prepared to determine the effective order of nonlinearity, k, where k is the apparent number of photons involved in a given process:

$$k \equiv \partial \ln(\text{signal})/\partial \ln(\text{energy}) .$$

The plot of the fluorescence data had a slope of 2, which is expected for a two-photon process in the absence of saturation (Fig. 6).

An effective two-photon excitation cross section [$\hat{\sigma}^{(2)}(\omega)$] was calculated using the formula[12]

$$\hat{\sigma}^{(2)}(\omega) = \frac{S(\omega)}{E^2} \frac{\sum_{v''} A_{6v''} - Q}{A_{60}} \frac{4\pi^2 r_0^4 (\hbar\omega)^2}{N_0 D \int_{-\infty}^{\infty} F^2(t)dt} , \quad (1)$$

where $\hat{\sigma}^{(2)}(\omega)$ (also known as the two-photon rate coefficient[10]) is the effective two-photon cross section in units of cm^4 s; $S(\omega)/E^2$ is the fluorescence signal in volts divided by the square of the pulse energy: r_0 is the $1/e^2$ radius of the laser beam intensity (fit to a Gaussian profile; averaged over the fluorescence viewing region); $\hbar\omega$ is the energy of a single laser photon; N_0 is the density of molecules in the initial state of the two-photon transition; and D is the calibration constant for the fluorescence detection system.[11] $F(t)$ is the measured temporal laser profile, defined as in Ref. 12:

$$I(r,z,t) = U(r,z)F(t) ,$$

$$\int_{-\infty}^{\infty} F(t)dt = 1 ,$$

where $I(r,z,t)$ is the beam intensity and $U(r,z)$ is the fluence. The fluorescence quantum yield is

$$\frac{A_{60}}{\sum_{v''} A_{6v''} + Q} ,$$

where A_{60} is the Einstein A coefficient for the detected fluorescence in the E,F ($v'=6$)$\rightarrow B$ ($v''=0$) band, Q is the rate of collisional quenching, and $\sum_{v''} A_{6v''}$ is the sum of Einstein A coefficients for fluorescence in all bands ($\sum_{v''} A_{6v''} = 1.01 \times 10^7$ sec^{-1}). The quantity A_{60} was obtained from a theoretical calculation[17] of the band transition moment (Table I).

The fluorescence detection system was calibrated with spontaneous Raman scattering of a visible laser beam by a static fill of ~ 1 atm H_2 in the experimental cell to produce a known photon flux at the wavelength of interest.[11] The most important fluorescence wavelengths and calculated branching ratios are listed in Table I. The ratio of the strengths of two rotational lines originating at the same level within a band equals the ratio of the Hönl-London factors for the two lines. We collected photons from two lines only, the $P(2)$ and $R(0)$ lines originating at the E,F ($v'=6$, $J'=1$) level and terminating in the B ($v''=0$, $J''=2,0$) levels, at wavelengths 752.7 and 746.2 nm, respectively. The ratio of the calculated Hönl-London factors for these two lines in a Σ-Σ transition is 2.[18] The calibration constant D [see Ref. 11, Eq. (1)] was measured in each run at an intermediate wavelength,

TABLE I. Fluorescence wavelengths, Einstein A coefficients, and branching ratios for H_2 E,F ($v'=6, J'=1$).

Lower level	$\lambda[R(0)]$ (nm)	$\lambda[P(2)]$ (nm)	$A_{6v''}$ (s^{-1})[a]	Branching ratio
B ($v''=0$)	746.2	752.7	3.6×10^{6}	0.36
B ($v''=1$)	827.6	835.2	4.9×10^{6}	0.49
B ($v''=2$)	925.7	934.9	2.6×10^{5}	0.03
B ($v''=3$)	1047	1058	2.4×10^{4}	0.002
B ($v''=4$)	1070	1082	7.7×10^{4}	0.008
B ($v''=5$)	1396	1415	4.6×10^{5}	0.05
All others	> 1400	> 1400	7.3×10^{5}	0.07
Total			1.01×10^{7}	1.00

[a]Reference 17.

748.8 nm; then D was measured once at several wavelengths. Combining the ratio of line strengths and the wavelength dependence of the apparatus responsivity, it was found that $D_{\text{eff}}=0.89D_{748.8}$, where $D_{\text{eff}}=\frac{2}{3}D_{752.7}+\frac{1}{3}D_{746.2}$.

The two-photon excitation cross section was measured several times, varying the beam diameter at the focus. The measured parameters for Eq. (1) are listed in Table II for each run. In run 6, a cylindrical beam profile was obtained by sending the collimated laser beam through an aperture just before the fluorescence cell, in which case the radius of the cylindrical profile could be directly substituted for r_0 in Eq. (1). [See the derivation of Eq. (1) in Ref. 12.] Large variations between runs in the photomultiplier calibration constant D were caused primarily by the use of different photomultiplier tube bias voltages to obtain optimum signals for data acquisition.

The two-laser absorption cross-section measurement at 193 nm was performed several times in a two-day period. Successive runs agreed to within about 2%, while all the data agreed to within 10%. We attribute the 10% spread to random error in calibrating the fluence of the delayed laser. An uncertainty of 20% for the fluorescence depletion measurements includes possible systematic errors (mainly pyroelectric detector calibration). We found an excited-state absorption cross section of $(6.4\pm1.3)\times10^{-18}$ cm^2 at 193 nm.

The two-laser absorption cross-section measurement at 355 nm showed a greater run-to-run variation ($\sim$15%) than the 193-nm measurement. This was probably due to the pronounced spatial mode structure of the Nd:YAG laser output which makes it more difficult to uniformly irradiate the excited molecule region with the 355-nm laser output. We obtained a value of $(9.7\pm2.4)\times10^{-18}$ cm^2 for the excited-state absorption cross section at 355 nm.

C. Role of photon statistics

The line-shape-independent, two-photon excitation cross section $\sigma_0^{(2)}$, which is a fundamental property of the molecule, is related to the effective cross section defined by Eq. (1) as follows:[16]

$$\hat{\sigma}^{(2)}(\omega)=\sigma_0^{(2)}g(\omega)G^{(2)}, \tag{2}$$

where $g(\omega)$ is the area-normalized line-shape function, and $G^{(2)}$ is the second-order intensity autocorrelation function of the laser,

$$G^{(2)}=\frac{\langle f^2(t)\rangle}{\langle f(t)\rangle^2}, \tag{3}$$

TABLE II. Experimental parameter values for $\sigma_0^{(2)}$ measurement.

Parameter (units)	Run 1	Run 2	Run 3	Run 4	Run 5	Run 6
S/E^2 (10^{7} V/J^2)	68.4	7.04	0.395	0.217	0.372	2.42
ω_0^2 (10^{-3} cm^2)	1.81	0.848	2.03	1.57	1.73	3.39
$A_{6v''}\Big/\left\lvert\sum A_{6v''}+Q\right\rvert$	0.114	0.109	0.115	0.114	0.135	0.110
$N_{J''}$ (10^{14} cm^{-3})[a]	7.15	7.57	7.04	7.08	5.41	7.41
D (10^{-7} V cm sr)	168	15.2	4.94	1.25	2.71	80.5
$\int F^2(t)dt$ (10^{5} s^{-1})	3.01	3.00	0.755	0.800	0.772	0.871
$\hat{\sigma}^{(2)}(0)$ (10^{-47} cm^4 s)	1.25	0.660	1.11	1.74	1.76	0.599
$G^{(2)}\sigma_0^{(2)}$ (10^{-46} cm^4)	4.3	2.0	3.6	3.9	5.8	1.3
Laser type	dye	dye	ArF	ArF	ArF	ArF
$G^{(2)}$ (assumed)	1.4	1.4	2.0	2.0	2.0	2.0
$\sigma_0^{(2)}$ (10^{-46} cm^4)	3.1	1.4	1.8	1.9	2.9	0.65

[a]Density in the $J''=1$ rotational level of H_2. The quenching rate Q was calculated using the total density with $N_J=1.52N_{J''}$.

where $f(t)$ is the true area-normalized temporal profile of the laser pulse measured with an infinitely fast detector. The angular brackets denote time averaging over a scale long compared to the coherence time of the laser, but short compared to the laser pulse length:[19]

$$\langle f(t)\rangle = \frac{1}{\Delta t}\int_t^{t+\Delta t} f(t')dt' ,$$

$$\langle f^2(t)\rangle = \frac{1}{\Delta t}\int_t^{t+\Delta t} f^2(t')dt' ,$$

The response time of the photodiode used is in the proper range; thus $\langle f(t)\rangle$ equals the observed $F(t)$. The bandwidth of the excimer laser was considerably smaller than that of the Raman-shifted laser, but the observed linewidths [and hence $g(\omega)$] were mainly determined by the sizable Doppler width for H_2 (0.90 cm^{-1}). The quantity $G^{(2)}\sigma_0^{(2)}$ is obtained in absolute units by integrating $\hat{\sigma}^{(2)}(\omega)$ over the excitation profile, as discussed previously.[12,19]

The factor $G^{(2)}$ characterizes the photon statistics of the pump beam, which must be taken into account when a multiphoton cross section is compared with theory. Our detection apparatus is too slow to capture the intensity variations (on a time scale of ps) of the multimode laser output. The factor $G^{(2)}$ may be thought of as expressing the amount of "spikiness" in the beam intensity that cannot be resolved by the photodiode. This point has been more fully discussed for two-photon excitation in atomic oxygen in Ref. 19.

We used $G^{(2)}=1.4$ for the Raman-shifted dyer laser,[19] and 2.0 for the excimer laser (i.e., the excimer laser was assumed to be a chaotic source). These choices are reasonably consistent with the present results: the average value of $G^{(2)}\sigma_0^{(2)}$ for the Raman-shifted laser measurements (runs 1 and 2) is 3.1×10^{-36} cm^4, while for the excimer laser (runs 3–6) it is 3.7×10^{-36} cm^4. The ratio $3.7/3.1=1.2$, which is fairly close to $2.0/1.4=1.4$. The scatter is too large to consider the difference significant. The average of $G^{(2)}\sigma_0^{(2)}$ from runs 1 and 2 divided by 1.4, and runs 3–6 divided by 2.0, is $\sigma_0^{(2)}=(2.0\pm0.9)\times10^{-36}$ cm^4.

III. THEORY

A. Comparison of $\sigma_0^{(2)}$ with previous calculations

The theoretical value of the integrated two-photon excitation cross section $\sigma_0^{(2)}$ (in cm^4) was obtained from the calculated two-photon transition moment[5] using the formula[16]

$$\sigma_0^{(2)} = (2\pi)^3\left[\frac{e^2}{\hbar c}\right]^2(\hbar\omega)^2P^2 , \tag{4}$$

where

$$P = \sum_k \frac{\langle f|r|k\rangle\langle k|r|g\rangle}{E_g - E_k + \hbar\omega} \tag{5}$$

is the two-photon transition moment for excitation by one laser beam; here g, k, and f refer to the ground, virtual intermediate, and final states of the transition, respectively; r is the dot product of the dipole moment operator with the laser beam polarization; and ω is the angular frequency of the laser. It is necessary to be careful in applying the results of Ref. 5. When the value of P^2 from Ref. 5 of 19.7 a.u. is entered into Eq. (4), the result is much larger than our measured value. However, the authors of Ref. 5 originally calculated a transition moment M for absorption of one photon from each of two statistically independent laser beams:

$$M = \sum_k \left[\frac{\langle f|r|k\rangle\langle k|r'|g\rangle}{E_g - E_k - \hbar\omega'} + \frac{\langle f|r'|k\rangle\langle k|r|g\rangle}{E_g - E_k - \hbar\omega}\right] \tag{6}$$

(where the prime denotes the second laser beam). They then set $r'=r$ and $\omega'=\omega$. To avoid double counting, the resulting transition moment must be divided by 2 in order to use it in Eq. (4).[20] Since the transition moment is squared in Eq. (4), the cross section is reduced by a factor of 4. The correctly calculated cross section, $\sigma_0^{(2)}=2.8\times10^{-36}$ cm^4, is in reasonable agreement with our measurements.

B. Direct photoionization of the E,F state

Several processes fall under the general category of photoabsorption by the E,F state. In this section we con-

TABLE III. Calculated cross sections for H_2 (E,F, $v=6$)$+\hbar\omega$.

Process	σ_{355} (10^{-18} cm^2)	σ_{193} (10^{-18} cm^2)
Direct photoionization		
to $v_+=1$	0.37	0.10
to $v_+=2$	8.11	2.03
to $v_+=13$		0.52
Sum over all open channels	8.50	3.15
Photoexcitation of $^1\Sigma_u$		
autoionization	0	7.13
dissociation (neutral+ionic)	3.55	0.52

sider direct (i.e., conventional) photoionization:

$$H_2^* + \hbar\omega \rightarrow H_2^+ + e^- ,$$

which is described by the matrix element between the bound E,F state and the electronic continuum plus the bound H_2^+ state. The cross section for this process may be estimated from calculations in the literature. The work of Cohn[21] provides tabulated cross sections as a function of the ejected electron energy. We interpolated these and multiplied by the appropriate Franck-Condon factors. The results are tabulated in Table III. This approximation neglects the R dependence and the electron energy dependence of the transition moment.

More sophisticated calculations of the direct photoionization process have been carried out by Rudolph *et al.*[22] These authors reported relative cross sections for the final vibrational states, but not the absolute numbers. An estimate of the direct photoionization cross section from the E,F ($v=6$) state to $H_2^+(v=2)$ obtained from their work[20] is 1.5×10^{-18} cm^2, which is about 25% smaller than the corresponding value in Table III.

C. Photoexcitation of the $^1\Sigma_u$ autoionizing state from the E,F state

Since the measured cross section for absorption by the E,F ($v'=6$) state is larger than the calculated upper limit for direct molecular photoionization, another mechanism may play a role. Recent work in this laboratory[9,23] and elsewhere[24,25] has demonstrated that excitation to a doubly excited, dissociating autoionizing state is an important channel in the photoionization of the $C\,^1\Pi_u$ state of H_2. We therefore performed quantitative calculations to assess the role of this channel in the present situation.

The mechanism considered is illustrated in Fig. 7. The initial level is $v'=6$ of the E,F state. Excitation to the lowest $^1\Sigma_u^+$ autoionizing state is shown in the figure. This state has been calculated by Guberman[26] and its electronic configuration is $2p\sigma_u 2s\sigma_g$. It is the most likely candidate final state, because it is reached by a strong one-electron transition $2p\sigma_u \leftarrow 1s\sigma_g$ from the inner-well E $1s\sigma_g 2s\sigma_g$ component of the E,F state, and by a one-electron $2s\sigma_g \leftarrow 2p\sigma_u$ transition from the outer-well F $(2p\sigma_u)^2$ component of the E,F state. Once excitation has occurred, the nuclei start to move outward on the $^1\Sigma_u^+$ potential curve. This electronic state is unstable with respect to autoionization, which occurs as the nuclei dissociate. This process, electron emission, leads to the final state $H_2^+ + e^-$. If autoionization does not occur, the nuclei continue to follow the $^1\Sigma_u^+$ curve and ultimately reach an asymptotic state of the form $H(1s)+H^*(nl)$, or $H^+ + H^-$.

The process just described, which leads to molecular autoionization ($H_2^+ + e$), neutral dissociation ($H^* + H$), or ionic dissociation ($H^+ + H^-$), was treated using the technique developed by Hickman.[9] The method treats the dynamics of nuclear motion by solving Schrödinger's equation with a nonlocal, complex potential. Cross sections for total dissociation and molecular autoionization were obtained, as well as the distribution of final vibra-

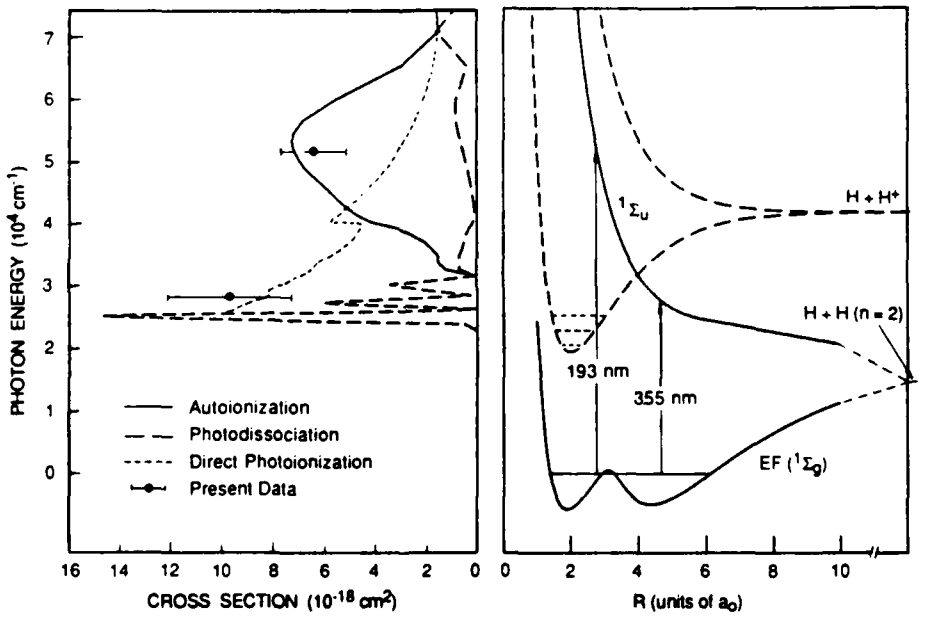

FIG. 7. (a) Calculations for direct photoionization (- - - - -), photodissociation through the $^1\Sigma_u$ state (— — —), and autoionization (——) through the $^1\Sigma_u$ state of H_2. (b) Potential curves of H_2 illustrating the mechanisms contributing to the calculations in the left panel. Notice that the energy (vertical) scales are the same in both panels, thereby clearly exhibiting the threshold behavior of all the cross sections.

tional states resulting from molecular autoionization. The necessary quantities for the calculation are the following: (1) the transition matrix element $\mu(R)$ connecting the initial E,F state with the $^1\Sigma_u^+$ state (R is the internuclear distance); (2) the potential curve for the $^1\Sigma_u^+$ state; and (3) the matrix element $V_{el}(R)$ connecting the $^1\Sigma_u^+$ state with the final-state continuum $H_2^+ + e^-$. The determination of these potentials and matrix elements is described in the following paragraph.

To calculate the transition moment $\mu(R)$ connecting the $^1\Sigma_u^+$ autoionizing state, one must take into account the R dependence of the E,F electronic wave function. This can be done in an approximate way by considering the two dominant electronic configurations, $1s\sigma_g 2s\sigma_g$ and $(2p\sigma_u)^2$. Each of these configurations corresponds to a diabatic potential curve; the avoided crossing of these curves leads to the well-known double-well nature of the E,F state. We can approximate the adiabatic electronic wave function as follows:

$$\Psi_{E,F}(R)=[\cos\Theta(R)](1s\sigma_g 2s\sigma_g)+[\sin\Theta(R)](2p\sigma_u)^2 . \tag{7}$$

Estimates of the mixing angle Θ may be obtained from the diabatic potential curves and coupling matrix elements determined by Hazi *et al.*[27] and Ross and Jungen.[28] One sets up a two-state Hamiltonian in the standard way: $H_{11}(R)$ is the energy of the $(2p\sigma_u)^2$ state; H_{22} is the energy of the $1s\sigma_g 2s\sigma_g$ state; and

$$H_{12}=v_0/[2-\delta_s(R)]^{3/2} ,$$

where $v_0=0.048$ a.u.,[27] and $\delta_s(R)$ is the quantum defect function. There is some uncertainty in the estimate of H_{12} because it was necessary to extrapolate v_0 beyond the range in which it was calculated by Hazi *et al.* The result is

$$\tan[2\Theta(R)]=2H_{12}/(H_{11}-H_{22}) .$$

We must now evaluate

$$\begin{aligned}\mu(R)&=\langle\Psi_{E,F}(R)|\mu_z|2p\sigma_u 2s\sigma_g\rangle\\&\cong[\cos\Theta(R)]\langle 1s\sigma_g|r\cos\theta|2p\sigma_u\rangle\\&\quad+[\sin\Theta(R)]\langle 2p\sigma_u|r\cos\theta|2s\sigma_g\rangle ,\end{aligned} \tag{8}$$

where r and θ are spherical electronic coordinates.

The first matrix element is for the $2p\sigma_u \leftarrow 1s\sigma_g$ core transition and has been evaluated by Bates.[29] Its value is $-R/2$ times a correction factor close to unity. The second matrix element is for the $2s\sigma_g \leftarrow 2p\sigma_u$ transition. It was evaluated numerically using single center wave functions determined from quantum defects. The results are well approximated by the polynomial $1.571-0.3807R+0.06268R^2$ (atomic units are used).

The $^1\Sigma_u^-$ potential curve has been calculated by Guberman.[26] The matrix element $V_{el}(R)$ is obtained from the resonance width $\Gamma(R)$ calculated by Tennyson and Noble,[16] using the relation

$$V_{el}(R)=[\Gamma(R)/2\pi]^{1/2} .$$

Tennyson and Noble calculated $\Gamma(R)$ for $R\le 2.8$ a.u.; for larger values we took the value at $R=2.8$ a.u.

With these potential curves, and the estimates of the matrix elements, we can treat photoexcitation of the $^1\Sigma_u$ autoionizing state. The calculated results are presented and compared with our experimental measurements in Sec. IV.

IV. DISCUSSION

The measurements of the two-photon excitation $(E,F\leftarrow X)$ cross section are in reasonable agreement with theory, as discussed in Sec. III A. The excitation process is straightforward and appears to need no further discussion.

Photoabsorption by the E,F ($v'=6$) state is more complex, because several alternate channels are available. We write several possibilities schematically as follows:

$$H_2^*(E,F)+\hbar\omega\rightarrow\begin{cases}H_2^+ + e^- , & (9a)\\ H_2^{**}\rightarrow H_2^+ + e^- , & (9b)\\ H_2^{**}\rightarrow H^* + H , & (9b')\\ H_2^{**}\rightarrow H^+ + H^- , & (9b'')\\ H + H^+ + e^- . & (9c)\end{cases}$$

Some of these channels have already been observed or discussed in the literature. Direct photoionization, (9a), is well known.[22] Channels (9b), (9b'), and (9b'') denote the excitation and subsequent decay of highly excited autoionizing states. Competition between autoionization and dissociation of these channels has been studied.[31] Channel (9c) is possible for sufficiently energetic photons, and has been inferred from observations of proton production.[10] A complicating feature of the experimental analysis of this channel is that other possible sources of H^+ ions are photoionization of the excited atomic hydrogen, H^*, produced by (9b'), or photodissociation of H_2^+.

Previous experiments have provided relative cross sections for several of the channels listed in (9). For example, the photoelectron energy distribution has been measured for (9) at 193 nm and provides evidence of a strongly non-Franck-Condon distribution of final vibrational states of H_2^+.[32,33] These results suggest that (9a) is not the only important channel. The present work provides complementary information, because absolute cross sections are measured and compared with theoretical calculations. Since the measured cross section for photoabsorption was significantly larger than the theoretically calculated cross section for channel (9a), additional channels probably play a role.

Theoretical calculations were carried out for comparison with the experimental data, which were obtained at values of $\hbar\omega$ corresponding to 355 and 193 nm. The calculations treat channels (9a), (9b), (9b'), and (9b''), for which estimates of the coupling terms could be obtained as described in Sec. III. These calculations suffice to demonstrate the importance of channels (9b), (9b'), and (9b''). Coupling terms to treat channel (9c) have not been

TABLE IV. Comparison of experimental and theoretical cross sections.

	$\sigma_0^2(E,F\ (v'=6)\leftarrow(v''=0))$ $(10^{-36}\ cm^4)$	$\sigma_{abs}(E,F\ (v''=6)+193\ nm)$ $(10^{-18}\ cm^2)$	$\sigma_{abs}(E,F\ (v''=6)+355\ nm)$ $(10^{-18}\ cm^2)$
Experimental	2.0±0.9	6.4±1.3	9.7±2.4
Calculated	2.8	10.8	12

calculated, and thus only qualitative comments can be made about this channel.

The theoretical calculations are summarized in Table III and in Fig. 7. An interesting implication of the calculations is that the relative importance of the various channels (9) changes dramatically with photon energy. This behavior can be best understood by examining Fig. 7. Cross sections for the various channels are shown. The short-dashed curve is direct photoionization, and is summed over all open final vibrational channels. It is shown for energies above the threshold for excitation of the $v=2$ vibrational state of H_2^+. The jump at about 40 000 cm^{-1} corresponds to the opening of the $v=13$ state of the ion. The Franck-Condon factor for this state (0.089) is second only to that for the $v=2$ state (0.754), and comes from the portion of the wave function in the outer F well. The long-dashed curve is photodissociation (including both neutral and ionic channels) on the $^1\Sigma_u$ autoionizing state. The details of this curve are uncertain because of the approximate transition matrix element used, but the general features make physical sense. The threshold occurs at the energy at which $H(n=2)+H$ may be formed. The oscillatory structure reflects the oscillations of the vibrational wave function in the outer well. In the region of oscillations, photodissociation is effectively the only available channel. The overlap between the dissociating wave function (H^*+H) and the H_2^+ vibrational wave functions is negligible up to about 30 000 cm^{-1}. Above this energy, the solid curve starts to rise. This curve corresponds to photoexcitation of the $^1\Sigma_u$ state, followed by autoionization, which can only be large when the wave function of the dissociating state (determined by the photon energy) has a good overlap with the wave functions of the open vibrational channels. It is interesting to note that the oscillations in the photodissociation curve are quenched once autoionization becomes probable.

These calculations suggest the following interpretation of the observed photoabsorption signal. At 355 nm, the process is predominantly direct photoionization, with a small component of photodissociation. Dissociative ionization, (9c), and ionic dissociation, (9b''), are not energetically allowed. At 193 nm, direct photoionization is much smaller, and photoexcitation of the $^1\Sigma_u$ state followed by autoionization is quite important. Dissociative ionization is possible at this energy, but our present data do not distinguish between the production of H_2^+ and H^+ ions. Anderson *et al.*[32] argued that less than 5% of all the ions were H^+, although Buck *et al.*[10] measured this fraction to be about 33%. Further studies are in progress to investigate this point.

We find that the sum of the calculated cross sections for (9a), (9b), (9b'), and (9b'') compares reasonably well with the measured data, as summarized in Table IV. Channels (9a) and (9b) may interfere, so that the total cross section may not be equal to the sum of the cross sections calculated for individual channels. We have not taken that into account. The crucial point we wish to make is that the measured cross section for photoabsorption is larger than the cross section calculated for direct photoionization (a factor of 2 larger at 193 nm). The additional channels considered clearly provide a substantial contribution to the total signal.

V. CONCLUSIONS

The measured integrated two-photon excitation cross section, $\sigma_0^{(2)}=(2.0\pm0.9)\times10^{-36}\ cm^4$, was in good agreement with the calculated value, $\sigma_0^{(2)}=2.8\times10^{-36}\ cm^{-4}$, for the H_2 $E,F\ ^1\Sigma_g^+$ $(v'=6)\leftarrow X\ ^1\Sigma_g^+$ $(v''=0)$ $Q(1)$ transition. The cross section for absorption by the excited E,F state of a third 193-nm photon, $\sigma_{abs}=(6.4\pm1.3)\times10^{-18}$ cm^2, was found to be substantially larger than our estimated value for direct photoionization, $3.2\times10^{-18}\ cm^2$. Excitation of the $^1\Sigma_u$ dissociating, autoionizing state was treated and shown to contribute significantly to the photoabsorption. Agreement was good between theory and experiment for absorption by the E,F state of a 355-nm photon. The sum of cross sections calculated for the separate channels was $12\times10^{-18}\ cm^2$; we measured $\sigma_{abs}=(9.7\pm2.4)\times10^{-18}\ cm^2$.

The technique of two-photon excited fluorescence (TPEF) appears promising as an analytical technique to measure densities of vibrationally excited H_2. Scaling from our demonstrated signal-to-noise ratios for $v''=0$, we estimate that densities of $10^{10}\ cm^{-3}$ per quantum state could be detected by using TPEF, using a laser pulse of 10 mJ focused to $10^{-2}\ cm^{-2}$ with a 10-ns pulse length. If the two-photon absorption cross sections for $v''=1$–14 are as large as the cross section reported here for $v''=0$, it should be possible to determine the vibrational state distributions in the multicusp H^- ion sources currently under development.[6,34]

Note added. The theoretical value of σ_0^2 has recently been reevaluated by Huo.[36] The new value is 3.6×10^{-36} cm^4. This will be discussed further in subsequent publications.

ACKNOWLEDGMENTS

This work was sponsored by the U.S. Air Force Office of Scientific Research, under Contract Nos. F49620-88-C-0112 and F49620-88-K-0005. Helpful conversations are acknowledged with Dr. Winifred Huo concerning the work of Ref. 22.

*Present address: Optical Shields, Ltd., 1390 Willow Rd., Menlo Park, CA 94025.
†Present address: Deacon Research, 900 Welch Rd., Ste. 203, Palo Alto, CA 94304.

[1]H. Eichert and M. Fischer, Int. J. Hydrogen Energy **11**, 117 (1986).
[2]W. T. Huntress, Jr., Adv. At. Mol. Phys. **10**, 295 (1974).
[3]H. Pummer, H. Egger, T. S. Luk, T. Srinivasan, and C. K. Rhodes, Phys. Rev. A **28**, 795 (1983).
[4]E. W. Rothe, G. S. Ondrey, and P. Andresen, Opt. Commun. **58**, 113 (1986).
[5]W. M. Huo and R. L. Jaffe, Chem. Phys. Lett. **101**, 463 (1983).
[6]R. L. York, R. R. Stevens, K. N. Leung, and K. W. Ehlers, Rev. Sci. Instrum. **55**, 681 (1984).
[7]D. C. Robie, L. E. Jusinski, and W. K. Bischel (unpublished).
[8]C. Cornaggia, A. Giusti-Suzor, and Ch. Jungen, J. Chem. Phys. **87**, 3934 (1987).
[9]A. P. Hickman, Phys. Rev. Lett. **59**, 1553 (1987).
[10]J. D. Buck, D. H. Parker, and D. W. Chandler, J. Phys. Chem. **92**, 3701 (1988).
[11]W. K. Bischel, D. J. Bamford, and L. E. Jusinski, Appl. Opt. **25**, 1215 (1986).
[12]D. J. Bamford, L. E. Jusinski, and W. K. Bischel, Phys. Rev. A **34**, 185 (1986).
[13]J. D. Buck, S. Kroll, and W. K. Bischel (unpublished); T. Ebata, N. Mikami, and M. Ito, J. Chem. Phys. **78**, 1132 (1983).
[14]D. C. Robie, J. D. Buck, and W. K. Bischel (unpublished).
[15]D. J. Kligler and C. K. Rhodes, Phys. Rev. Lett. **40**, 309 (1978).
[16]R. P. Saxon and J. Eichler, Phys. Rev. A **34**, 199 (1986).
[17]M. Glass-Maujean, P. Quadrelli, and K. Dressler, At. Data Nucl. Data Tables **30**, 274 (1984).
[18]G. Herzberg, *Molecular Spectra and Molecular Structure I. Spectra of Diatomic Molecules*, 2nd ed. (Van Nostrand, New York, 1950).
[19]D. J. Bamford, A. P. Hickman, M. J. Dyer, and W. K. Bischel, J. Opt. Soc. Am. B **5**, 1369 (1988).
[20]W. M. Huo (personal communication).
[21]A. Cohn, J. Chem. Phys. **57**, 2456 (1972).
[22]H. Rudolph, D. L. Lynch, S. N. Dixit, V. McKoy, and W. M. Huo, J. Chem. Phys. **86**, 1748 (1987).
[23]E. Y. Xu, T. Tsuboi, R. Kachru, and H. Helm, Phys. Rev. A **36**, 5645 (1987).
[24]W. A. Chupka, J. Chem. Phys. **87**, 1488 (1987).
[25]M. A. O'Halloran, S. T. Pratt, P. M. Dehmer, and J. L. Dehmer, J. Chem. Phys. **87**, 3288 (1987).
[26]S. L. Guberman, J. Chem. Phys. **78**, 1404 (1983).
[27]A. U. Hazi, C. Derkits, and J. N. Bardsley, Phys. Rev. A **27**, 1751 (1983).
[28]S. Ross and Ch. Jungen, Phys. Rev. Lett. **59**, 1297 (1987).
[29]D. R. Bates, J. Chem. Phys. **19**, 1122 (1951).
[30]J. Tennyson and C. J. Noble, J. Phys. B **18**, 155 (1985).
[31]J. W. J. Verschuur, L. D. Noordam, J. H. M. Bonnie, and H. B. van Linden van den Heuvell, Chem. Phys. Lett. **146**, 283 (1988).
[32]S. L. Anderson, G. D. Kubiak, and R. N. Zare, Chem. Phys. Lett. **105**, 22 (1984).
[33]E. Y. Xu, A. P. Hickman, R. Kachru, and H. Helm (unpublished).
[34]K. N. Leung, G. J. DeVries, K. W. Ehlers, L. T. Jackson, J. W. Stearns, M. D. Williams, M. G. McHarg, D. P. Ball, W. T. Lewis, and P. W. Allison, Rev. Sci. Instrum. **58**, 235 (1987).
[35]K. P. Huber and G. Herzberg, *Molecular Spectra and Molecular Structure IV. Constants of Diatomic Molecules* (Van Nostrand, New York, 1979).
[36]W. M. Huo (personal communication).

APPENDIX D

Photoelectron Spectroscopy of Vibrationally Excited H_2 ($E,F\ ^1\Sigma_g^+$)

Phys. Rev. A, **40**, 7031 (1989).

PHYSICAL REVIEW A VOLUME 40, NUMBER 12 DECEMBER 15, 1989

Photoelectron spectroscopy of vibrationally excited H_2 ($E,F\,{}^1\Sigma_g^+$)

E. Xu, A. P. Hickman, R. Kachru, T. Tsuboi, and H. Helm
Molecular Physics Laboratory, SRI International, Menlo Park, California 94025
(Received 24 July 1989)

Photoelectron energy spectra following (2+1)-multiphoton ionization of H_2 via the double-well $E,F\,{}^1\Sigma_g^+$ state have been measured using a magnetic-bottle electron spectrometer. The range of vibrational levels studied, $v_{E,F}=3$–9, includes states localized at the bottom of the E well, and also states that span both wells. The branching among the vibrational ionization channels is governed by the strong R dependence of the electronic wave function and the degree of localization of the vibrational wave function in the E or the F well. Theoretical analysis confirms that at least two mechanisms contribute to the observations: a direct process involving only the E,F state and the H_2^+ ionization continuum, and an indirect process involving the ${}^1\Sigma_u^+$ autoionizing state. Mass spectroscopic measurements carried out for $v_{E,F}=9$, $J=1$ show that about 25% of the ions produced were H^+. Qualitative arguments suggest that most of these protons arise from dissociative ionization to the H_2^+ continuum.

I. INTRODUCTION

Dynamical processes in diatomic molecules can be investigated by multiphoton ionization and measurement of the photoelectron energy. Such spectra directly provide final-state distributions, from which many features of the molecular interactions may be inferred. For example, recent studies of the multiphoton ionization of H_2 (Refs. 1–9) revealed anomalous distributions of final vibrational states of H_2^+. Although surprising at first, these distributions were shown to arise[10,11] from an indirect process involving dissociating, autoionizing states in the H_2 continuum. A feature of the indirect ionization process is that final vibrational states may be populated that have a poor Franck-Condon factor with the vibrational level of the neutral intermediate state.

This paper reports the extension of our previous measurements of multiphoton ionization (MPI) of H_2 to the case where specific vibrational levels of the E,F state are prepared by two-photon excitation and are photoionized by a third photon. The E,F states present new features because of the unusual double-well structure of the potential curve, and have been studied by several groups.[1–3,12–14] The electronic structure of these states exhibits a strong dependence on the internuclear separation R. Depending on whether the vibrational state is localized mostly in the E well or mostly in the F well, one expects different channels to come into play. By tuning the laser to alternate vibrational levels in the E,F state $v_{E,F}$ we have observed dramatic changes in the final-state distributions. Furthermore, theoretical analysis suggests a consistent interpretation of this behavior in terms of the interplay of several alternate ionization channels.

This paper is organized as follows. Section II describes the experimental procedure. Section III reviews the indirect autoionizing channel and describes theoretical calculations based on the nonlocal complex potential model that include this channel. Section IV describes and discusses our results and Sec. V presents concluding remarks.

II. EXPERIMENTAL PROCEDURE

The multiphoton ionization scheme is shown in Fig. 1: two photons in the energy range around 6.5 eV resonantly excite intermediate E,F levels of known rovibrational quantum number. The E,F double-minimum potential contains low vibrational states which are trapped mostly in either the inner E well or the outer F well, as well as vibrational states with their wave functions spread over the potential barrier and out to large R. The third photon from the same laser ionizes the molecule. Photoelectrons from the various resulting ionic states are collected in a time-of-flight (TOF) electron spectrometer.

We use a YAG (yttrium aluminum garnet) pulsed laser system and a high-pressure H_2 Raman cell to generate tunable light in the wavelength range from 180 to 200 nm at 100 μJ/pulse energy level. The laser beam is focused by a 15-cm focal length lens and forms a 500-μm size spot at the center of the electron spectrometer. Simultaneously injected into the same spot is a supersonic jet of H_2 from a pulsed valve. The spectrometer is of magnetic-bottle-type design, energized by permanent magnets. It has a 2π collection efficiency due to its angular integration and a high time and energy resolution due to its field design. The principle and details of this instrument have been published by Tsuboi *et al.*[15] The spectrometer is differentially pumped with two turbo molecular pumps to 10^{-8} torr, and the average background pressure of H_2 gas in the magnet chamber is kept in the 10^{-5}-torr range during the experiment. Photoelectrons created by laser-H_2 interaction follow the magnetic field lines into the 65-cm TOF tube and are collected on a multichannel plate detector. We record the photoelectron signal with an eight-channel real-time time-to-digital converter (TDC) (Le Croy's model 4208), which works in a multihit mode

 ©1989 The American Physical Society

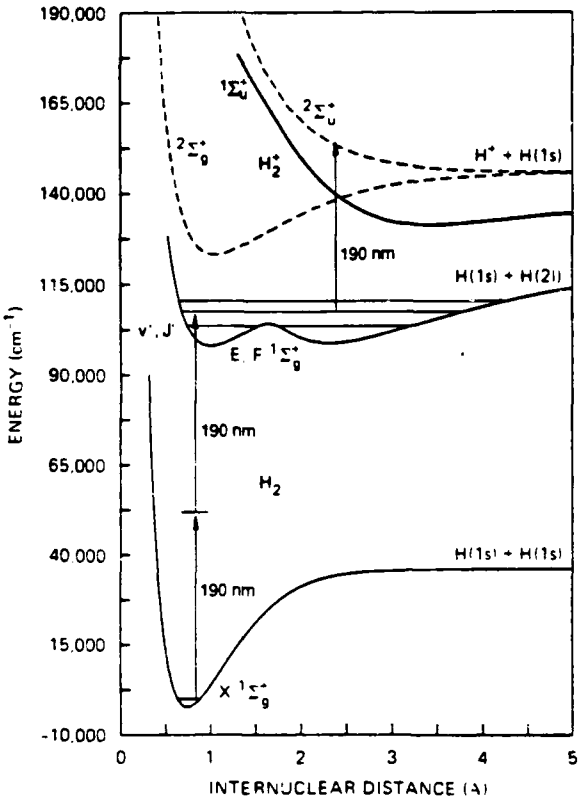

FIG. 1. Diagram of the relevant potential curves for the multiphoton ionization of H_2 through the E,F state. Solid curves are H_2 states, dashed curves are H_2^+.

in this experiment. Its intrinsic time resolution is 1 nsec, which should enable us, in principle, to resolve rotational splitting for 4-eV electrons. Data acquisition is controlled by a PDP-11 computer. The use of the TDC in replacement of the analog averaging method that was applied in our previous[6] photoelectron experiment involving H_2 has greatly improved our signal-to-noise ratio and time-energy resolution. Nevertheless, we still have to subtract each data spectrum with its corresponding background spectrum taken when the laser is detuned from the resonance frequency, owing to an unidentified impurity that generates photoelectrons in the energy range from 0.5 to 2 eV.

Currently we do not apply any external field to extract or retard electrons. However, an unidentified source of contact potential limits collection of photoelectrons to those above 400 meV. The retardation of electrons caused by the contact potential is corrected by calibrating the spectra against the known ionization potential of H_2 and the vibrational spacings of H_2^+. We have also set up a time-of-flight ion spectrometer to monitor the creation of ion species in the same multiphoton processes.

III. THEORY

Recent theoretical[10,11,16] and experimental[6-9] studies have led to a realization of the importance of dissociating, autoionizing states in the photoionization of electronically excited molecules. Photoexcitation of these states, followed by autoionization, provides an additional contribution to photoionization and may lead to strongly non-Franck-Condon distributions of final vibrational states. Photodissociation to excited neutral products is also possible. This section summarizes the mechanism responsible for these effects.

Figure 1 shows the relevant potential curves in the present situation. We use the term direct photoionization to denote the one-electron transition between the initial state H_2 E,F and the electronic continuum $e+H_2^+$. This transition is caused by the dipole-matrix element coupling the excited-state orbital and the Coulomb scattering function. An additional process that must be considered is the photoexcitation of the dissociating, autoionizing $^1\Sigma_u^+$ state, which has the electronic configuration $2s\sigma_g 2p\sigma_u$, and is also coupled to the E,F state by a one-electron transition. If the transition to the $^1\Sigma_u^+$ state occurs, then the nuclei start to dissociate just as in photodissociation. However, the autoionizing state is unstable with respect to electron emission. As the nuclei move, there is a competition between autoionization and dissociation. Roughly speaking, if autoionization occurs before the nuclei separate to the R^* for which the $^1\Sigma_u^+$ state is lower in energy than the $^2\Sigma_g^+$ state of H_2^+ ($\sim 4a_0$), then the final state will be H_2^+ plus a continuum electron, corresponding to indirect photoionization. For the present system and for others studied in our laboratory,[6,11] our calculations indicate that this outcome occurs with at least 90–95 % probability. If the nuclei reach R^* without autoionization, they encounter a series of curve crossings with the Rydberg potential curves converging to the $^2\Sigma_g^+$ state of H_2^+. Depending on the outcome of the curve crossings, the nuclei may ultimately dissociate or undergo a transition to a bound state and vibrationally autoionize or radiate.

For the present situation, the lifetime for electron emission is on the order of 8×10^{-16} sec.[17] A typical dissociation time estimated by classical mechanics is about 4×10^{-15} sec, or about five times longer. Therefore significant nuclear motion is likely during the time it takes to autoionize. During this time, electronic energy may be converted to nuclear kinetic energy. Contrast this situation to direct photoionization in which the electron is emitted before the nuclear position and momentum have time to change substantially. From this point of view, one can see why the Franck-Condon approximation is applicable to direct photoionization, but not to the indirect process.

The mechanism just described has been treated by solving a modified Schrödinger equation with a nonlocal complex potential. The first application[11] of this method was to the photoionization of the $C\,^1\Pi_u$ state, and a calculation for the photoionization of the H_2 ($v_{E,F}=6$) has been compared with other experiments from this laboratory.[18] In this section, we summarize the determination of the necessary potential curves and describe calculations of the distribution of final vibrational states for several initial vibrational states of the E,F potential. Cross sections for the direct photoionization process are

estimated and added to those for the autoionization process. The results presented in Sec. III will show each contribution independently. In principle, the processes of direct photoionization and excitation-autoionization interfere. One should add complex amplitudes and then square, rather than add cross sections as we have done. Dixit *et al.*[16] have carried out such calculations on related systems. However, because we are invoking approximate coupling terms from several sources with various phase conventions, attempting to treat interference does not seem warranted.

The potentials and coupling terms used to treat the photoexcitation from the E,F state are discussed in detail elsewhere. We briefly list these terms and how they were obtained. (i) The $^1\Sigma_u^+$ autoionizing potential was calculated by Guberman.[19] (ii) The width $\Gamma(R)$, or electron emission rate, was taken from calculations of Tennyson and Noble.[17] (iii) The transition moment $\mu(R)$ connecting the E,F state with the $^1\Sigma_u^+$ state was estimated by considering the two dominant electronic configurations of the E,F states, as described in Ref. 18.

The direct photoionization cross sections may be determined from previous work. Cohn[20] tabulated values for several excited states of H_2 using the Coulomb approximation for the continuum wave function. More recently, Rudolph *et al.*[21] have carried out more sophisticated calculations. They calculated the distribution of final vibrational states following direct photoionization, but they did not report the absolute values of the cross sections. Their results appear to indicate[22] that the calculations of Cohn are accurate to within 30%. For the present calculations, we have evaluated direct photoionization cross sections by interpolating Cohn's photoionization cross sections as a function of photoelectron energy and multiplying them by the appropriate Franck-Condon factor.

In summary, we calculated the distribution of final vibrational states by the following procedure. We calculate the cross section for the direct photoionization process, using the Franck-Condon approximation. To this we add the cross section for reaching the same final state by going through the $^1\Sigma_u^+$ autoionizing state, using the nonlocal complex potential method.[11] It is this second contribution that causes the strongly non-Franck-Condon nature of the distribution.

IV. RESULTS AND DISCUSSION

A. Available channels

We have measured the TOF spectra of photoelectrons obtained in the multiphoton ionization of H_2 through several vibrational states of the $E,F\,^1\Sigma_g^+$ double-well potential. We first indicate schematically the open channels that could lead to the electrons:

$$\mathrm{H}_2\,E,F\,^1\Sigma_g^+\,(v_{E,F},J=1)\rightarrow\begin{cases}\mathrm{H}_2^+(v^+)+e & \text{(1a)}\\ \mathrm{H}_2^{**}(^1\Sigma_u^+)\rightarrow\begin{cases}\mathrm{H}^*+\mathrm{H}\\ \mathrm{H}_2^+(v^+)+e\\ \mathrm{H}+\mathrm{H}^++e\end{cases} & \text{(1b)}\\ \mathrm{H}+\mathrm{H}^++e\,. & \text{(1c)}\end{cases}$$

We focus our attention on the channels available after the first two photons have been absorbed to form the E,F state. Channels (1a) and (1b), direct photoionization, and excitation of the autoionizing state, respectively, were discussed in Sec. III. Channel (1c) is dissociative ionization, and will be discussed in more detail below.

A simple molecular-orbital picture of the wave functions of the E,F states and of the H_2 states created in channels (1a)–(1c) suggests that each of these channels can be related to specific one-electron transitions. The transitions can be easily assigned by considering the form of the initial and final electronic states for each channel. Near the E well, the E,F electronic wave function is predominantly $1s\sigma_g 2s\sigma_g$, and direct ionization of the E state corresponds to ionization of the $2s\sigma_g$ orbital. Channel (1b) corresponds to core excitation of the $1s\sigma_g$ orbital to create the $2s\sigma_g 2p\sigma_u\,^1\Sigma_u^+$ autoionizing state. Near the F well, the electronic wave function is a linear combination of $1s\sigma_g 2s\sigma_g$ and $(2p\sigma_u)^2$. In this range, the autoionizing state can also be formed by the $2p\sigma_u\rightarrow 2s\sigma_g$ transition.

In the third process (1c) atomic fragments are formed following one-photon absorption of the E,F level. Direct dissociative photoionization to the continuum of the ground state and first excited state of H_2^+ is also possible from the F well. The electronic wave function's $1s\sigma_g 2s\sigma_u$ component permits coupling to the $^2\Sigma_g^+$ H_2^+ ground state and the $(2p\sigma_u)^2$ component to the excited state of $^2\Sigma_u^+$. The various channels shown will occur with amplitudes that are weighted according to the radial distribution of the E,F vibrational wave function.

B. Photoelectron spectra

We now discuss our results for specific intermediate vibrational states of the E,F potential. We use the notation $v_{E,F}$ to denote the vibrational quantum number according to the Dressing convention, which combines E- and F-well states. To indicate states localized predominantly in the inner or the outer well, we use v_E and v_F, respectively. The inner E-well potential curve is approximately parallel to the H_2^+ ground state $^2\Sigma_g^+$. Therefore direct photoionization of E-well states is expected to have a

large component from transitions with $|v^+ - v_E| = 0$. An example for this is the vibrational level $v_{E,F} = 3$ for which the wave function is almost entirely localized in the E well ($v_E = 1$). The most likely final H_2^+ state in this case is $v^+ = 1$, as shown in Fig. 2. Similarly, as shown in Fig. 3, $v_{E,F} = 6$ ($v_E = 2$) leads to a large proportion of $v^+ = 2$. However, in both cases the population of the other vibrational states is larger than one would expect from simple Franck-Condon arguments. This result agrees well with the result of a similar experiment by Anderson, Kubiak, and Zare,[1] which stimulated theoretical activity to explain the anomalous final-state distribution. We note that Anderson, Kubiak, and Zare[1] did not observe the $v^+ = 13$ peak in their electron spectrum on the $v_{E,F} = 6$ state, which may have been caused by a low sensitivity in measuring less energetic photoelectrons in their electron collector.

Our theoretical results for $v_{E,F} = 3$ and 6 are also shown in Figs. 2 and 3. The calculations allow us to assess how much of the total photoionization comes from the direct process and how much from the indirect process through the autoionizing state. The shaded bars show the Franck-Condon portion, and the open bars show the total calculated cross section. In general, the agreement with experiment is good, and confirms the following interpretation of the data. The dominant channels are (1a) and (1b), with the excitation to the autoionizing state contributing to the broad distribution of final states. However, other mechanisms should not be neglected. Rudolph *et al.*[21] have shown that effects such as the R dependence of the transition matrix element also contribute to the broadening. There is also a significant component of direct photoionization of $v_{E,F} = 6$ leading to $v^+ = 13$. The two largest Franck-Condon factors for these E,F states are to $v^+ = 2$ (0.754) and to $v^+ = 13$ (0.089). The latter component arises because the small outer-well component of the $v_{E,F} = 6$ state contributes to a substantial Franck-Condon factor with $v^+ = 13$ of H_2^+. The calculations also show that the indirect ionization channel contributes significantly to the $v^+ = 13$ peak.

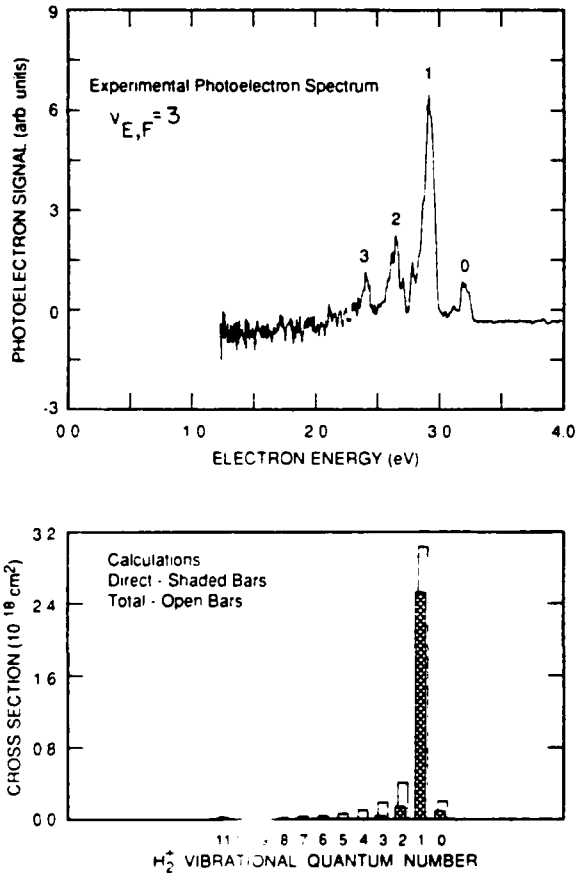

FIG. 2. Experimental photoelectron spectrum for the $v_{E,F} = 3$ ($v_E = 1$), $J = 1$, intermediate state, and the theoretical distribution of final vibrational states. The shaded bars correspond to the calculated direct cross sections, and the open bars to the sum of the direct and indirect cross sections. The indirect contribution corresponds to the difference between the two bars.

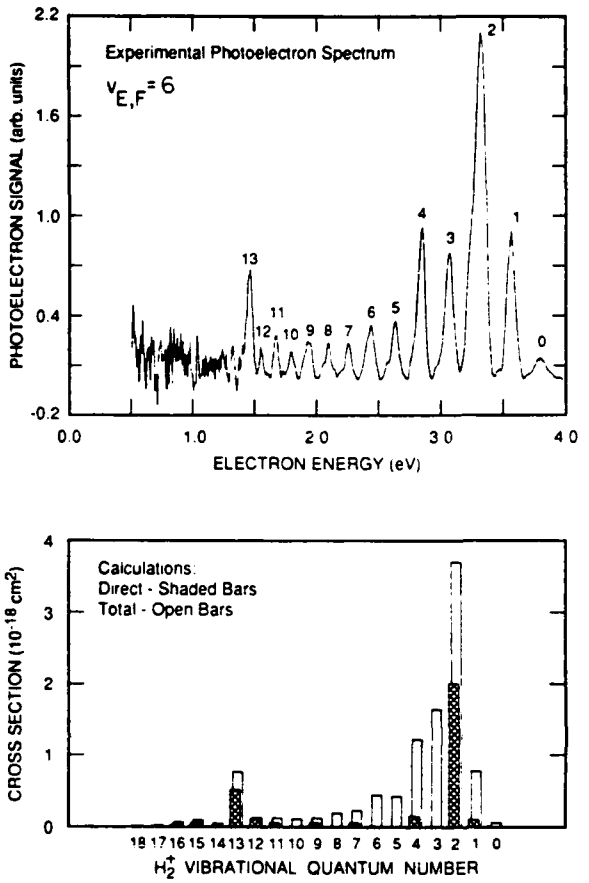

FIG. 3. Same as Fig. 2, for $v_{E,F} = 6$ ($v_E = 2$).

The predominantly inner-well vibrational states would not be expected to have a large cross section for dissociative ionization channel (1c) because of the poor Franck-Condon factor at the wavelength used in this experiment. The experimental data confirm this expectation. In a separate apparatus that monitors ion species using the same laser intensity and frequency, H^+ was observed

only as a small percentage of the total ion production. This conclusion agrees with Anderson, Kubiak, and Zare's[1] observation on the $v_{E,F}=6$ state. However, Buck, Parker, and Chandler[23] observed a somewhat larger proportion of H^+.

We also investigated states associated with the outer, F well. The $v_{E,F}=7$ ($v_F=4$), $J=1$ state was an interesting choice because it is only 252.25 cm^{-1} higher than its E-well neighbor, the $V_{E,F}=6$ ($v_E=2$), $J=1$ state. The final-state distributions from the two states are completely different. Figure 4 shows the measured spectrum. Several low v^+ states have comparable signals, and the large v^+ states that have a good overlap with the outer-well wave function become the dominant feature in the spectrum. The spectrum from $v_{E,F}=9$, shown in Fig. 5, also exhibits features at large v^+ that can be attributed to the overlap between the outer-well intermediate state and the H_2^+. This electron energy spectrum is composed of two groups of peaks. One corresponds to the state with the largest Franck-Condon overlap with the inner-well portion of the E,F wave function. The other group is dominated by $v^+=14$, a high vibrational state from exciting the outer well. We also notice in this spectrum a broad electron signal below 1.5 eV after the general background was subtracted from the total signal.

Theoretical calculations for $v_{E,F}=7$ and 9 are also shown in Figs. 4 and 5. The interpretation of the data is not as clear for these states as for $v_{E,F}=3$ and 6. Because the E,F wave functions are spread over both wells, the Franck-Condon factors for the direct process cover many values of v^+. The theoretical calculations indicate that most peaks have substantial contributions from both direct and indirect ionization mechanisms.

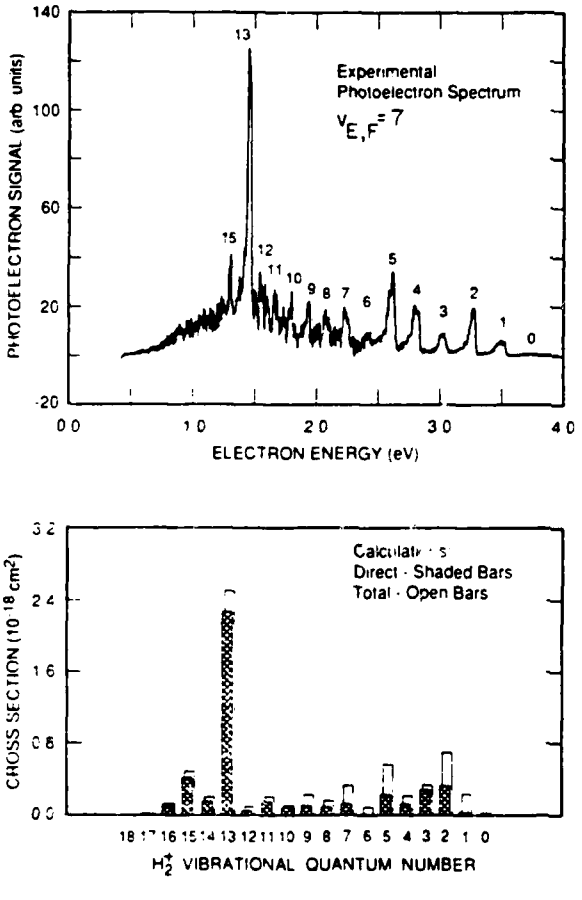

FIG. 4. Same as Fig. 2, for $v_{E,F}=7$ ($v_E=4$).

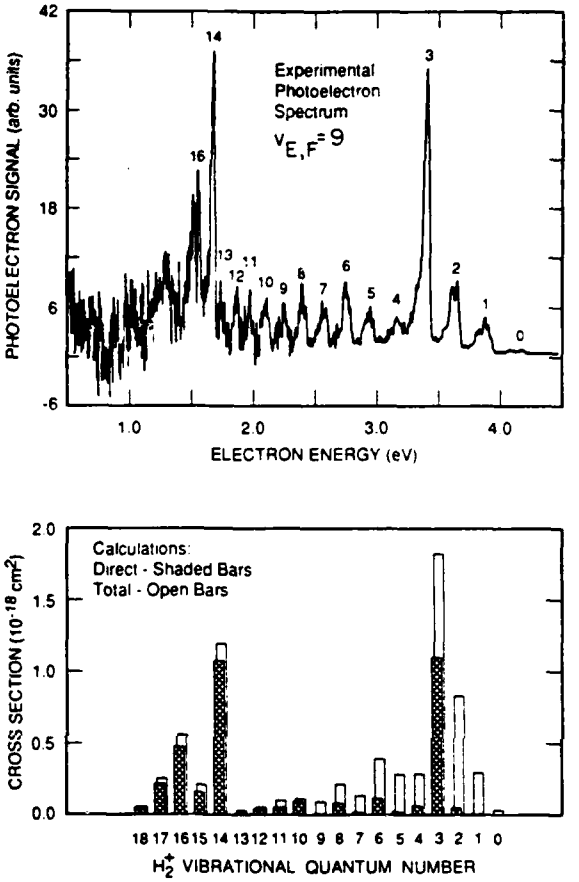

FIG. 5. Same as Fig. 2, for $v_{E,F}=9$ ($v_E=3$).

The ion mass spectrometry measurements show that ionization via the $v_{E,F}=9$ ($v_E=3$) state produces a significant amount of H^+. Figure 6 shows the TOF spectrum of ion species of this state; the H^+ signal is about 30% that of H_2^+. The origin of this large fraction of protons will be discussed in Sec. IV C.

C. Origin of H^+

Although protons account for a significant fraction of the photoions observed for $v_{E,F}=9$ in the present experiment and in other recent studies, no definitive explanation of their origin exists. Several alternative mechanisms are possible. Referring back to the available channels (1a)–(1c), we note that excited hydrogen atoms H^* or molecular ions H_2^+ can be produced. Photoionization of H^* or photodissociation of H_2^+ can produce protons. Channel (1c) produces protons directly by dissociative ionization. Both the $^2\Sigma_g^+$ and the $^2\Sigma_u^+$ potential curve of

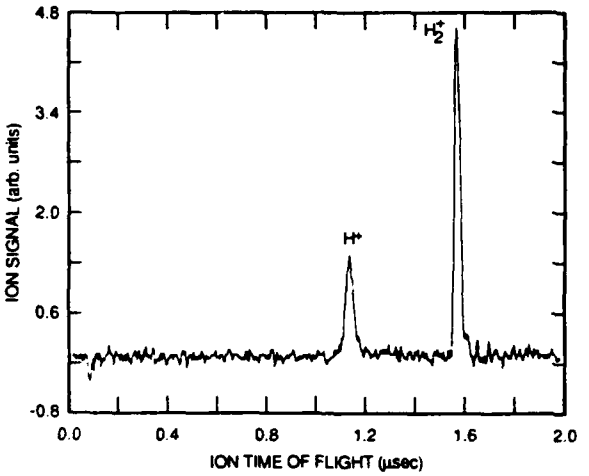

FIG. 6. Time-of-flight spectrum for the ion mass spectrometry measurements.

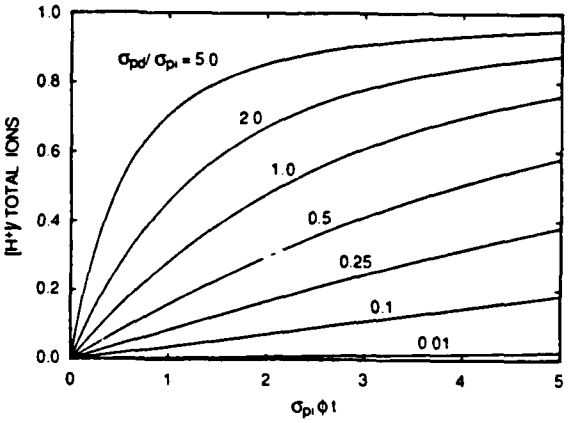

FIG. 7. Results of rate-equation model for the fraction of H_2^+ ions that are photodissociated to form H^+.

H_2^+ are available for this process. The present photoelectron spectra provide additional information to address this point.

The data allow us to rule out photoionization of H^* using a fourth photon from the laser pulse as a significant source for the observed protons. Excited atoms are produced by those molecules in the $^1\Sigma_u^+$ autoionizing state that "survive" the autoionization process and dissociate. When the excited atoms produced by the dissociation are ionized, the photoelectron energies are 3.129 eV for $n=2$, 5.017 eV for $n=3$, and 5.678 eV for $n=4$ (at the laser wavelength employed for $v_{E,F}=9$). We have not observed electrons of these energies. If they were present, they would be observed, as they were in our previous experiment[6] involving photoionization of H_2 ($C\,^1\Pi_u^+$).

We have also estimated the production of protons by photodissociation of H_2^+, using a rate-equation model. Let N_0, $N_{E,F}$, N_{v^+}, and N_{H^+} denote the number densities of $H_2(X)$, $H_2(E,F)$, $H_2^+(v^+)$, and protons, respectively. Let $\sigma_{pi}(v^+)$ be the cross section for photoionizing the E,F state and producing $H_2^+(v^+)$, and let $\sigma_{pd}(v^+)$ be the cross section for photodissociating $H_2^+(v^+)$. $\sigma_{pi}(v^+)$ depends on the vibrational state of the E,F potential and $\sigma_{pd}(v^+)$ depends on wavelength. We define also $\sigma_{pi}=\sum\sigma_{pi}(v^+)$, the total photoionization cross section of the E,F state and $N_{H_2^+}$, the total H_2^+ population. The two-photon excitation cross section is σ_0 and has units of (length)$^4\times$(time). We write the following rate equations, assuming only that the laser pulse is not strong enough to deplete the ground-state population N_0:

$$\frac{dN_{E,F}}{dt}=\phi^2\sigma_0 N_0-\phi\sigma_{pi}N_{E,F}\,,$$
$$\frac{dN_{H_2^+}}{dt}=\phi\sigma_{pi}N_{E,F}-\phi\sigma_{pd}N_{H_2^+}\,, \qquad (2)$$
$$\frac{dN_{H^+}}{dt}=\phi\sigma_{pd}N_{H_2^+}\,.$$

These equations involve explicitly only the total H_2^+ ion population. The dependence on the specific population of a vibrational level v^+, N_{v^+}, is contained in σ_{pd}, which is a weighted average over the photodissociation cross sections for the individual vibrational levels:

$$\sigma_{pd}=\sum_{v^+}(N_{v^+}/N_{H_2^+})\sigma_{pd}(v^+)\,. \qquad (3)$$

A useful estimate of the proton population can be obtained by solving the above equations analytically, using a constant value for σ_{pd}. We can obtain an estimate of σ_{pd} by noting that the H_2^+ states are populated, at least initially, in proportion to the cross sections σ_{pi}. We therefore assume $N_{v^+}/N_{H_2^+}\cong\sigma_{pi}(v^+)/\sigma_{pi}$.

The set of equations (2) with constant coefficients is easily solved using Laplace transforms. The important dimensionless parameters are (i) $\phi\sigma_{pi}t$, where ϕ is the laser fluence in photons per cm^{-2}s^{-1}, and (ii) σ_{pd}/ϕ_{pi}. Figure 7 shows the calculated results for the fraction of total ions (H_2^+ and H^+) that are protons. The rate of converting the H_2^+ to protons by photodissociation competes with the production of new H_2^+ by photoionization; the balance depends on the ratio σ_{pd}/σ_{pi}.

Typical values of σ_{pd}/σ_{pi} are in the range 0.4–0.6. These values were determined from the present calculations of σ_{pi} and from direct calculations of the photodissociation cross section similar to Dunn's.[24] From Fig. 7 it is clear that for photodissociation of H_2^+ to contribute substantially ($\sim$10%) to the proton fraction, $\phi\sigma_{pi}t\sim 1$ is necessary. Typical parameters for the present experiment are 100 μJ per 5 ns pulse, and spot size 500 μm. These values, combined with the calculated values of $\sigma_{pi}\sim 7\times10^{-18}$ cm^2, yield ar estimate of $\phi\sigma_{pi}t\sim 0.1$.

The rate-equation analysis leads to the conclusion that photodissociation of H_2^+ is likely to account for, at most, a few percent of the observed protons in the present experiment. We note that substantially more protons would be expected from this mechanism at greater laser intensities.

Another mechanism for producing protons is dissocia-

tive ionization of the E,F states. Continuum translational states on both the $^2\Sigma_g^+$ and $^2\Sigma_u^+ H_2^+$ potential curves are possible final states for this process. Dissociative ionization can also occur following excitation of the $^1\Sigma_u^+$ autoionizing state. Here we discuss qualitatively the direct photoionization to continuum states of the $^2\Sigma_g^+$ and $^2\Sigma_u^+$ potentials. The cross section for this process can be written[25]

$$\frac{d\sigma}{dE} = \frac{8\pi^3 \nu}{c} \left| \int \chi_f(R)\mu(R)\chi_i(R)dR \right|^2 , \quad (4)$$

where $\chi_i(R)$ is the initial vibrational wave function on the E,F curve, $\mu(R)$ is the transition dipole-matrix element, and $\chi_f(R)$ is the translational wave function on the $H+H^+$ potential curve. The energy supplied by the photon is shared by the photoelectron and the nuclei; one must calculate the photoelectron spectra expected by evaluating Eq. (4) for wave functions $\chi_f(R)$ for the range of $H+H^+$ energies possible. Calculations of $\mu(R)$ are not available, but qualitative conclusions follow from comparing the Franck-Condon factors for transitions to the final states $^2\Sigma_g^+$ and $^2\Sigma_u^+$. Direct numerical integration of Eq. (4) for $\mu=1$ and for photon energies corresponding to $v_{E,F}=9$ shows that the Franck-Condon factors to the continuum of the $^2\Sigma_g^+$ state are large only for nuclear translational energy states in the energy range $\lesssim 100$ meV. For large translational energies, the Franck-Condon factors greatly favor the $^2\Sigma_u^+$ final state.

An estimate of the absolute contributions of dissociative ionization via the continuum of the ground state of $H_2^+, X\,^2\Sigma_g^+$ can be obtained by summing the calculated contributions of direct photoionization to all bound levels of $H_2^+ X$. In Table I we give these sums for the vibrational levels investigated here. It is apparent that only for $v_{E,F}=9$ does a substantial contribution from the ground-state continuum exist ($\sim 6\%$). It is most likely that this contribution together with the transition to $^2\Sigma_u^+$ are responsible for the proton yield observed in $v_{E,F}=9$.

The processes (1c) must give rise to photoelectrons at energies below 1.53 eV in Fig. 5. The data suggest that electrons are detected which correspond to this dissociative ionization process, although more refined experiments will be required to prove the undulatory electron energy distributions predicted by Eq. (4).

TABLE I. Summed Franck-Condon factors to the ground state of H_2^+ (calculated for $J=0$).

$v_{E,F}$	$\sum_{v^+=0}^{18} \lvert\langle v_{E,F} \rvert v^+ \rangle\rvert^2$
3	1.000
6	0.999
7	0.989
9	0.942

V. CONCLUDING REMARKS

We have reported measurements and calculations of the photoelectron energy spectra following resonant multiphoton ionization of H_2 involving intermediate vibrational states on the double-well E,F potential curve. The available ionization channels include direct photoionization, indirect photoionization through a dissociative autoionizing state, and dissociative ionization. Our results show that the relative importance of these channels depends sensitively on whether the intermediate E,F wave function is localized in the E or the F well. In the latter case, qualitative arguments based on Franck-Condon factors support the interpretation that most of the dissociative ionization occurs through the $^2\Sigma_u^+$ state. Another likely source of H^+ production, photodissociation of H_2^+, does not appear to be a dominant mechanism at the present power levels.

ACKNOWLEDGMENTS

We gratefully acknowledge the stimulating discussions with Dr. K. Gillen. This research was supported by the U.S. Air Force Office of Scientific Research under Contracts No. F49620-86-K-0017 and No. F49620-88-K-0005.

[1] S. L. Anderson, G. D. Kubiak, and R. N. Zare, Chem. Phys. Lett. **105**, 22 (1984).
[2] C. Cornaggia, J. Morellec, and D. Normand, J. Phys. B **18**, 1501 (1985).
[3] C. Cornaggia, D. Normand, J. Morellec, G. Mainfray, and C. Manus, Phys. Rev. A **34**, 207 (1986).
[4] H. M. Bonnie, J. W. J. Verschuur, H. J. Hopman, and H. B. van Linden van den Heuvell, Chem. Phys. Lett. **130**, 43 (1986).
[5] H. M. Bonnie, P. J. Tenhuistra, J. Los, and H. J. Hopman, Chem. Phys. Lett. **125**, 27 (1986).
[6] E. Y. Xu, T. Tsuboi, R. Kachru, and H. Helm, Phys. Rev. A **36**, 5645 (1987).
[7] M. A. O'Halloran, S. T. Pratt, P. M. Dehmer, and J. L. Dehmer, J. Chem. Phys. **87**, 3288 (1987).
[8] M. A. O'Halloran, S. T. Pratt, F. S. Tomkins, J. L. Dehmer, and P. M. Dehmer, Chem. Phys. Lett. **146**, 291 (1988).
[9] J. W. J. Verschuur, L. D. Noordam, J. H. M. Bonnie, and H. B. van Linden van den Heuvell, Chem. Phys. Lett. **146**, 283 (1988).
[10] W. A. Chupka, J. Chem. Phys. **87**, 1488 (1987).
[11] A. P. Hickman, Phys. Rev. Lett. **59**, 1553 (1987).
[12] N. Sen, K. Rai Dastidar, and T. K. Rai Dastidar, Phys. Rev. A **38**, 841 (1988).
[13] C. Cornaggia, A. Giusti-Suzor, and Ch. Jungen, J. Chem. Phys. **87**, 3934 (1987).
[14] E. E. Marinero, R. Vasudev, and R. N. Zare, J. Chem. Phys. **78**, 692 (1983).
[15] T. Tsuboi, E. Y. Xu, Y. K. Bae, and K. T. Gillen, Rev. Sci. Instrum. **59**, 1357 (1988).
[16] S. N. Dixit, D. L. Lynch, B. V. McKoy, and A. U. Hazi, Phys. Rev. A **40**, 1700 (1989).

[17]J. Tennyson and C. J. Noble, J. Phys. B **18**, 155 (1985).
[18]J. D. Buck, D. C. Robie, A. P. Hickman, D. J. Bamford, and W. K. Bischel, Phys. Rev. A **39**, 3932 (1989).
[19]S. L. Guberman, J. Chem. Phys. **78**, 1404 (1983).
[20]A. Cohn, J. Chem. Phys. **57**, 2456 (1972).
[21]H. Rudolph, D. L. Lynch, S. N. Dixit, V. McKoy, and W. M. Huo, J. Chem. Phys. **86**, 1748 (1987).
[22]W. M. Huo (private communication).
[23]J. D. Buck, D. H. Parker, and D. W. Chandler, J. Phys. Chem. **92**, 3701 (1988).
[24]G. H. Dunn, Phys. Rev. **172**, 1 (1968).
[25]K. Kirby, T. Uzer, A. C. Allison, and A. Dalgarno, J. Chem. Phys. **75**, 2820 (1981).

APPENDIX E

Dissociative Attachment of Electrons to Vibrationally Excited H_2

Phys. Rev. A, **43**, in press (1991).

DISSOCIATIVE ATTACHMENT OF ELECTRONS TO VIBRATIONALLY EXCITED H_2

A. Peet Hickman
Molecular Physics Laboratory
SRI International
Menlo Park, CA 94025

ABSTRACT

Calculations are reported of the dissociative attachment of low energy (< 5eV) electrons to molecular hydrogen in the states v = 0-9 and J = 0. The dynamics are treated using resonant scattering theory, fully including the nonlocal and energy-dependent shift and width operators. The necessary coupling terms are taken from the *ab initio* calculations of fixed-R electron-H_2 scattering performed by Mündel, Berman, and Domcke. Good agreement with the available experimental data of Schulz and Asundi and of Allan and Wong is achieved. Exploratory calculations were performed to investigate various local approximations to the nonlocal shift operator. The results suggest that the optimum local approximation will, in general, differ from the curve obtained in a fixed-nuclei structure calculation.

MP 90-034
March 30, 1990

INTRODUCTION

Dissociative attachment (DA) of electrons to molecular hydrogen is a process of great fundamental and practical interest. It is thought to be a primary source of the H^- ions produced in hydrogen plasmas. The process may be schematically written

$$e + H_2(v,J) \rightarrow H^- + H \qquad (1)$$

where v and J denote the vibrational and rotational quantum numbers of the H_2. Measurements for the absolute cross section for attachment to the ground state (v = J = 0) were reported by Schulz and Asundi,[1] and Allan and Wong[2] showed that the cross section increases dramatically as the internal energy of the H_2 increases. They measured relative values of sigma for v = 0-4 (J = 0), and found that the cross section increased roughly an order of magnitude for each increment of v.

This behavior was explained in 1978 by the analysis of Wadehra and Bardsley[3] based on the local complex potential model. They used *ab initio* potential curves available at that time, and fit a parameterized coupling function to the experimental data. The same coupling function was then used[3-6] to extend the calculations to other values of (v,J), for which experimental data are not available.

Recent work in the calculation of potential curves and coupling terms for electron molecule scattering has provided *ab initio* information of much greater reliability than was available ten years ago, and this information can be used to reexamine the treatment of dissociative attachment. For example, the recent calculations of Mündel, Berman and Domcke[7] have provided the necessary matrix elements for a treatment of dissociative attachment of H_2 that fully includes the energy dependent and nonlocal shift and width operators. These authors also report calculations[8] of DA of H_2 for v = 0-2 (J = 0), but the emphasis of their work was on vibrational excitation. We have

found that their work, with some additional analysis, provides a basis for much broader calculations of DA.

This paper is organized as follows: Section II presents the theory, including a summary of the resonant scattering theory and a discussion of specific coupling terms. Particular care is taken to handle the potentials and couplings in the range of internuclear separations R near 3.0 a_0 where the $^2\Sigma_u^+$ resonant state H_2^- crosses the H_2 potential curve. Section III presents and discusses the numerical results, and Section IV contains concluding remarks.

THEORY

A. SUMMARY OF RESONANT SCATTERING THEORY

The formal theory of DA is well developed,[8-11] and we will present only the essential points to facilitate discussion of our implementation. The following summary follows the notation of Wadehra's review[12] to a large extent. We begin with the expression for the total wave function of the electron-molecule system:

$$\Psi(q,R) = \phi_d(q,R)F(R) + \sum_{\substack{v \\ \text{open}}} \int d\varepsilon\, f_v(\varepsilon)\, \psi_\varepsilon(q,R)\, \chi_v(R) \qquad (2)$$

q refers collectively to the electron coordinates, and R is the internuclear separation. It is assumed that the fixed-R electron-molecule wave functions have been determined: ϕ_d is a discrete state, corresponding to H_2^- and ψ_ε is an electron-molecule scattering wave function. The vibrational wave functions of H_2 are χ_v. The treatment of DA requires the determination of F(R), the wave function describing the nuclear motion. By substituting Eq.(2) into Schroedinger's equation and formally solving for the expansion coefficients $f_v(R)$, one can derive the following equation for F(R):

$$\left[\frac{\hbar^2}{2M}\frac{d^2}{dR^2} - V_d(R) + E\right]F(R) = V(R,E-E_{v_o})\,\chi_{v_o}(R) + (\underset{\sim}{\Delta} - \frac{i}{2}\underset{\sim}{\Gamma})\,F(R) \qquad (3)$$

The total energy E is the sum of the asymptotic ($R \rightarrow \infty$) kinetic energy of the electron and the vibrational energy of the molecule, which is E_v for vibrational state v. The initial vibrational state of H_2 is v_o. $V_d(R)$ is defined as a matrix element of the electronic Hamiltonian H_{el}

$$V_d(R) = \langle \phi_d \mid H_{el} \mid \phi_d \rangle \qquad (4)$$

$\underset{\sim}{\Delta}$ and $\underset{\sim}{\Gamma}$ are nonlocal, energy-dependent operators whose action on the function F(R) yields a function of R defined as follows:

$$(\underset{\sim}{\Delta} - \frac{i}{2}\underset{\sim}{\Gamma})F = \int dR' \sum_{\substack{v \\ \text{open}}} \chi_v(R)\,\chi_v(R')\left[\Delta(R,R',E-E_v) - \frac{i}{2}\Gamma(R,R',E-Ev)\right] F(R') \quad (5)$$

where

$$\Delta(R,R',\varepsilon) = P\int d\varepsilon' \frac{V(R,\varepsilon')\,V(R',\varepsilon')}{\varepsilon-\varepsilon'} \quad (6)$$

$$\Gamma(R,R',\varepsilon) = 2\pi\, V(R,\varepsilon)\, V(R',\varepsilon) \quad (7)$$

$$V(R, E) = \langle\phi_d \mid H_{el} \mid \psi_\varepsilon\rangle \quad (8)$$

Equation (3) is solved for the boundary conditions that F(R) = 0 for R = 0, and F(R) is a outgoing wave asymptotically. The cross section for DA is then

$$\sigma_{DA} = \frac{\pi^2}{\varepsilon}\frac{\hbar k}{M}\lim_{R\to\infty}|F(R)|^2 \quad (9)$$

This formulation can be related to the parameters describing the fixed-R resonant scattering. At each R, the electron scattering cross section from the molecule exhibits a resonance of width $\Gamma(R)$ at an electron kinetic energy $E_{res}(R)$. It is convenient to define a potential curve $V_{res}(R)$ that combines the electron scattering energy with the energy of the bound state H_2 target:

$$V_{res}(R) = V_{H_2}(R) + E_{res}(R) \quad (10)$$

where $V_{H_2}(R)$ is the ground state H_2 potential. $V_{res}(R)$ is shifted by an amount $\Delta(R)$ from the zeroth order discrete state energy $V_d(R)$. $V_{res}(R)$, $E_{res}(R)$ and $\Gamma(R)$ are related as follows:

$$V_{res}(R) = V_d(R) + \Delta(R) \tag{11}$$

where

$$\Delta(R) = \Delta(R,R,E_{res}(R)) \tag{12}$$

The width (R) of the resonance at fixed R is given by

$$\Gamma(R) = V(R,E_{res}(R))^2 \tag{13}$$

The distinction between $V_{res}(R)$ and $V_d(R)$ has not always been maintained. It is often assumed that the operator Δ on the right hand side (rhs) of Eq.(3) can be neglected, and that $V_d(R)$ on the lhs can be replaced by $V_{res}(R)$. This simplification corresponds to approximating the dynamical operator $\underset{\sim}{\Delta}$ by $\Delta(R)$ in Eq.(3), and then assuming the closure relation for the sum over open vibrational states. In the present work, we utilize recent calculations[7,8] for $V(R,\varepsilon)$, which allows us explicitly to include the nonlocal shift operator.

B . ELECTRONIC MATRIX ELEMENTS

Calculations are available in the literature for nearly all the necessary coupling terms for DA of H_2. Excellent potential curves for H_2 have been obtained[13]; these were used to calculate the vibrational wave functions χ_v. $E_{res}(R)$ has been calculated by Mündel et al.[7] These authors showed that $E_{res}(R)$ could be unambiguously defined as the electron scattering energy at which the eigenphase sum equals $\pi/2$.

For the essential matrix element $V(R,\varepsilon)$, we have fit the numerical values calculated by Mündel et al.[7,8] by a convenient analytic function. Although Mündel et al.[8] reported a nine-parameter analytic fit to their calculations, we have found it preferable to repeat the fit using a

different analytic form. Some difficulty was encountered in trying to use the functional form reported in Ref. 8. $V(R,\varepsilon)$ approaches a nonzero constant asymptotically (as $R \rightarrow \infty$). Also, Table I in Ref. 8 contains typographical errors.

A good fit to the calculated points was obtained with the following analytic function:

$$V(R,\varepsilon) = \frac{A(R)\varepsilon^{3/4}}{(\varepsilon + B)^2} \tag{14}$$

This formula is physically plausible. If we consider the matrix element between a bound hydrogenic function and an energy-normalized p wave scattering function $(2k/\pi)^{1/2} j_1(kr)$, the result is[14]

$$(2k/\pi)^{1/2} \int_0^\infty e^{-r/r_o} j_1(kr)\, r^2\, dr \propto \frac{k^{3/2}}{(k^2 + r_o^{-2})^2} \tag{15}$$

Since $\varepsilon = (1/2)k^2$, Eq.(15) is consistent with Eq.(14) and yields the correct threshold behavior.

The most accurate fit could be achieved by letting both A and B be functions of R in Eq.(14). However, considerable simplification of the calculations results if B is a constant. This point will be discussed below. Fortunately, we found that a reasonably accurate fit could still be obtained if B is a constant. Fig. 1 shows the results of a least squares fit to the calculations of Mündel et al.,[7] using the analytic form of Eq.(14). The constant B = 7.15 eV was obtained in the fit. This approach also provides a natural way to extrapolate $V(R,\varepsilon)$ to large values of R: one keeps the same B and adopts a sensible asymptotic form for A(R). As shown in Fig. 2, the values of A(R) fit in the range $1.4\ a_o < R < 2.75\ a_o$ (for which calculations were reported) suggest a linear extrapolation out to the R for which A(R) is zero.

The advantage of the form Eq.(14) for $V(R,\varepsilon)$ is twofold. First, the principal part integral in the definition of the shift operator [Eq.(6)] can be done analytically. Second, a separable form

of the shift operator results, permitting Eq.(3) to be solved by Bardsley's Green function method.[15,16] We consider the principal part integral in this section, and defer discussion of the method of solution to the next section.

We now consider

$$\Delta(R,R',\varepsilon) = P \int_0^\infty \frac{A(R)\, A(R')\, (\varepsilon')^{3/2}\, d\varepsilon'}{(\varepsilon'+B)^4\, (\varepsilon-\varepsilon')} \tag{16}$$

where P denotes the principal part integral. Simplification follows by change of variable to $x = \varepsilon'/B$, and by the introduction of a factor of $\pi/16$ for future convenience:

$$\Delta(R,R',\varepsilon) = -\frac{\pi}{16} A(R)\, A(R')\, B^{5/2}\; p(\varepsilon/B) \tag{17}$$

where

$$p(a) = \frac{16}{\pi}\; P \int_0^\infty \frac{x^{3/2}\, dx}{(x+1)^4\, (x-a)} \tag{18}$$

The function p(a) only needs to be evaluated in the interval [-1,1]. The value of p elsewhere follows from the symmetry relation

$$p(1/a) = -a\, p(a), \tag{19}$$

which is easily verified by writing the integral expression Eq.(18) for p(1/a), and then changing variables to $y = 1/x$.

Fig. 3 illustrates the values of p(a) calculated numerically. The special values p(0) = 1, p(1) = 0, and dp/da (0) = 5 follow from Eqs.(18) and (19).

We now illustrate the explicit values of the coupling matrix elements used. Particular attention is paid to the region of R near 3 a_o. For R > 3 a_o, there exists a well defined bound state H_2^- at an energy below the corresponding H_2 energy. For fixed R < 3 ao, there exists a scattering resonance at an energy $E_{res}(R) > 0$. Formally, one expects[17] the bound state at large R to join smoothly with the resonance at small R; the potential curves adopted to treat DA must behave this way as well. Using the values of $E_{res}(R)$ calculated bu Mündel et al.[7] for R < 3 a_o, and the potential curve calculated by Senekowitsch et al.[18] for R > 3 a_o, we found indeed that the H_2^- curve at large R could be smoothly joined with the curve $V_{res}(R)$ defined by Eq.(10). Another way of stating this is that for R > 3 a_o, $E_{res}(R)$ is negative and corresponds to a bound state.

We can now define the potential curve $V_d(R)$ for all values of R. Since $E_{res}(R)$ has been shown to be a smooth and well-behaved function of R near R = 3 a_o, there is no difficulty in using the definition of the shift [Eqs. (11), (12), and (17)] to determine $V_d(R)$ for both positive and negative values of $E_{res}(R)$:

$$V_d(R) = V_{H_2}(R) + E_{res}(R) - \Delta(R) \qquad (20)$$

The potential curves determined are shown in Fig. 4.

C. WORKING EQUATIONS

We now describe the solution of Eq.(3). The analysis of the previous section has led to explicit forms of the shift and width operators that can be handled with standard methods. The crucial point is that the R and R' dependence of Δ and Γ is identical. One can rewrite Eq.(3) as

$$\left[\frac{\hbar^2}{2M}\frac{d^2}{dR^2} - V_d(R) + E\right]F(R) = V(R, E-E_{v_o})\ \chi_{v_o}(R)$$

$$+ \int dR' \sum_{\substack{v \\ \text{open}}} \chi_v(R)\,\chi_v(R')\,A(R)\,A(R')$$

$$\times \left[g_\Delta(E-E_v) - i\pi\, g_\Gamma(E-E_v)\right] F(R') \qquad (21)$$

where

$$g_\Gamma(\varepsilon) = \frac{\varepsilon^{3/2}}{(\varepsilon + B)^4} \qquad (22)$$

and

$$g_\Delta(\varepsilon) = -\frac{\pi}{16} B^{-5/2}\, p(\varepsilon/B) \qquad (23)$$

Bardsley's Green function method[15,16] can be used to reduce the problem to a set of linear equations whose coefficients involve the matrix elements of the Green function for the lhs of Eq.(20). This function is defined as

$$G(R',R) = C^{-1}\, F_1(R_<)\, F_2(R_>) \qquad (24)$$

where $F_1(R)$ is the regular solution of Eq.(20) with the rhs set to zero that satisfies the boundary conditions $F_1(0) = 0$ and $F_1(R) \rightarrow \sin(kR+\delta)$ as $R\rightarrow\infty$. The irregular solution $F_2(R)$ satisfies $F_2(R)\rightarrow \exp[i(kr+\delta)]$ as $R\rightarrow\infty$. For this choice of asymptotic normalization, the Wronskian $C = -k/2M$. The matrix elements $G_{vv'}$ are defined by

$$G_{vv'} = \int_0^\infty dR \int_0^\infty dR'\ A(R)\chi_v(R)\ G(R,R')A(R')\chi_{v'}(R') \qquad (25)$$

One then solves the set of linear equations $\mathbf{Ax} = \mathbf{b}$, where

$$x_v = \int_0^\infty \chi_v(R)\, A\,(R)\, F\,(R)\, dR \tag{26}$$

$$b_v = g_\Gamma\,(E\text{-}E_{v_0})\, G_{vv_0} \tag{27}$$

and

$$A_{vv'} = \delta_{vv'} - \left[g_\Delta(E\text{-}E_{v'}) - i\pi\, g_\Gamma(E\text{-}E_{v'})^2\right] G_{vv'} \tag{28}$$

The asymptotic form of F(R) can be determined from the x_v just as in previous work,[16-19] and from that the cross sections can be evaluated.

RESULTS AND DISCUSSION

A. CALCULATIONS OF CROSS SECTIONS AND RATES

Cross sections for DA of H_2 through the $^2\Sigma_u^+$ H_2^- state have been calculated for J = 0 and v = 0-9, and for electrons from threshold up to 4-5 eV. Results for the cross sections as a function of incident electron energy are shown in Fig. 5. These calculations include the full energy-dependent and complex shift and width operators. The cross sections exhibit oscillatory structure near threshold that appears to be related to the energy dependence of the width operator. We found that the oscillations persisted when the nonlocal shift was replaced by a local shift. However, the structure was not present in earlier calculations we performed with an nonlocal but energy-independent width, nor was it seen in the calculations of Wadehra and Bardsley,[3] who used a local shift and a local width. This comparison suggests that the energy-dependent factors in the sum over vibrational states in Eq.(21) are the origin of the structure. These terms spoil the closure approximation, in which the sum is replaced by a Dirac delta function, and which underlies the reduction to the local complex potential model.

A more physical explanation is the following: The local width approximation means that the resonant H_2^- state decays at a smoothly varying rate as the nuclei move apart after electron capture. This decay rate is independent of the details of the final channels available. The nonlocal width restricts the decay of the resonant state, by introducing a dependence on the matrix element of that state with the wave functions of the available vibrational levels of H_2. The decay is then sensitive to the details of the matrix elements between the vibrational levels of H_2 and the translational wave function on the H_2^- state. Because the matrix elements change with energy, the oscillatory structure results. This structure may also be an analog of the vibrational fine structure discussed by Domcke et al.[11] in e-H_2 vibrational excitation.

The calculations can be compared with experimental data, and with other calculations in the literature, in several different ways. Fig. 6 shows the cross section for attachment by H_2 (v = 0) as a function of energy. Several recent calculations are compared with the data of Schulz and Asundi.[1] The calculated peak values are very similar. It is plausible that the calculations are all larger than the experiment; Gauyacq[20] has pointed out that convoluting his calculation with an electron energy distribution whose full width at half maximum is 300 meV would decrease the calculations from 2.3 to 1.5×10^{-5} Å^2. The primary difference between the calculations is the width of the threshold peak. The present calculation agrees closely with that of Gauyacq,[20] and obtains a FWHM of about 340 meV; the calculated widths of Wadehra and Bardsley[3] and Mündel et al.[8] are about 500 and 530 meV, respectively. Schultz and Asundi[1] reported two sets of data taken under different conditions. The set with the narrower width, about 400 meV, is shown; the width of the other set was about 600 meV. Further experimental data would be desirable to differentiate between the various calculations.

Allan and Wong[2] have measured the relative cross sections at threshold for v = 0-4, and we compare our calculations with their data in Fig. 7. The relative experimental measurements have been converted to absolute cross sections by using the measurements of Schulz and Asundi for v = 0 (= 1.6×10^{-5} A^2). Comparision with other calculations is also possible over the range v = 0-9. We note that Wadehra and Bardsley[3,4] and Wadehra[5,6] fit their calculations to the experimental data, and used the same coupling potentials and matrix elements for the calculations at higher v. The present calculations are closest to those of Mündel et al.[8] for v = 0-2, who also took into account the nonlocal, energy-dependent shift and width operators. The present calculation rests on a fully numerical solution of the nuclear wave equation [Eq.(21)], which was facilitated by a particular choice of the form of the electronic coupling matrix element [Eq.(14)]. Mündel et al. fit $V_d(R)$ with a Morse potential, and treated the shift and width operators by an expansion in a Lanczos basis. We believe that the present approach uses more accurate potentials for the range of internuclear distance where the H_2 potential crosses the H_2^- curve. This range is

crucial to DA, but less important to vibrational excitation, which was the emphasis of the work of Mündel et al.[8] Finally, we note that the present calculations agree well with those of Gauyacq,[20] which were based on the zero-range-potential formalism.

Extensive calculations were carried out by Wadehra and Bardsley[3,4] and Wadehra[5,6] using the local complex potential model; many of the results were presented as rate constants depending on an average energy $\bar{E} = (3/2)kT$. We adopt the same nomenclature for easy comparision with their results. Fig. 8 shows rather close agreement between the present calculations and the previous calculations based on the local complex potential model. Although the logarithmic scale minimizes the quantitative differences, all general trends are in essential agreement.

Finally, the dynamical calculations of DA depend on the potentials and matrix elements in the range of $R > 3\ a_0$, where H_2^- is a true bound state. A series of calculations was performed in which A(R) was arbitrarily set to zero for $R > 3\ a_0$, thereby eliminating any contribution from this range of R. The total cross sections for DA decreased about 20-30%. Since Mündel et al.[7,8] only reported numerical values for $V(R,\varepsilon)$ in the range $R = 1.4$ to $2.75\ a_0$, the A(R) we used for larger R is an extrapolation. This test provides a measure for the uncertainty in our calculations due to our extrapolation of A(R).

B. ACCURACY OF THE LOCAL COMPLEX POTENTIAL MODEL

The most surprising aspect of the present results is that the calculations based on the local complex potential (LCP) appear to be fairly satisfactory, at least when one looks at an averaged quantity like the rate constant. Is there a physical basis for replacing the nonlocal operators $\underset{\sim}{\Delta} - (i/2)\underset{\sim}{\Gamma}$ with a simpler, local form? Mündel et al.[8] performed a comparison for $v = 0$ and concluded that the LCP was a "stunning failure". They noted that the results of the LCP could be as much as a factor of ten large. The explicit expressions we have used for the width and particularly the shift operator provide a tool for monitoring the accuracy of the final calculation as

successive approximations are invoked to simplify the shift or width. Our results confirm the need to consider the full operators, but suggest situations where an optimum local shift can be defined.

We begin our analysis with the explicit expression for the action of the shift operator on the nuclear wave function, which follows from Eqs.(21) and (23)

$$\underset{\sim}{\Delta F} = \frac{\pi}{16} B^{-5/2} A(R) \int dR' \sum_{\substack{v \\ \text{open}}} \chi_v(R) \chi_v(R') p\left(\frac{E-E_v}{B}\right) A(R') F(R') \qquad (29)$$

The operator $\underset{\sim}{\Delta}$ is both nonlocal, because of the integrals over R', and energy dependent, because of the terms involving $(E-E_v)$. We note that the constant B was determined to be 7.15 eV, and that for electrons at threshold for DA, $(E-E_v)$ ranges from 3.7 eV (v = 0) to 0.14 eV (v = 9). Hence for our calculations $(E-E_v)/B < 0.5$. From Fig. 3 it appears that the energy variation of $p((E-E_v)/B)$ in this range is not large and that $p(0) = 1$ could be substituted into Eq.(29) as an approximation. If this is done, the shift operator is reduced to an energy-independent but still nonlocal operator. The arguments for further simplification are well known; one assumes that the sum over open channels in Eq.(29) is close to the sum over all channels (including the continuum), which satisfies the completeness relation

$$\sum_v \chi_v(R) \chi_v(R') = \delta(R-R') \qquad (30)$$

Again specializing to H_2, we note that the sum always includes at least 10 terms, since the asymptotic energy of $H + H^-$ is greater than the vibrational energy of H_2 for v = 0-9. If we assume that the sum is complete, the shift operator is reduced to the following local operator:

$$\Delta F = -\frac{\pi}{16} B^{-5/2} A(R)^2 F(R) \qquad (31)$$

This form provides a simple analytic form for the shift. Determination of an explicit analytic form for the coupling matrix element $V(R,\varepsilon)$ has led to an approximate form of a local shift that is different from the normal local approximation to the shift. It is usually argued that the local shift is the static shift that is obtained when one solves the fixed nuclei scattering problem [Eq.(11)]. We have tested these two forms of the local shift.

A similar argument can be used to reduce the nonlocal width operator to a local form. In this case, however, there is no clear way to eliminate the energy dependence as there was for the shift. Substituting $E_{res}(R)$ for $E-E_v$ in the expression for $\Gamma(R,R,E-E_v)$ in Eq.(5) is the most straightforward approach. As expected,[12,21] test calculations with such an energy-independent but nonlocal width show spurious threshold behavior: the cross section decreases discontinuously (generally less than 10%) as a new channel for vibrational excitation opens up. The calculations also suggested that the sum over open vibrational states was converged within 10-20%.

We performed a series of calculations to test the various approximations to the shift operator. In all cases the nonlocal and energy-dependent width was preserved. We found that the local shift defined by Eq.(31) was a reasonably good approximation. Fig. 9 compares the results with the local shift and with the full shift operator. The largest error, about a factor of two, occurs for $v = 0$, and the approximation rapidly converges for increasing v. This behavior is completely consistent with the arguments that led to the local approximation in the first place. $(E-E_v)/B$ at threshold is largest for $v = 0$, and becomes progressively smaller for larger v. Hence approximating $p((E-E_v)/B)$ by $p(0)$ should become progressively more accurate for larger initial v, and this behavior is exhibited by Fig.9.

We also performed calculations in which the local shift was approximated by the fixed-R shift defined by Eq.(11). As before, the energy-dependent and nonlocal width operator was used. For $v = 0$ the cross sections were about an order of magnitude too large, confirming the observation of Mündel et al.[8] that this form of the local shift is a poor approximation. The cross

sections were generally less accurate than those obtained with Eq.(31), although the results were within a few percent for v = 5-9.

The two local potentials corresponding to the alternative local shifts are compared in Fig. 10. V_{local} is obtained by adding the local shift defined by Eq. (31) to V_d; it led to reasonably accurate cross sections. V_{res} was defined earlier in Eqs. (11) and (12) as the position of the fixed-nuclei electron scattering resonance. It is the curve that would be obtained in a standard fixed-nuclei calculation and we have seen that it does not lead to accurate cross sections.

These results demonstrate that part of the failure of the LCP reported in Ref. 8 can be attributed specifically to the choice of a local shift, and that the LCP can be improved by alternative choices of $\Delta(R)$. However, the optimum choice in the present case is not the fixed-nuclei form one might expect on physical grounds. These results provide a rationale for the success of Wadehra's and Bardsley's calculations[3-6] based on the LCP model. Because of the accuracy of a local shift constructed by well defined mathematical approximations, it appears plausible that a fitting procedure would lead to a legitimate, approximate local shift and width. However, using *ab initio* fixed-nuclei shifts and widths in an LCP model calculation can lead to serious errors.

CONCLUDING REMARKS

Calculations have been reported of the dissociative attachment of low energy electrons to molecular hydrogen in several vibrational levels. The calculations are based on fully *ab initio* calculations, obtained from the literature, of the potential curves and electronic structure matrix elements that characterize the fixed-R electron-H_2 scattering. The present calculations have fully included the energy-dependent and nonlocal width and shift operators.

By monitoring the accuracy of the calculations as the shift and width operators are reduced to local form, we have demonstrated that a poor choice of the local shift can seriously degrade the accuracy of the results, even if the correct, energy-dependent and nonlocal width is used. Unfortunately, the best choice of a local resonance potential curve, which follows from the optimum local shift, is not the one available from fixed-nuclei calculations of the resonant potential curve. Furthermore, our results suggest that a satisfactory local approximation to the shift operator may not always exist. Our experience with H_2 suggests that an important requirement is that several vibrational channels be open at the threshold for DA. For H_2, 10 vibrational channels are available at this energy, so the requirement is satisfied. The situation could be quite different for other systems.

This analysis of the results underscores the need for detailed electronic structure calculations of the fixed-R electron-H_2 scattering. In particular, the energy dependent matrix element $V(R,\varepsilon)$ coupling the resonant state with the continuum must be obtained for a definitive calculation. The present work has shown that once the necessary fixed-nuclei information has been determined, the dynamics equations involving energy-dependent and nonlocal operators can be efficiently formulated and solved.

ACKNOWLEDGEMENTS

The author acknowledges helpful conversations with W. Domcke, T. O'Malley, and J. Wadehra. This research was supported by the U.S. Air Force Office of Scientific Research under Contract No. F49620-88-K-0005.

REFERENCES

1. G. J. Schulz and R. K. Asundi, Phys. Rev. **158**, 2 (1967).

2. M. Allan and S. F. Wong, Phys. Rev. Lett. **41**, 1791 (1978).

3. J. M. Wadehra and J. N. Bardsley, Phys. Rev. Lett. **41**, 1795 (1978).

4. J. M. Wadehra and J. N. Bardsley, Phys. Rev. A **20**, 1398 (1979).

5. J. M. Wadehra, Appl. Phys. Lett. **35**, 917 (1979).

6. J. M. Wadehra, Phys. Rev. A **29**, 106 (1984).

7. M. Berman, C. Mündel and W. Domcke, Phys. Rev. A **31**, 641 (1985).

8. C. Mündel, M. Berman and W. Domcke, Phys. Rev. A **32**, 181 (1985).

9. T. F. O'Malley, Phys. Rev. A **150**, 14 (1966).

10. J. N. Bardsley, Proc. Phys. Soc. **89**, 321 (1966).

11. W. Domcke, C. Mündel, and L. S. Cederbaum, Comments At. Mol. Phys. **20**, 293 (1987).

12. J. M. Wadehra, "Vibrational Excitation and Dissociative Attachement," in *Nonequilibrium Vibrational Kinetics*, ed. by M. Capitelli, Springer-Verlag, Berlin, 1986.

13. W. Kolos and L. Wolniewicz, J. Chem. Phys. **46**, 1426 (1967).

14. I. S. Gradshteyn and I. M. Ryzhik, *Table of Integrals, Series, and Products*, Academic Press, New York, 1980.

15. J. N. Bardsley, J. Phys. B **1**, 349 (1968).

16. A. Giusti-Suzor, J. N. Bardsley, and C. Derkits, Phys. Rev. A **28**, 682-(1983).

17. W. Domcke, J. Phys. B. **14**, 4889 (1981).

18. J. Senekowitsch, P. Rosmus, W. Domcke, and H.-J. Werner, Chem. Phys. Lett. **111**, 211 (1984).

19. A. P. Hickman, J. Phys. B. **20**, 2091 (1987).

20. J. P. Gauyacq, J. Phys. B **18**, 1859 (1985).

21. J. P. Gauyacq, *Dynamics of Negative Ions*, World Scientific, Singapore, 1987, pp 160-161.

FIGURE CAPTIONS

1. Comparision of the numerical values $\Gamma(R,\varepsilon) = 2\pi|V(R,\varepsilon)|^2$ calculated by Mündel et al. with the analytic fit used in the present work.

2. Determination of the least squares fit to A(R). The values of $\Gamma(R,\varepsilon) = 2\pi|V(R,\varepsilon)|^2$ shown in Fig. 1 and calculated in Ref. 8 can be inverted using Eq.(14) to give a value of A(R) for each (R,ε) pair. The range of values of A thereby calculated at each R is indicated by the boxes.

3. The reduced function used to determine the principal part integral defined by Eq.(18).

4. The relevant potential curves for the dissociative attachment of electrons to H_2.

5. Calculated cross section for dissociative attachment of electrons with $H_2^+(v,J = 0)$ through the $^2\Sigma_u$ resonant state. The full energy dependent and nonlocal shift and width operators were used for these calculations.

6. The calculated cross section for dissociative attachment of electrons with $H_2(v = 0,J = 0)$ is compared with several previous calculations and with the experimental data of Schulz and Asundi.

7. The peak cross section for dissociative attachment as a function of the internal energy of the molecule. The scale on the top of the figure shows the corresponding vibrational quantum number for J = 0.

8. Comparision of rate constants for dissociative attachment with the corresponding calculations of Wadehra based on the local complex potential model.

9. Comparision of the cross section for dissociative attachment calculated using the full energy-dependent, nonlocal shift operator with a calculation using the local shift defined by Eq.(31). The energy-dependent, nonlocal width operator was used for both calculations.

10. Comparison of two forms of the local potential used for the results presented in Fig. 9. The local potentials V_{res} and V_{local} are obtained by adding to the potential V_d different local approximations for the shift operator.

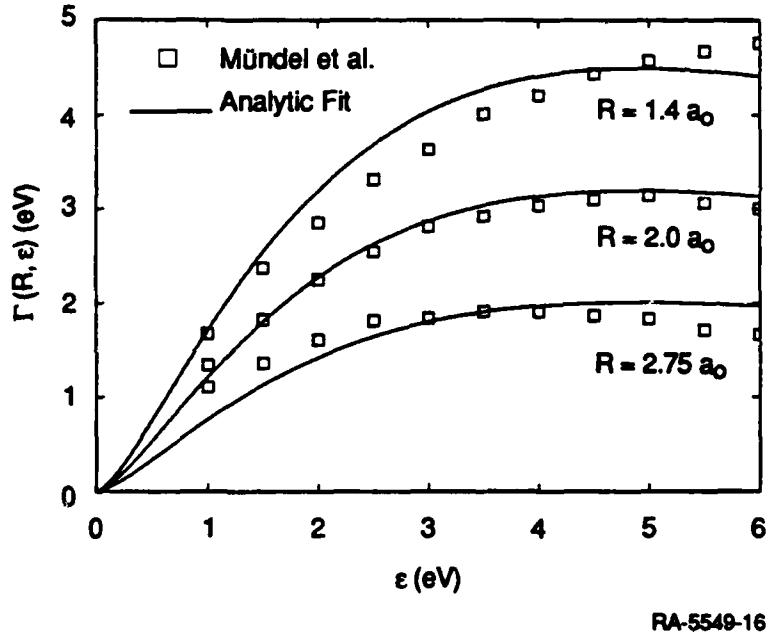
Mündel et al.
Analytic Fit
R = 1.4 a0
R = 2.0 a0
R = 2.75 a0
Γ(R,ε) (eV)
ε (eV)
0
1
2
3
4
5
6
RA-5549-16

Figure 1

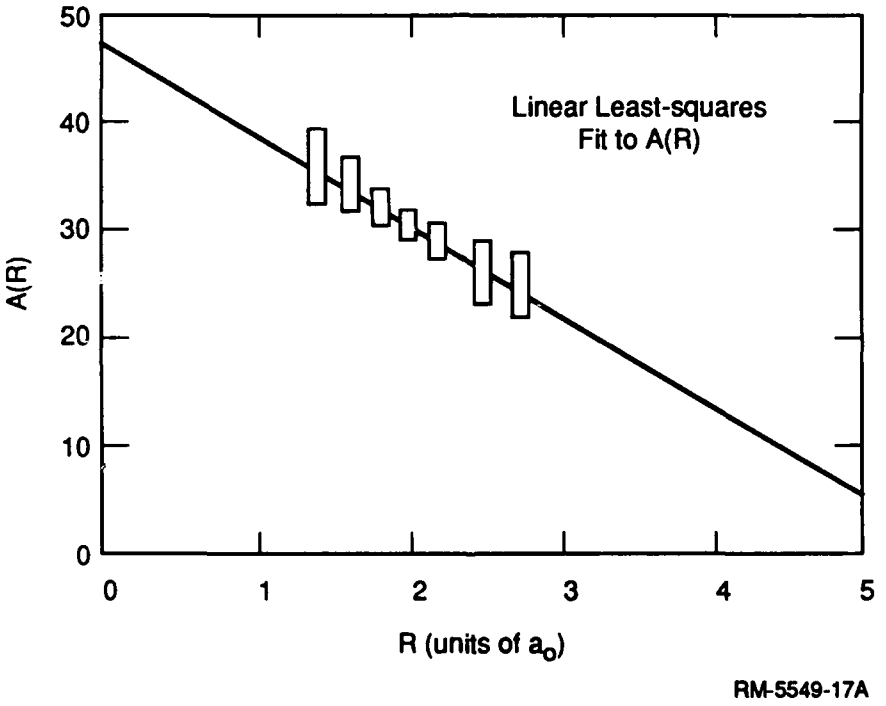
50
40
30
20
10
0
A(R)
0
1
2
3
4
5
R (units of a_o)
Linear Least-squares
Fit to A(R)
RM-5549-17A

Figure 2

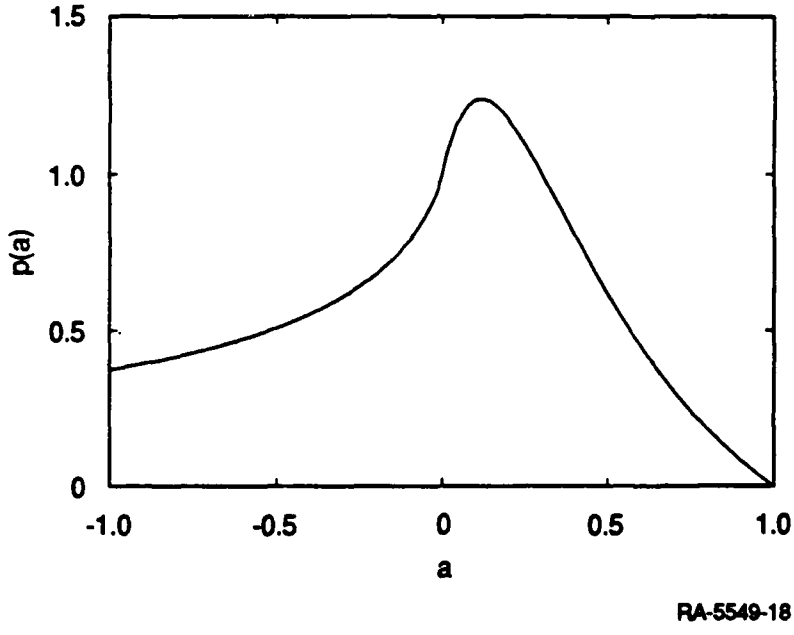

Figure 3

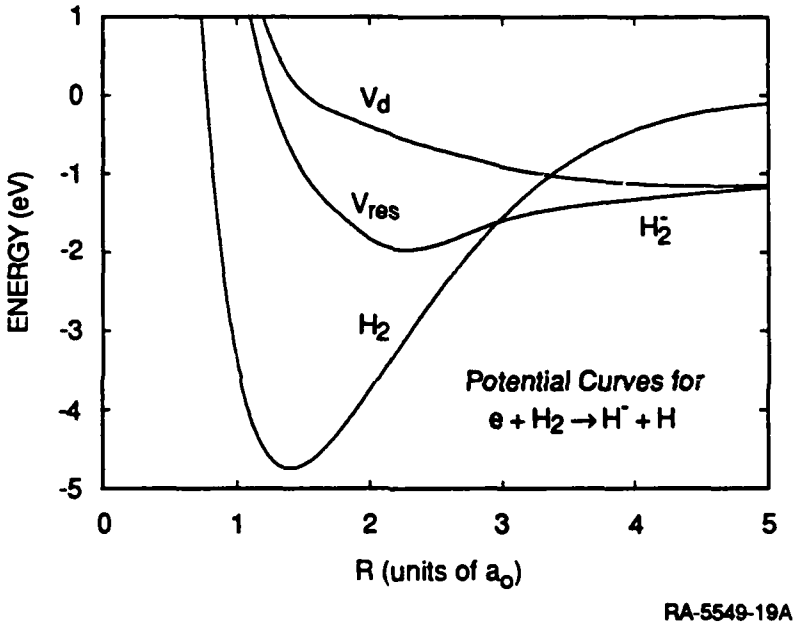
1
0
-1
-2
-3
-4
-5
ENERGY (eV)
0
1
2
3
4
5
R (units of a_o)
V_d
V_{res}
H_2^-
H_2
Potential Curves for
$e + H_2 \rightarrow H^- + H$
RA-5549-19A

Figure 4

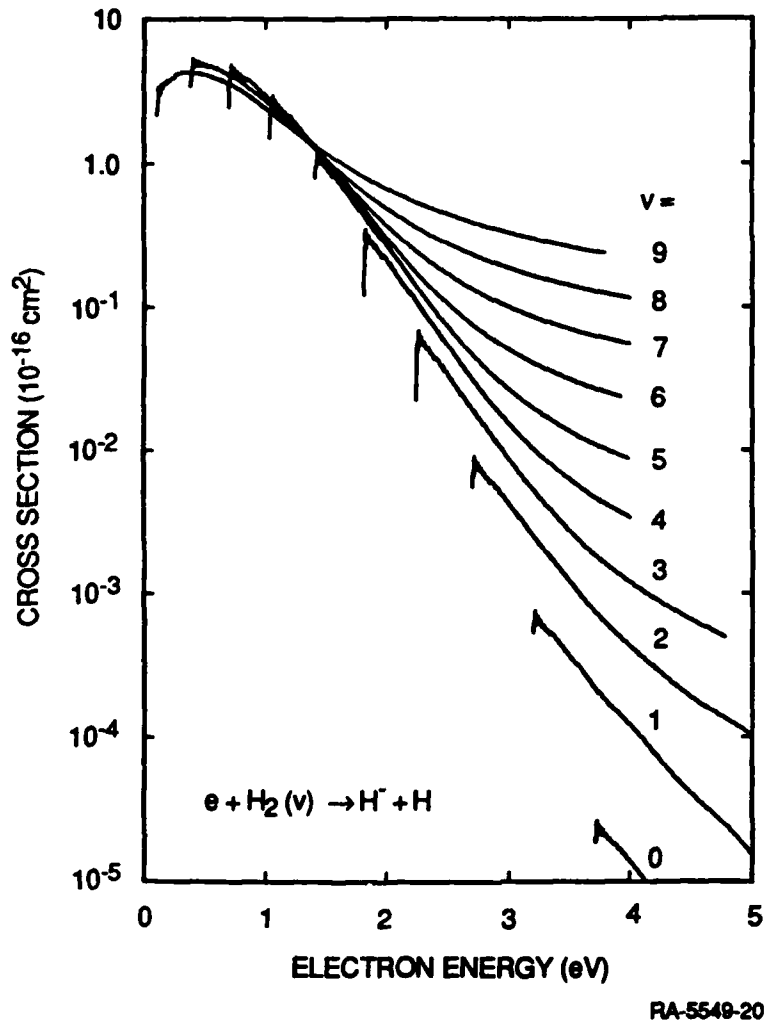
10
1.0
10^{-1}
10^{-2}
10^{-3}
10^{-4}
10^{-5}
CROSS SECTION (10^{-16} cm^2)
v=
9
8
7
6
5
4
3
2
1
0
$e + H_2(v) \rightarrow H^- + H$
0
1
2
3
4
5
ELECTRON ENERGY (eV)
RA-5549-20

Figure 5

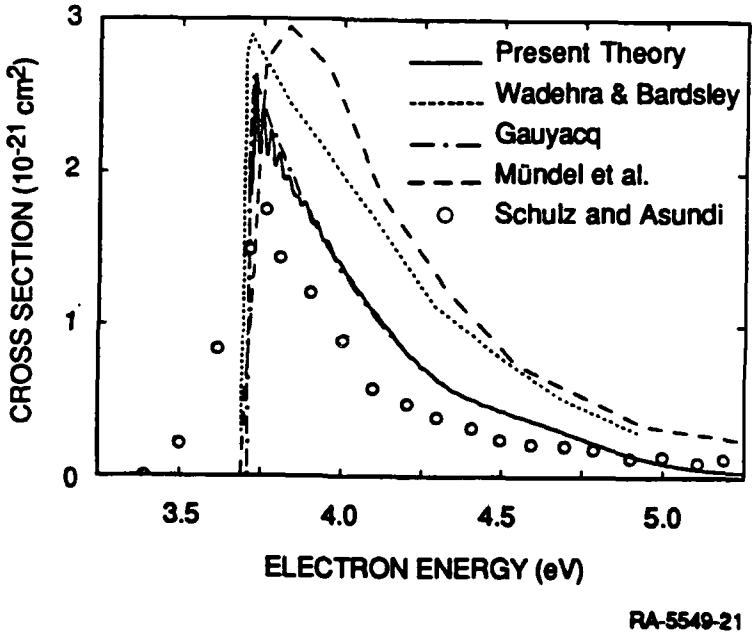
Present Theory
Wadehra & Bardsley
Gauyacq
Mündel et al.
Schulz and Asundi
CROSS SECTION (10^{-21} cm^2)
ELECTRON ENERGY (eV)
0
1
2
3
3.5
4.0
4.5
5.0
RA-5549-21

Figure 6

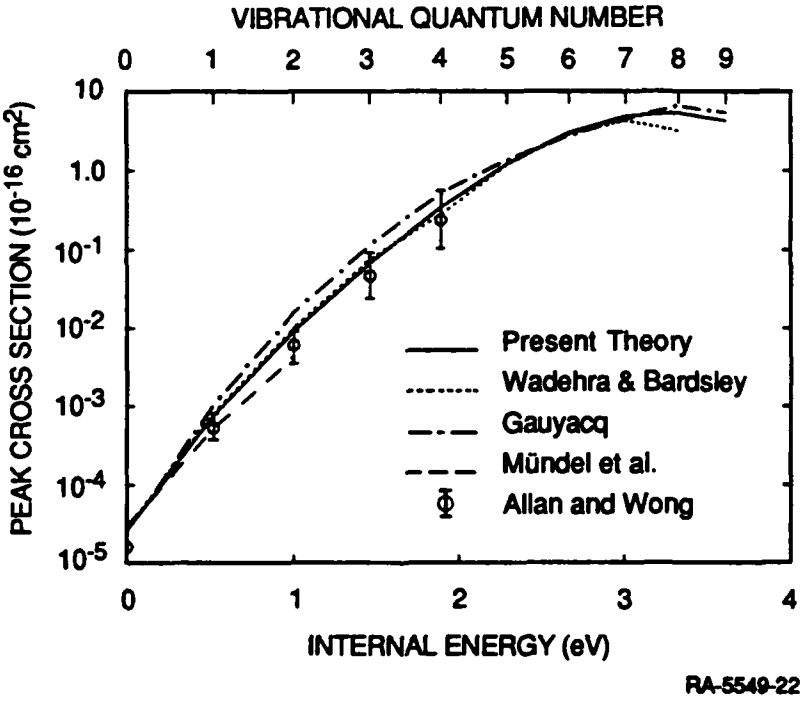
VIBRATIONAL QUANTUM NUMBER
0 1 2 3 4 5 6 7 8 9
PEAK CROSS SECTION (10^{-16} cm^2)
10
1.0
10^{-1}
10^{-2}
10^{-3}
10^{-4}
10^{-5}
Present Theory
Wadehra & Bardsley
Gauyacq
Mündel et al.
Allan and Wong
0 1 2 3 4
INTERNAL ENERGY (eV)
RA-5549-22

Figure 7

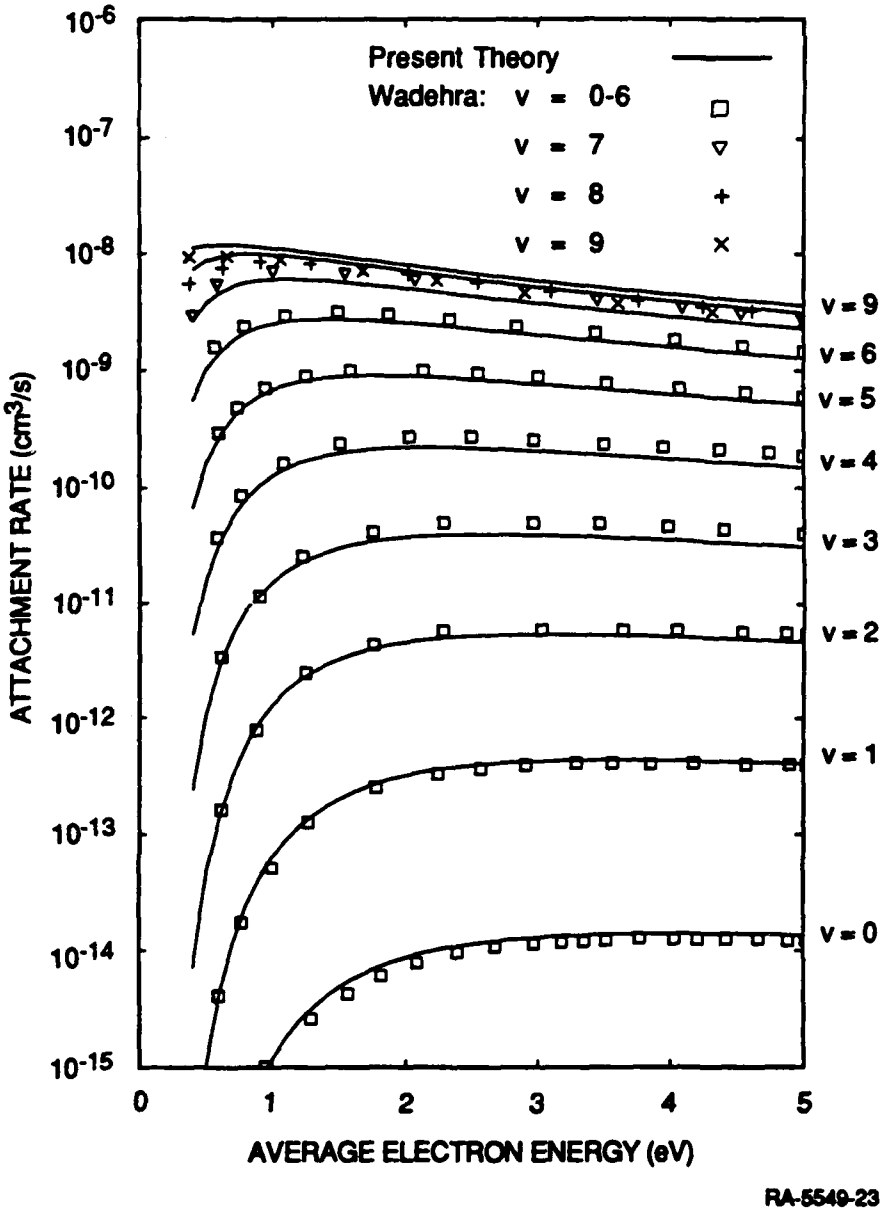
Present Theory
Wadehra: v = 0-6
v = 7
v = 8
v = 9
v = 9
v = 6
v = 5
v = 4
v = 3
v = 2
v = 1
v = 0
ATTACHMENT RATE (cm³/s)
AVERAGE ELECTRON ENERGY (eV)
RA-5549-23

Figure 8

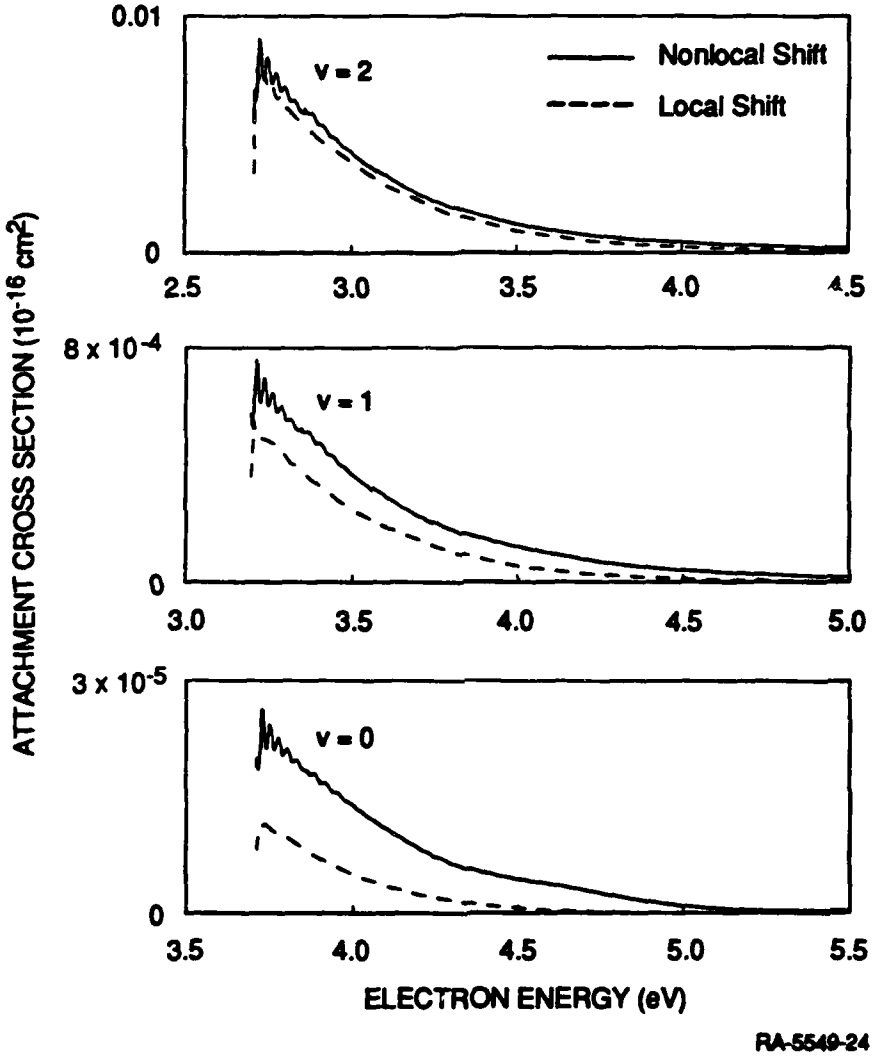
0.01
0
v = 2
Nonlocal Shift
Local Shift
2.5
3.0
3.5
4.0
4.5
8 x 10-4
0
v = 1
3.0
3.5
4.0
4.5
5.0
3 x 10-5
0
v = 0
3.5
4.0
4.5
5.0
5.5
ATTACHMENT CROSS SECTION (10-16 cm2)
ELECTRON ENERGY (eV)
RA-5549-24

Figure 9

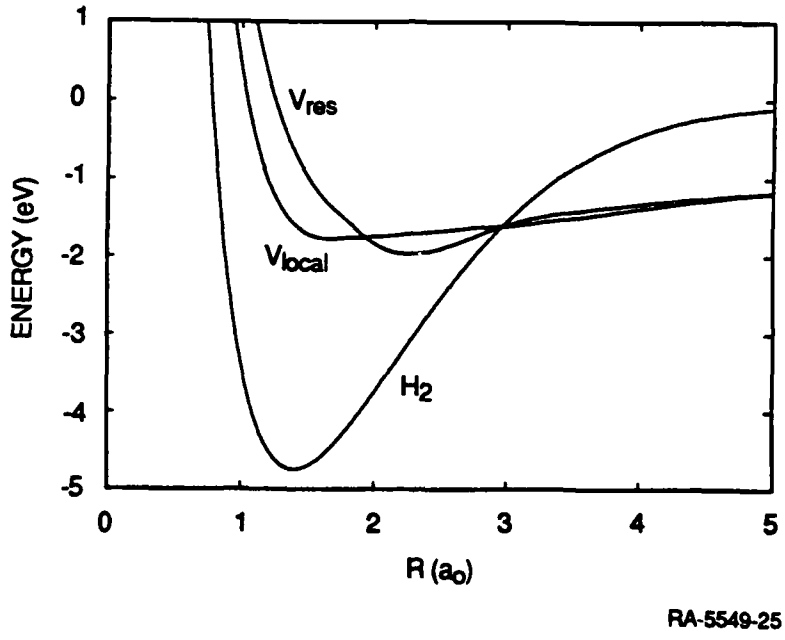

Figure 10